Palaeoenvironmental Reconstruction of the Jurassic, using Plant Macrofossils from a site at Lune River, Southeast Tasmania

Kate Eilleen Bromfield

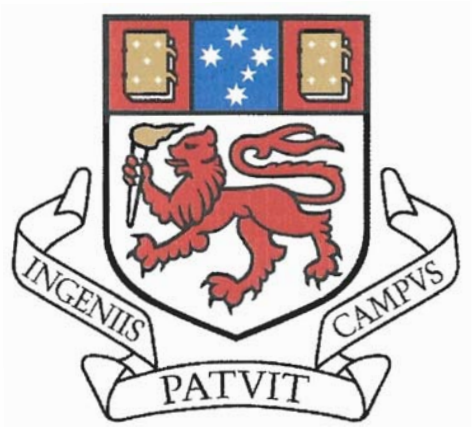

A research thesis submitted in partial fulfilment of the requirements of the Degree of Bachelor of Science with Honours.

School of Earth Sciences

University of Tasmania

November 2004

The view from the Lune River fossil site, looking across Southport Lagoon.

For Oliver and Matilda

Declaration

This thesis contains no material which has been accepted for the award of any other degree or diploma in the university and, to the best of my knowledge and belief, contains no material previously published or written by another person, except where due reference has been made in the text.

Kate Bromfield

November, 2004

Abstra

Jurassic plants excavated from a 12 by 5 m site, at Lune River, southern-most Tasmania, include an araucarian tree and numerous pteridophytes, belonging to the orders Osmundales, Filicales and Bennetitales. Deposition occurred in an aqueous, probably fluvial environment, where the plants underwent variable degrees of decomposition prior to burial. Stems of the fossil pteridophytes are in a non-life position, oriented southeast with an average dip of 40° indicating that a unidirectional force acted on them during deposition. The fossils occur in two to three metres of immature volcanilithic sandstone beds that are each up to 1 m thick. The sandstone consists primarily of clasts from granitic basement rocks, mafic clasts containing feldspathic microlathes, and primary, phreatomagmatic quartz crystals. Zircons from the volcanic deposits show a minor Triassic age distribution (226 Ma); but the majority are Jurassic, with an age of 182+/- 4 Ma.

Thermal alteration index of microfossils (3-3.3) and reflectance of organic material within the sediments (0.63-0.77 R_O) resulted from contact metamorphism resulting from intrusions of Jurassic basalt. Jurassic basalt (MgO 5.4-5.6 wt %, SiO_2 55.1-55.5-wt %) caps the volcanilithic units. It displays very similar ratios of fluid-immobile trace elements (eg, Zr/Nb, Ti/V and Zr/Y), to the Jurassic dolerite found in the state, indicative of a common source. The basalts are correlated with the Kirkpatrick Basalts (Trans-Antarctic Mountains, Antarctica) based on their field relationships with bounding strata, age, and distinctive similarities in major element composition and fluid-immobile trace element ratios. The basalt is interpreted as an extrusive equivalent of the Tasmanian dolerite, and core containing rip-up-clasts of basalt in fine-grained dolerite indicates that the basalt predates the dolerite at Lune River.

Based on comparative morphology of the plants, the sedimentology and stratigraphy of the depositional environment plus the presence of hydrophilic pteridophytes and gymnosperms with unusually large tracheids (40 μm across), and wide growth rings (1-2 cm), the Toarcian environment, at 82° south, was temperate to warm and humid with an abundant supply of water. Lune River was the location of a wide, meandering river.

Acknowledgments

This project could not have come to fruition without the logistical support of Forestry Tasmania, especially Kerri Spicer, who coordinated the project, Daniel Tuan who helped with supervision of excavator, Mark Bradley and Ken Borland, who helped with water cartage, pump equipment, and setting up the site and taking everything away at the end of the field season, Michael Giudici, Tim McDermott and Mathew Reid who surveyed the site for me, and the members of the committee, who made everything run smoothly. In addition, I would not have had the opportunity to work on this project if not for inspiration from Dr. Clive Burrett. Thanks Clive for giving me the space to find my way, while gently guiding me towards the product.

Credit goes to Borris and Chrystine, for finding the site and informing the University of its possible significance, being excited about the project, putting me up during the field work, and remaining so positive throughout the year. Good luck to you both in the future.

I would like to thank the staff and technical team at the university for advice, assistance and for making the past few years so easy to enjoy. In particular, I would like to thank Wally Herman, Sebastian Meffre, Tony Crawford, Rob Scott, and Michael Roach for helping with the little things that made the whole thing work. In addition, thankyou to Max Banks, Jim Basinger of Saskatchewan University, Clive Calver and Mike Jacobson from MRT, Geoffrey Playford from the University of Queensland, Alan Cook, Wayne Knowles and Dr. Gordon Henry. My special thanks go to Chris Sharples and Andrew Stacey. You have both been fantastic and I cannot thank you enough. Thankyou to Catherine Reid and Jocelyn McPhie for advice and support, and Greg Jordan, for being a mentor and mocking me endlessly. Thankyou also to Noel Kemp, for your friendship and advice, and access to the Tasmanian Museum and Art Gallery geological collection.

My thanks to everyone who worked as a fieldy for me: Teghan, Mark, Kylie, Kieren, Nic, Roman, Jo, Oliver (you are beautiful), Nathan, and little Clive. Finally, thankyou to my family and friends, particularly Val, for your endless patience and support, not just this year.

Contents

List of Figures

List of Plates

List of Tables

Chapter 1 Introduction

Preamble

Early in 2003, Nigel Ellis and Christyne Klimek followed fragments of silicified wood occurring as float, up slope, until it disappeared, then began to dig. They unearthed a significant portion of a fossil tree and numerous pieces of pteridophytic flora, both fossil fern stems and leaf moulds. The location of these fossils falls within the fossicking area designated and administered by Mineral Resources Tasmania (MRT) under the Mineral Resources Development Act. The land surrounding the site of the tree is managed by Forestry Tasmania, and is adjacent to a juvenile eucalypt plantation managed by Forestry Tasmania on behalf of the Tassie Trees Trust.

Mr Ellis approached Dr. Clive Burrett, at the University of Tasmania, with a proposal to study the significance of the fossils, and by June 2003, a committee comprising affected parties convened to manage the research and future development of the site. The committee members are: Steve Davis, Kerri Spicer and Daniel Tuan from Forestry Tasmania, Geeveston, Clive Burrett and Kate Bromfield from the University of Tasmania, Hobart, Clive Calver from Mineral Resources Tasmania, Rosny Park, Nathan Duhig and Penny Wells from the Forest Practices Board, Hobart, Michael Pemberton from the Department of Primary Industries, Water and Environment, and Nigel Ellis, from Lunaris Gemstones, Lune River.

In January 2004, Forestry Tasmania provided funding and logistical support for the excavation of the site. During ten days in the field, an area 12 by 5 m was excavated to a depth of 4 m depending on the overburden. The tree was exposed and found to be over twelve metres long, with much still buried in the ground at the end of the period. Fully unearthed, it may well be the longest petrified log in the state, rivalling Tasmania's largest fossil tree found at Coal Hill (Banks 1990) (Figure 1).

The committee, in light of the findings presented herein, will decide the future development of the site.

Aims and significance

The aim of the project was to undertake a palaeoenvironrnental reconstruction using evidence from the fossil site. In order to achieve this, identification of the plant fossils was important, and the stratigraphy of the site relative to the regional geology had to be established.

From Pb-U dates obtained from the site and from the constraints of field relations, the rocks are Toarcian (189-176.5Ma), from the early mid-Jurassic. This is the first time that definite Jurassic ***in situ*** sedimentary and extrusive volcanic rocks have been available for study in Tasmania. This is also the first time that precise age constraints can be placed on the fossil plants from Lune River.

It is clear that the extrusive rocks are important; the small study area comprises a suite of rocks confirming Tasmania's close links to Antarctica prior to the rifting of Gondwana. The basalt found at Lune River has a close geochemical affinity with the Kirkpatrick Basalts of Antarctica, which are extrusive equivalents of the Ferrar Igneous Complex (Siders and Elliot 1985). Further, the volcanilithic sandstone from the site has characteristics and physical components similar to widespread phreatomagmatic deposits linked to the groundwater-rich basin associated with the Jurassic rift zone of the Trans-Antarctic Mountains (Hanson and Elliot 1996).

Site Location

The fossil site lies in the southeast sector of the Tasmania Basin, near the western boundary of the basin, on an east-facing slope. It is approximately 5 krn south of Lune River and 6 km north of Laprena, on the western side of the Laprena Track, on Tasmania's south east coast (Figure 1). The site falls within the bounds of the public fossicking site at Lune River. However, Mineral Resources Tasmania (MRT) amended the dimensions of the public area on the 17th December 2003, such that under section 163(1) of the ***Mineral Resources Development Act 1995,*** a 50 m^2 area surrounding the site itself (Figure 2) is now a protected fossil site and is no longer open to amateur fossickers.

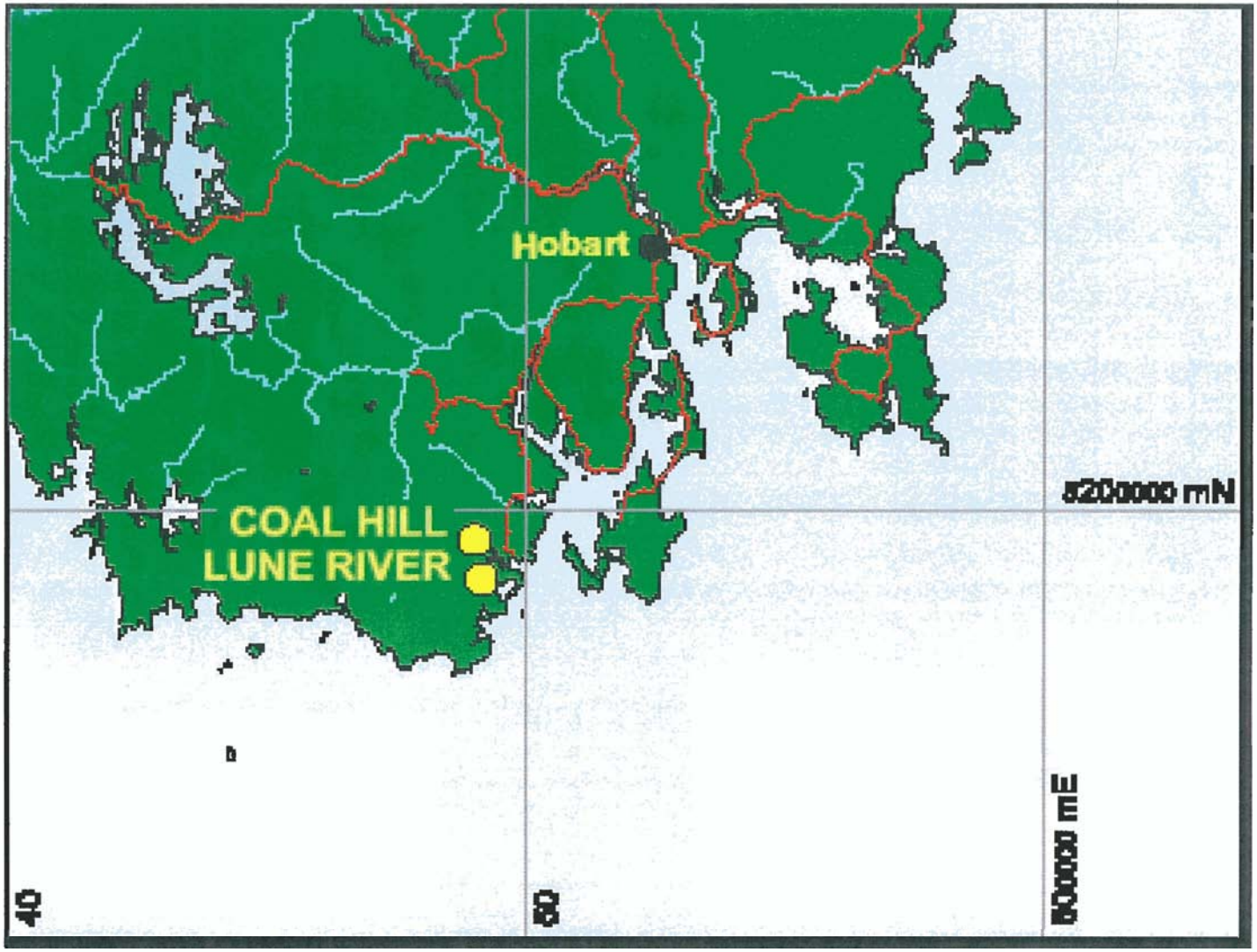

Figure 1. Location of Lune River, southeast Tasmania, with Coal Hill fossicking site marked on for reference. Map courtesy of MRT.

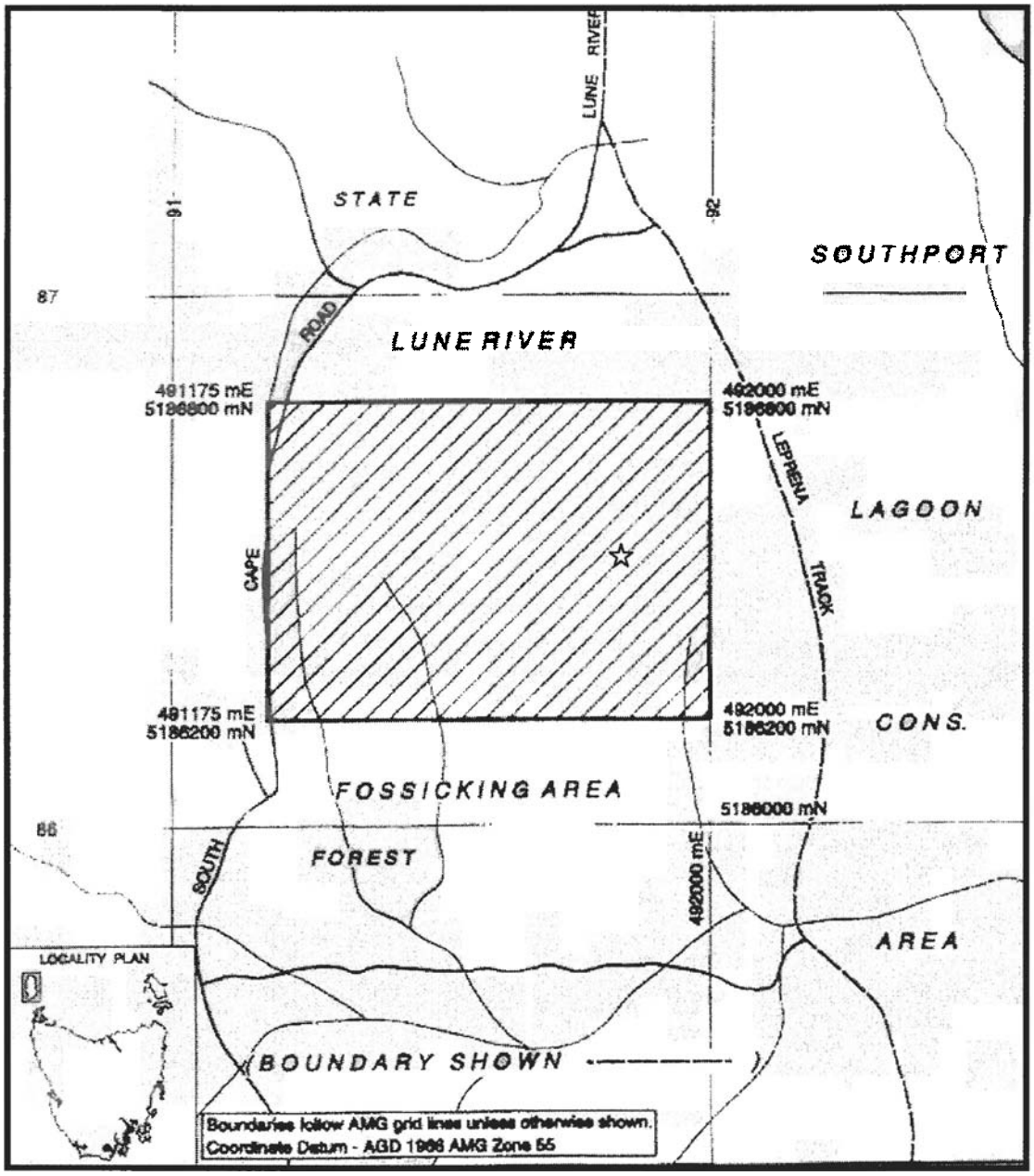

Figure 2. Boundary of protected fossil site within the Lune River public fossicking area. * indicates field site. Map curtesy of MRT.

Methodologies

Field Work:

During ten days field work, the site was excavated by Forestry Tasmania contractors. MRT supplied the permit to remove 50 kg of rock samples from a protected fossil site (28th October 2003). The site was surveyed, stratigraphic logs were made, samples were collected, and the site was photographed using a Sony DSC-P72 digital camera. The exact location and relationship of samples to host rock was recorded as samples were removed. Samples were labelled LN 1-120. Where the precise location of a sample was not recorded, samples were labelled LNX 1-30. Samples mentioned in the following text are housed at the University of Tasmania and have been ascribed a UTGD sample number in accordance with University procedure.

Lab work:

Zircons were separated and dated using the LA-ICPMS method with an HP4500 quadrupole ICPMS with a 213 nm Nd-YAG New Wave (Meffre et al. (in prep)). Appendix 1 outlines the analytical procedure, and appendix 1A shows the morphology and zonation of the zircons.

The method for whole rock analyses using X-ray fluorescence is outlined in Appendix 2. Raw data from this process is presented in appendix 2A.

PIMA analysis used PIMA SP software, with reference to the Spectral Interpretation Field Manual G-Mex vol 1 and Spectral Analysis Guide for Mineral Exploration, AusSpec International Pty. Ltd. (1997).

Electron microprobe analysis of a selection of amphiboles and plagioclase was done at the University of Tasmania. Mineral compositions were analysed using a CAMECA SX100 electron microprobe located in the Central Science Laboratory. The instrument is equipped with five wavelength dispersive spectrometers and a Rontec Xflash energy dispersive detector. The instrument was operated at an accelerating voltage of 15kV with a nominal beam current of 20nA (faraday cup) and beam size of 3um. X-ray lines were calibrated using a suite of well-characterised natural minerals, synthetic simple oxides, and pure metals. Measurement conditions were tailored to avoid analytical artefacts. Raw data is presented in appendix 3A.

Latex peels of fossils and leaf impressions were made using dental latex following method outlined by Jones and Rowe (1999). Peels were mounted and photographed using an ElectroScan 2020 Environmental Scanning Electron Microscope. The instrument operated in high vacuum mode at an accelerating potential of 15kV. Samples were coated with a nominal 40 nm thickness of Au.

Micrographs were taken using an Olympus BX60 microscope. The software for processing the images was "analysis - Soft Imaging System." Laola Pty Ltd prepared palynology samples and Professor Geoff Playford, from the University of Queensland, scanned the microscope slides for palynomorphs using a stereo-binocular microscope equipped with mechanical stage (Olympus model BH2).

Alan Cook, from Keiraville Consultants, using Leitz MPV1.1 photometer equipped with separate fluorescence illuminator, performed Vitrinite Reflectance analysis and Swift point counters. Whole rock samples were mounted in cold setting polyester resin and polished using chromium sesquioxide and Mg0 polishing powders. Wayne Knowles from Mirror Image also performed VR analysis, and appendix 4 outlines a detailed description of the method used.

Total Organic Carbon was measured on a Carlo Erba EA 1112 Series Elemental Analyser, using the Flash Combustion Technique, which is a worldwide standard test.

Palynomorphs were compared to standards in North (1984) to determine the Thermal Alteration Index. Plant identifications were made, where possible, by comparison to holotypes held at the Tasmanian Museum and Art Gallery. Fossils were photographed using a Nikon Coolpix 9500, using swan-head lights, following the method described by Jones and Rowe (1999).

Maps and stratigraphic logs were compiled using the programs ERmapper, Arcview, and Freehand 10. Core was logged at Mineral Resources Tasmania rock store. Thin sections and polished sections of wood and rocks were prepared at the University of Tasmania.

Previous work

Previous work on the Lune River region is available from both a geological and a palaeobotanical perspective. Mineral Resources Tasmania has produced a 1:25000 geological map series of the Southeast Tasmania (Forsyth et al. 1995), which encompasses the Lune River area. It also produced the Space-Time diagram of Tasmania (Seymour and Calver 1998).

Numerous authors have defined the geology of the Tasmania Basin and geochronology of in-filling strata has been established, up to the intrusion of dolerite during the Jurassic (Forsyth 1989a). Leaman (1975, 1995) described the form and mechanics of sill emplacement of the dolerite. Gould (1971) mentioned basalt outcropping at Lune River. Banks et al. (1989 and unpublished data), explored the relationship between clay sediments and the basalt. They suggested that the basalt and the dolerite may have shared the same magma source and that at Lune River, both intrusive and extrusive forms of the same event occur. Berry and Banks (1985) studied faulting in the Hobart region. However, timing of faulting in the Hobart area is still unresolved. Faults cross cutting dolerite intrusions are Tertiary (Leaman 1995); while Berry and Banks (1985), and Leaman (1975) indicate that some of the faults operating in southeast Tasmania may have been active during the Mesozoic. The fossils from Lune River have been described for the most part by Tidwell; Tidwell et al. (1987), Tidwell et al. (1991), Tidwell (1987), Tidwell and Jones (1987), Tidwell and Skogg (1992), and Tidwell (1991). Gould (1971) described, possibly erroneously, a species of *Cibotium* from the region. White (1986) collated many permineralised specimens from Lune River, proposed a sequence of taphonomic events for Lune River, and suggested a Jurassic age.

Concerning the use of palaeobotanical methods in the interpretation of fossil sites, numerous authors provide applicable techniques. Grant-Mackie et al. (2000) used Australian plant fossils to describe the Jurassic palaeobiogeography of Gondwana. Osborne and Beerling (2002) used tree ring analysis from fossil trees to estimate CO_2 levels and predict ancient greenhouse times while Niklas (1994) provided a means of predicting the original height of fossil trees using the basal stem diameter. Burnham (1989) and Burnham et al. (1992) used leaf litter assemblages to asses the degree to which fossil leaf litters reflect the composition of ancient forests. Thorne (2001)

reconstructed high palaeolatitude forests from plant fossils found in New Zealand, and Cúneo et al. (2003) used similar methods to study *in situ* forests in Antarctica. Hallam (1998) described a number of ways to determine Jurassic environments using palaeoecological methods. Finally, Jones and Rowe (1999) provided a definitive account of palaeobotanical techniques, from fossil collection and sample preparation, through to analyses.

Chapter 2 Geological Setting

The Lune River fossil site lies within the Tasmania Basin, neighbouring a fault scarp, which defines the western wall of a graben. It is adjacent to a knoll of Jurassic dolerite, and is associated with basalt flows and volcanic sandstone.

Basement rocks

Southern Tasmania is underlain by three major basement lithologies (Figure 3). The oldest rocks are the Precambrian Tyennan Complex (TY), which extends from the central highlands to the south coast. The complex subdivides into two lithological units, a quartzite-chloritic pelite, and a garnetiferous schist quartzite. The former, the quartzite-chloritic pelite, makes up the south-eastern part of the complex, close to Lune River (Turner 1989).

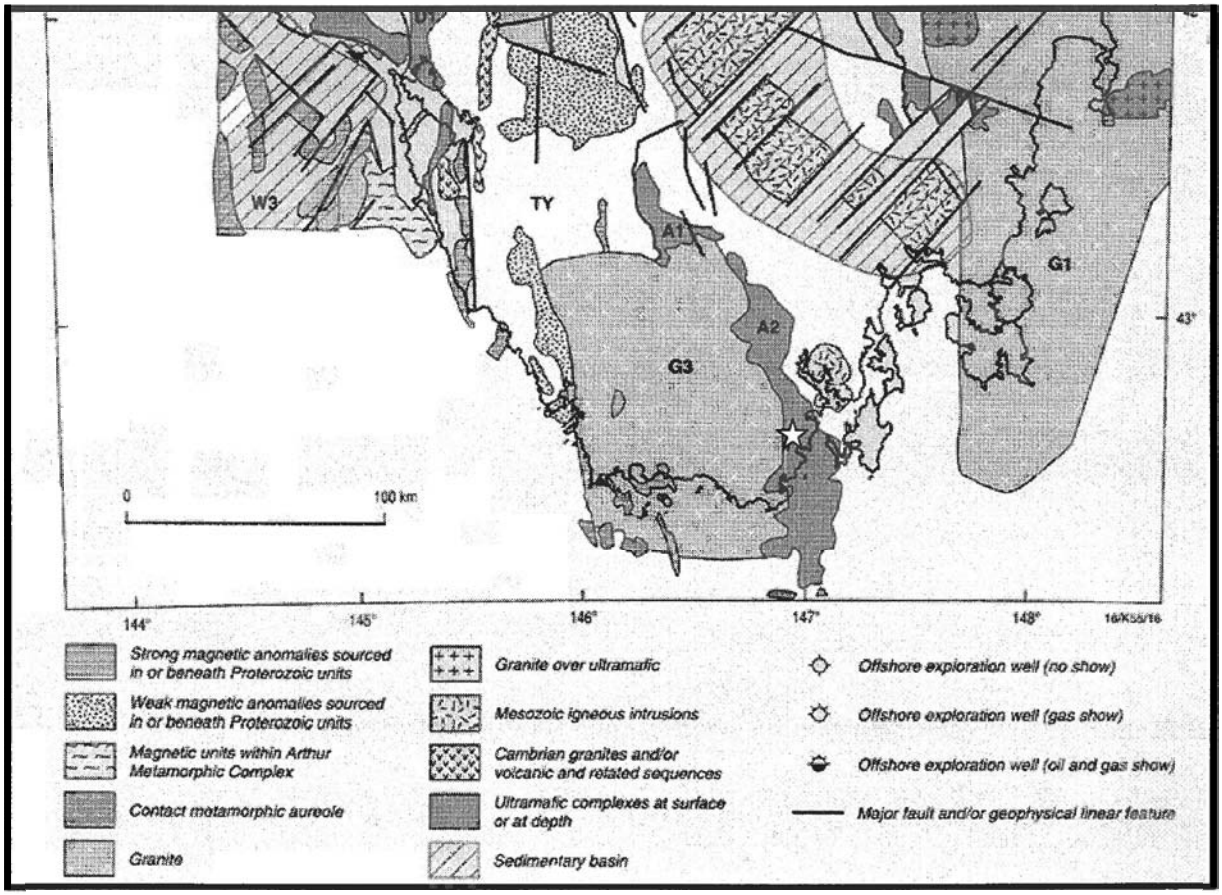

Figure 3. Basement lithology in southeast Tasmania. * indicates fossil site. Map from Gunn et al. (1997).

The second is the Cambrian Adamsfield Trough (A1 and A2), and equivalents (Gunn et al. 1997). These are basinal marine sedimentary deposits interleaved with ultra-

from high Mg boninitic andesites usually associated with oceanic fore-arc areas (Corbet and Turner 1989).

During the Devonian, granitoids passively intruded the Precambrian-Cambrian rocks. Those outcropping at South West Cape and Cox Bight on the southeast coast, derived from melting sediments, and are considered S-type granites. However, the Cox Bight body is a coarse-grained to sparse feldspar-porphyritic biotite granite, while the South West Cape granite is coarse-grained foliated biotite granite with feldspar and biotite phenocrysts. Isotope ages for both bodies lie well outside the range given for other west coast granites, but they differ from each other. The South West Cape granites were emplaced 310-330 Ma, while the Cox Bight granites were emplaced 370-390 Ma (McClenaghan 1989).

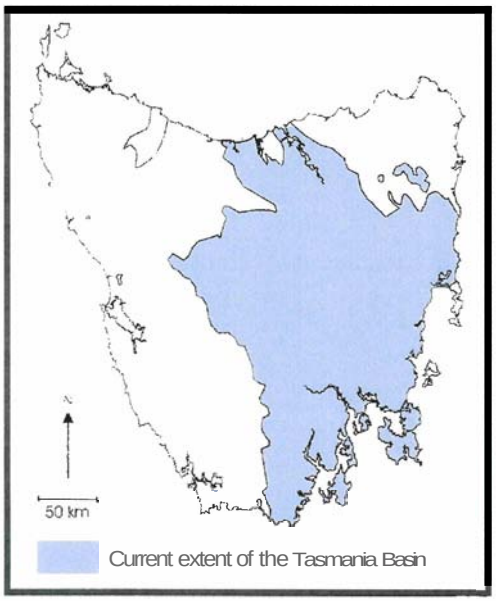

Figure 4. Current extent of the Tasmania Basin. From (Stacey and Berry 2004).

Tasmania Basin

The Tasmania Basin covers the eastern side of present-day Tasmania (Figure 4). It is a shallow epicratonic basin, 30, 000 km^2, although the present boundary is erosional, and the original basin may have been much larger (Bacon et al. 2000), containing horizontal to sub-horizontal, Late Carboniferous to Late Triassic strata. It formed due to stresses in the Tamar Fracture System, which allowed ongoing basin subsidence. Deposition occurred in a north northwest/south-southeast trending trough (Langford 1992) coincident with the axis of the Tamar Fracture System. Deposition was contemporaneous with minor faulting, producing local variations in facies architecture.

Deposits infilling the basin constitute the Parmeener Supergroup, which is divided into two units (Figure 5). The Lower Parmeener Supergroup consists of Upper Carboniferous to Permian glaciomarine deposits with limited freshwater coal measures. The Upper Parmeener Supergroup is composed of Upper Permian to

Triassic fluvial sequences, which are approximately 1500 m thick (Leaman 1975), with thick, abundant freshwater coal measures (Williams 1989).

During the Late Carboniferous, Tasmania was at a latitude of 75-80" south and was largely covered with ice. As the ice retreated, the Tmro Tillite was deposited, composed of detritus scraped from basement surfaces. The Woody Island Formation, made up of Permian units of pyritic, carbonaceous siltstone with ice rafted sediments and drop stones, and glendonites (calcitic pseudomorphs of calcium carbonate hexahydrate crystals grown at sub zero temperature), overlies this. The Woody Island Formation underlies the richly fossiliferous siltstone, calcareous siltstone, sandstone, and subordinate micrite of the Bundella Formation. In much of the state, the Faulkner Group overlies the Bundella Formation, although it pinches out stratigraphically near Cygnet. It consists of a variable succession of conglomerate, pebbly sandstone, coarse quartz siltstone and sandstone. The Hickman Formation and correlates conformably overlie it. These are comprised of pyritic mudstone; fossiliferous and unfossiliferous siltstone; fine-grained silty sandstone; medium-coarse grained quartz sandstone and pebble and granule conglomerate. The Harts Hill Limestone and its correlative, the Berriedale Limestone, overlie the Hickrnan Formation. These are richly fossiliferous, bioclastic limestones, interbedded with subordinate calcareous and sandy bioturbated siltstone. Dropstones are infrequent. The Harts Hill Limestone in turn underlies the Deep Bay Formation, which is a richly fossiliferous, shallow marine siltstone, with fine sandstone and silicic volcanic debris incorporated into some localities. Deposition of the Deep Bay Formation preceded deposition of the Minnie Point Formation, which

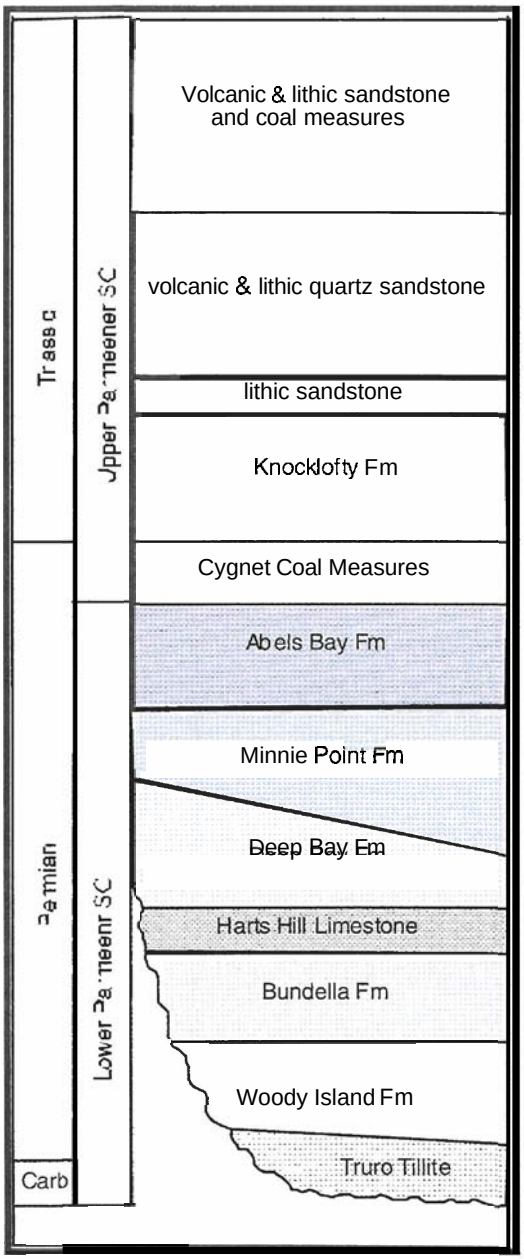

Figure 5. General stratigraphy of the Parmeener Supergroup in the Lune River region. Modified from Reid et al. (2004)

consists of conglomerates with granitic and quartzite clasts, and coarse to very coarse-grained sandstone. In southeastern Tasmania, the Minnie Point Formation underlies the Abels Bay Formation and the boundary is gradational and conformable. The Abels Bay Formation consists of inter-bedded pebbly siltstone and fine-grained sandstone; fissile and non-fissile, pebbly siltstone with subordinate fine-grained silty sandstone; and fine-grained pebbly sandstone with minor siltstone partings. The uppermost beds are carbonaceous mudstone with occasional siltstone bands and arenaceous laminae (Farmer 1985).

The Upper and Lower Parmeener Supergroup are separated in northeastern Tasmania by an hiatus spanning at least the Lower Triassic (Forsyth 1989a). However, the boundary is gradational elsewhere in the state.

The rocks of the Upper Parmeener Supergroup reflect a freshwater depositional environment, and occur as four separate units. In southern Tasmania, the Cygnet Coal Measures overlie the Abels Bay Formation. This unit contains carbonaceous beds inter-bedded with well sorted, cross-bedded or ripple laminated feldspathic sandstone. Basal beds contain quartz pebble conglomerate and pebbly sandstone. This unit passes laterally into the well-sorted, quartz sandstone of the Knocklofty Formation and correlatives. The unit regionally is in the order of 200-300 m thick. Regionally, the lower beds of the unit are generally sandstone and the upper beds are thinner, and dominate by lutite. The sandstone reflects low sinuosity rivers with palaeocurrents predominantly southeast to east, and the lutite intervals reflect abandoned channel and overbank deposits (Reid et al. 2004; Reid et al. in prep). Overlying the quartz sandstone, there is a change to lithic dominated sandstone. This unit is about 20 m thick and consists of lenticular quartz sandstone inter-bedded with lithic sandstone and lutite. It reflects depostition in a low sinuosity river flowing NNW (Forsyth 1989b). The uppermost unit of the Upper Parmeener Supergroup consists of volcanic lithic sandstone and lutites, with coal seams, tuff, and conglomeratic beds. This unit has a high proportion of igneous grains relative to the older Parmeener beds, and these range from acid to basic compositions. Sandstone dominates over the lutite and coal beds. The sandstone units typically have coarse-grained erosive bases, passing upwards into cross-bedded and ripple laminated fine-grained sandstone and lutite. Silicified plants are present in the sandstone beds. The volcanilithic sandstone was

deposited in high sinuosity rivers, with the finer grained beds representing channel fills. The coal developed in proximal peat swamps that were periodically eroded by the reappearance of major channels.

In southeast Tasmania, the Parmeener Supergroup is represented by Triassic coal measures and basal quartz sandstone, confined to the floor of the Lune River Graben (Figure 6). These represent the nearest Triassic sediments to the Lune River fossil site.

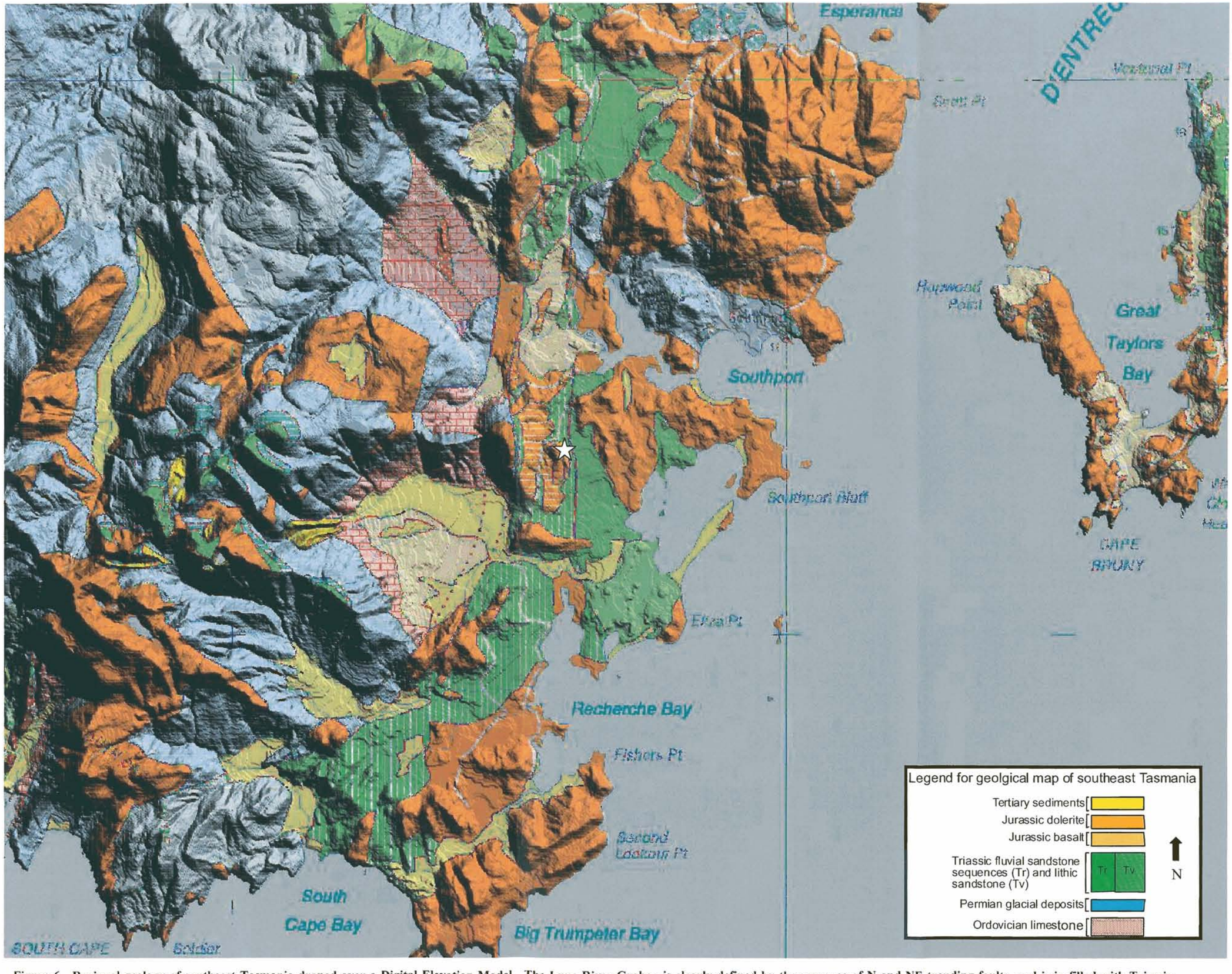

Figure 6. Regional geology of southeast Tasmania draped over a Digital Elevation Model. The Lune River Graben is clearly defined by the presence of N and NE trending faults, and is in-filled with Triassic sediments. * indicates Lune River fossil site. Map curtesy of MRT and compiled with the assistance of A. Stacey.

Faults

NNW compression forces acting on the state caused Mesozoic faulting. Two sets of faults exist in southeast Tasmania; strike-slip faults striking 100° and 170° (Berry and Banks, 1985) and reverse faults striking NE, seen confining the Lune River Graben. The NE striking faults were active during the Mesozoic, before and after the dolerite intrusion (Leaman 1975). Early Tertiary reactivation of the faults by extensional tectonics produced the Dement Graben. Strike-slip faults became normal dip-slip faults as a result of east to north-east extensional pressure.

Faults active in Antarctica in the region that is now the Transantarctic Mountains, demonstrate similar trends as those recorded by Berry and Banks (1985). Wilson (1993) provided abundant evidence that faulting in the region that is now the Transantarctic Mountains preceded emplacement of the Ferrar Igneous Province, and continued after it. In Victoria Land, only rarely are faults seen to cross cut dolerite, while in the region of the Beardmore Glacier, normal faults cutting dolerite intrusions are common. Both NNW and ENE striking normal fault sets occur in the Beardmore Glacier region, and of these, the faults trending NNW compare with the similar trending (170°) faults in Tasmania.

Reactivation of the Lune River fault probably produced the Lune River Graben (Figure 6). Older sediments from the Tasmania Basin step upwards on either side of the graben, leaving younger rocks protected from erosion along the graben floor. Throw on the Lune River fault is 400-600 m (Figure 7). This has produced horsts of uplifted Permian marine rocks at geographically elevated locations on the eastern wall of the graben, and Ordovician limestone and Permian sediments to the west of the graben wall.

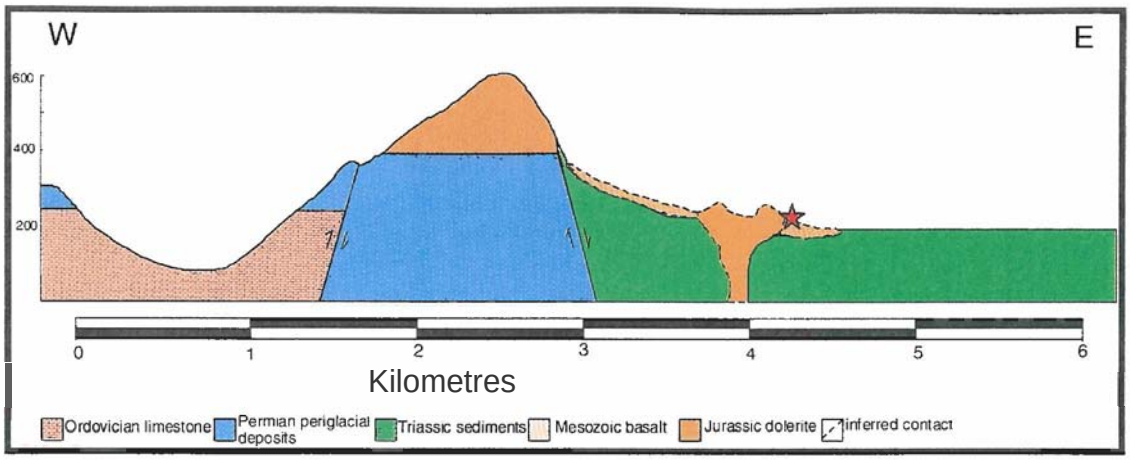

Figure 7. Cross-section through Lune River Graben. * indicates field site. Stratigraphic units have been drawn assuming sub-horizontal bedding.

Dolerite

Tasmanian Mesozoic intrusive rocks span a wide compositional range, from dolerite (diabase) to granophyre and quartz diorite (McDougall 1962), and will henceforth be referred to as dolerite *(sensu lato*). Intrusions resulted from extensional stresses between continental blocks within the Gondwana supercontinent (Baillie 1989). Overall, they are tholeiitic in composition, with relatively high FeO total, low total alkali content, and are characterised by a relatively high initial $^{87}Sr/^{86}Sr$ ratios (~0.711), suggestive of significant crustal contamination (Compston et al. 1968). The primary source region was probably upper mantle, as with the correlative Ferrar lgneous Province, Victoria Land, Antarctica (Siders & Elliot, 1985), although interaction with crustal lithologies during ascent likely resulted in significant contamination. Considering the variations in crustal lithology across the region intruded by Tasmanian and Ferrar dolerites, their homogenous chemical signatures indicate that contamination occurred on a large scale.

The dolerite mtruded in thick, stepped sheets, large transgressive bodies, and dykes. In three-dimensional view, each intrusion is broadly conical and axially flattened, and connected to a source at the deepest point on the cone (Figure 8). It intruded the flat-lying sediments infilling the Tasmania Basin, between 175-184 Ma (Minor and Mukasa 1997). Dolerites were emplaced in four or five pulses, with older magmatic episodes intruding lower into the rock column than overlying younger ones (Leaman

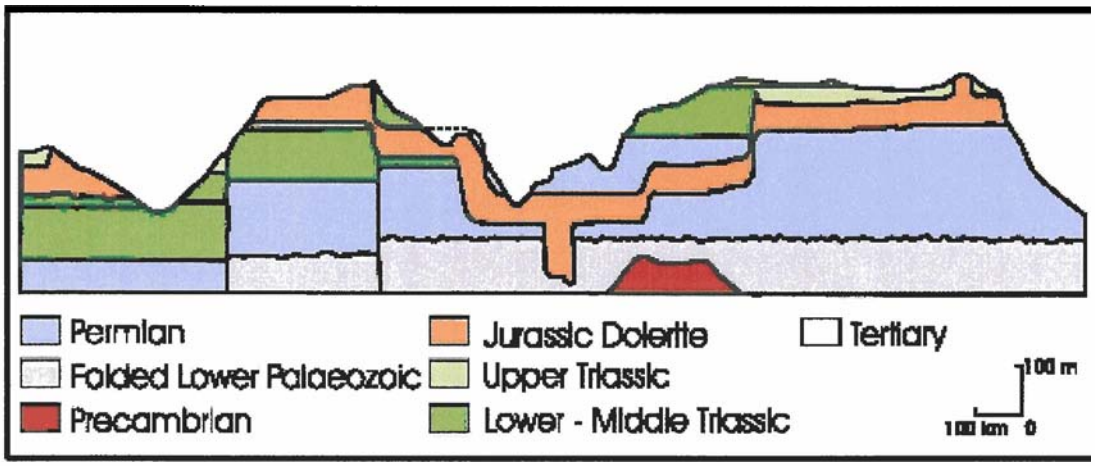

Figure 8. Form of intruding Jurassic dolerite. Curtesy of Stacey and Berry 2004 and modified from Leaman 1975.

1975). Doleritic bodies are typically either less than 1 metre thick, although some are between 300-450 metres thick. Rock textures display significant variability, ranging from glassy through fine-grained, up to medium-coarse grained.

Contact between dolerite and country sediments in Tasmania is typically sharp, with limited contact metamorphism associated with the intrusion. Associated hornfelsic contact aureoles are restricted to within only a few metres of the intrusion. Narrow metamorphic aureoles may be a result of an absence of catalysing fluids emanating from the intruding magma, or the low heat capacity of the magma (McDougall 1962), due to the high level crustal emplacement and the fact that the country rock was cold at the time of emplacement.

Columnar or platy jointing commonly occurs proximal to contact boundaries and develops at right angles to the margins of the intrusion. Such jointing is characteristic of the upper and basal margins of a hypabyssal intrusion cooling rapidly against the country rock (Forsyth 1989b).

Basalt

Banks et al. (1989) suggested a Mesozoic age for the basalt at Lune River, and Seymour and Calver (1998) ascribed it a Mid-Mesozoic age. From figure 6, it is clear that the basalt is confined to the floor of the Lune River Graben.

Areal magnetic survey

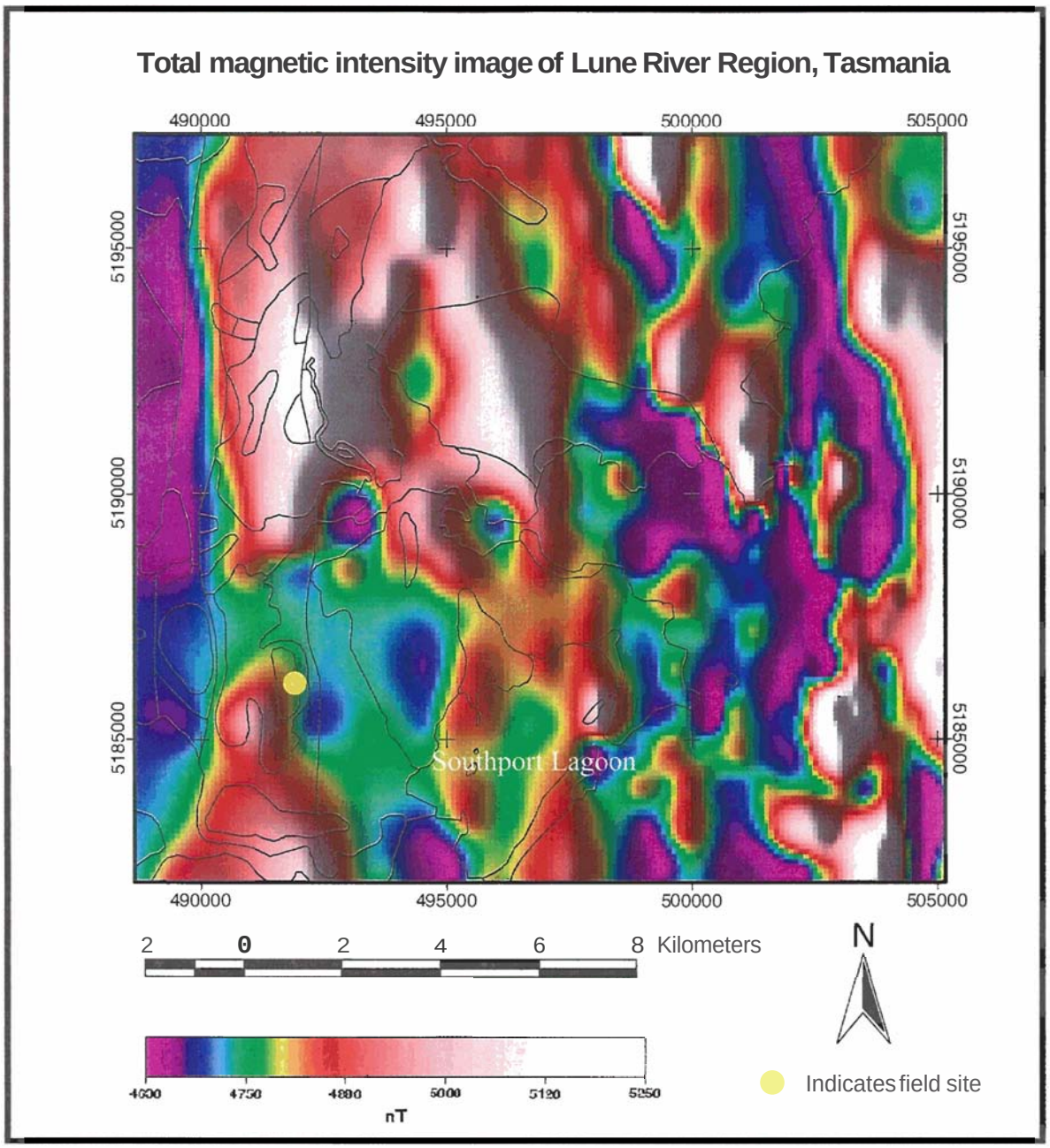

Figure 9. Total magnetic intensity (TMI) of the region surrounding the Lune River fossil site. Compiled with assistance of M. Roach, from data provided by MRT.

In 1982, Marathon Petroleum Australia Ltd. flew an areal magnetic survey over the Strathblane-Catamaran region, which covered the fossil site at Lune River. The survey flew at a mean altitude of 132 metres and a line spacing of 500 metres. The total magnetic intensity (TMI) image (Figure 9) is dominated by Jurassic dolerite, which shows as red-white highs on the image, and has a TMI from 5000-5250 nT. The basalt is associated with the dolerite intrusions and has a TMI of between 4800-5000 nT. However, it is difficult at this resolution to distinguish the basalt from the

dolerite and to determine whether they shared a vent orfissure associated with regional faulting. The Triassic sediments have a low TMI, between 4600-4800 nT, relative to the igneous rocks. The fault that forms the western wall of the Lune River Graben is clearly defined by the edge of the dolerite body. However, it is impossible to say whether emplacement of the igneous suite of rocks was controlled by the fault, or whether rocks uplifted by the western block have been eroded, leaving only younger rocks east of the fault. Again, it is clear that the basalt is confined to the floor of the Lune River Graben, as are the sediments of the Upper Parmeener Supergroup. The regional geology outline overlies the image, and correspondence between the image and the surface geology is poor at this resolution. The fossil site lies on the border between the intruding dolerite and the Upper Parmeener Supergroup, west of Southport Lagoon.

Chapter 3 Local Geology

Site description

The excavation site at Lune River is dominated by orange and yellow clay. Some lenses of clay are massive, and appear structureless, while others have a polygonal form. This clay surrounds grey to buff coloured fine-grained sediment, which encases the fossils. The fine-grained sediment is often very hard and silicifed, and usually does not extend more than a few centimetres from the plants. It is frequently jointed, with joint spacing 1-2 cm. The joints have variable trends, from 46°/066°E to 72°/060°E, and perpendicular joints are often present, trending 50°/062°W. In places, the silicified sediment forms micro-concentric rings, wrapping around the fossils (Figure 10).

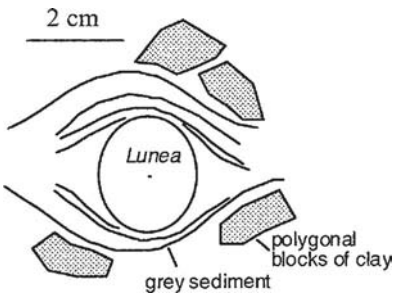

Figure **10.** Form of fine-grained sediment wrapping around fossils, **in** this example, ***Lunea jonesii***

Important features noted at the site include the lobe like appearance of orange clay bulging up from underneath the fossils (Plate 1.1), the polygonal form of the clay overlying, and adjacent to the fossil tree (Plate 1.2), and the relictual cracks in the yellow clay, in filled with fine-grained, grey sediment (Plate 1.3). These cracks appear in what may have been the palaeosurface, and the contact between the yellow clay and the grey sediments above trends 80°/030°S.

The arrangement of the fossils within the site is also an important feature. The petrified tree forms the core of the excavation, and trends 140°/20°SE. Islands of fossilised leaf impressions fi-om vegetation debris are associated with it. These islands are defined in the survey of the fossil site, presented in appendix 5. They occur within the very fine-grained grey sediment, as isolated, raft-like features on either side of the tree, and the impressions often have a ferruginous coating. Also associated with the tree are numerous petrified pteridophyte stems. These often overlie and obscure the tree trunk (Plate 1.4).

Plate 1.1. Basalt derived clay lobing up from under the site, and interacting with the fossiliferous sediments. **Plate 1.2.** Polygonal form of basalt derived clay adjacent to the petrified tree.

Plate 1.3. Desiccation cracks in the palaeosurface, in filled with fine-grained grey sediment. **Plate** 1.4. One of the rafts of pteridophytic vegetation associated with the petrified tree. "O" indicates the presence of a preserved *Osmundacaulis* sp. **Plate** 1.5. Polished sample of the volcanilithic sandstone (UTGD 154333), showing normal grading, centimetre scale bedding structures, and erosional scouring in filled with pebble sized conglomerate composed of charcoal, quartz and carbonaceous clasts.

Site Stratigraphy

The fossils at Lune River occur in very fine-grained, silicified, siltstone, found at the base of the stratigraphic log (Figure 11). (Other stratigraphic logs from the site are presented in Appendix 7.) The thickness of this rock type beneath the site is unknown. Three beds of normal graded quartz-rich volcanilithic sandstone, which also holds

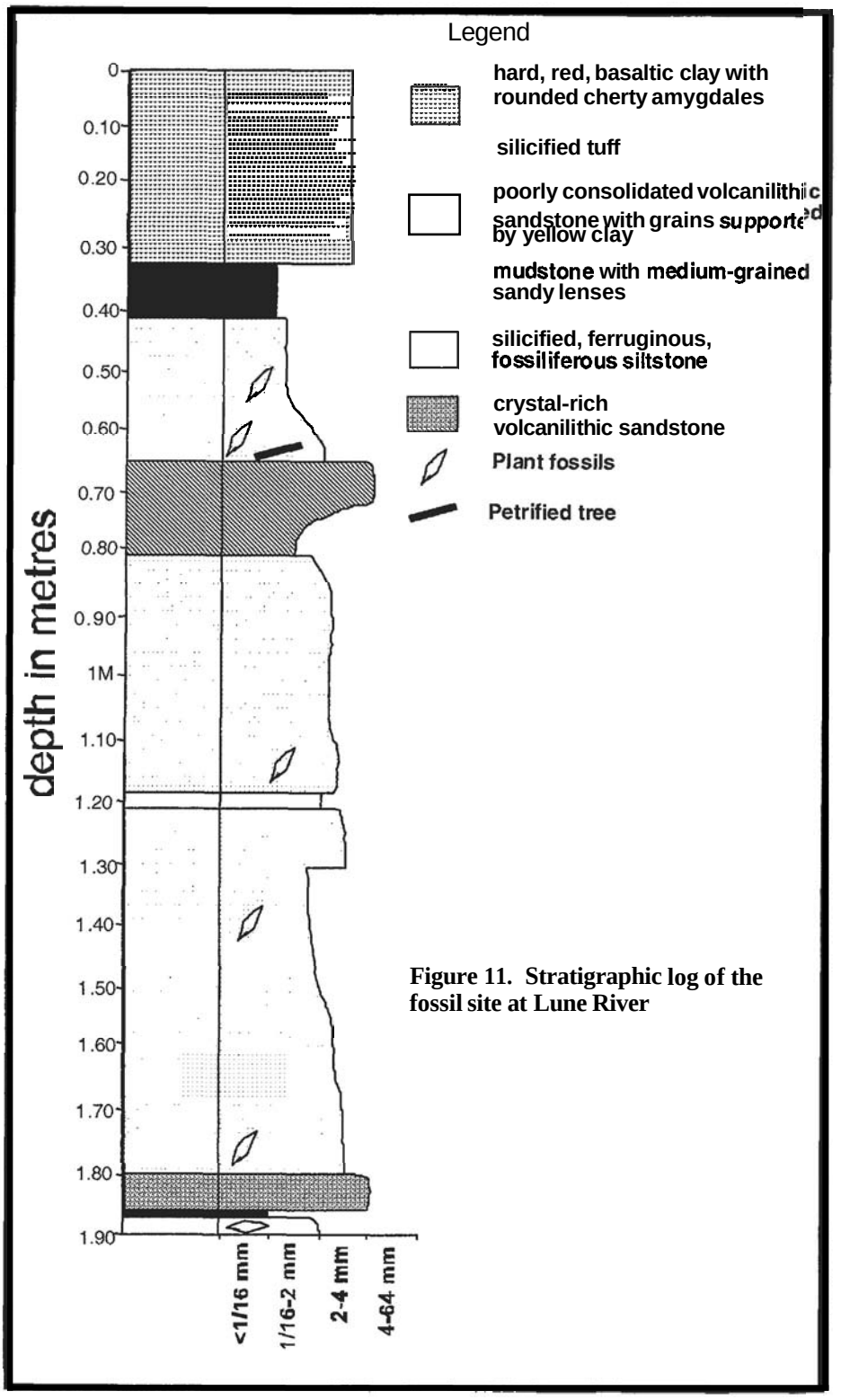

Figure 11. Stratigraphic log of the fossil site at Lune River

fossilised plant fragments, overlie it. Although the lowermost ten centimetres is not altered, much of this unit is extremely weathered and has a high clay content. A reverse graded horizon of mudstone with medium to coarse-grained sandy lenses occurs between the second and third clay rich sandstone beds. Thinly laminated silicified tuff separates the sandstone from ferruginous clay with cherty inclusions, interpreted as arnygdales, derived from the weathering of basalt that caps the site.

Volcanilithic fossiliferous sandstone

Much of the site consists of beds, up to 1 metre thick, of immature, crystal-rich volcanilithic sandstone with 50-60 % lithic clasts. It occurs in three fining upwards sequences, with one thin, reverse-graded bed towards the top of the sequence. The upper beds are altered to clay. Lateral continuity of the deposit was difficult to ascertain due to the small working area encompassed by the site boundaries. However, a similar deposit appears in core CA 106, drilled proximal to the site, so lateral continuity is likely. Sedimentary features at the site were difficult to determine due to weathering, however, polished sections revealed local scour-and-fill structures, in-filled with coarse-grained carbonaceous and quartz lag deposits (Plate 1.5). The rocks have SiO_2 76.2-80.5 wt % and MgO 1 wt % making them intermediate to dacitic in composition.

Different locations show slightly different grain sizes and balance of components. Overall however, it is a moderately to very well sorted, graded quartz and lithic rich lapilli tuff. The major components are quartz with angular, curviplanar margins and straight extinction (Plate 2.1), and rounded and angular lithic clasts, many of which are mafic and contain felspathic micro-lathes (Plate 2.2). The composition of the other lithic clasts is variable. Some are carbonaceous shale while others are granodioritic. The sandstone also contains intraclasts of mineralised peat and silicified natural charcoal (Plate 2.3). Clumps of tabular sodic plagioclase are common (Plate 2.4), as well as large, angular isolated potassium feldspar crystals, which often have altered or sieve texture cores. Some of the plagioclase crystals have melt inclusions entrained within them. Minor components include primary, euhedral hornblende (*sensu lato*), angular strained quartz crystals with polygonal recrystallisation fabrics, decrepitated biotite partially replaced by chlorite (Plate 2.5), zoned apatite, euhedral zircons (appendix 1A), and rare garnets. High aluminium

ilmenite and titanomagnetite are common. Two forms of devitrified glass occur between clasts; large blebs of recrystallised, axiolitic, black-brown glass, and fine golden-orange bubble wall shards (Plate 2.6). Secondary quartz cement in-fills some pore spaces. Some of the grains have rims of silica overgrowths. There are abundant iron oxides on clast rims, and sparse pyrite occurs.

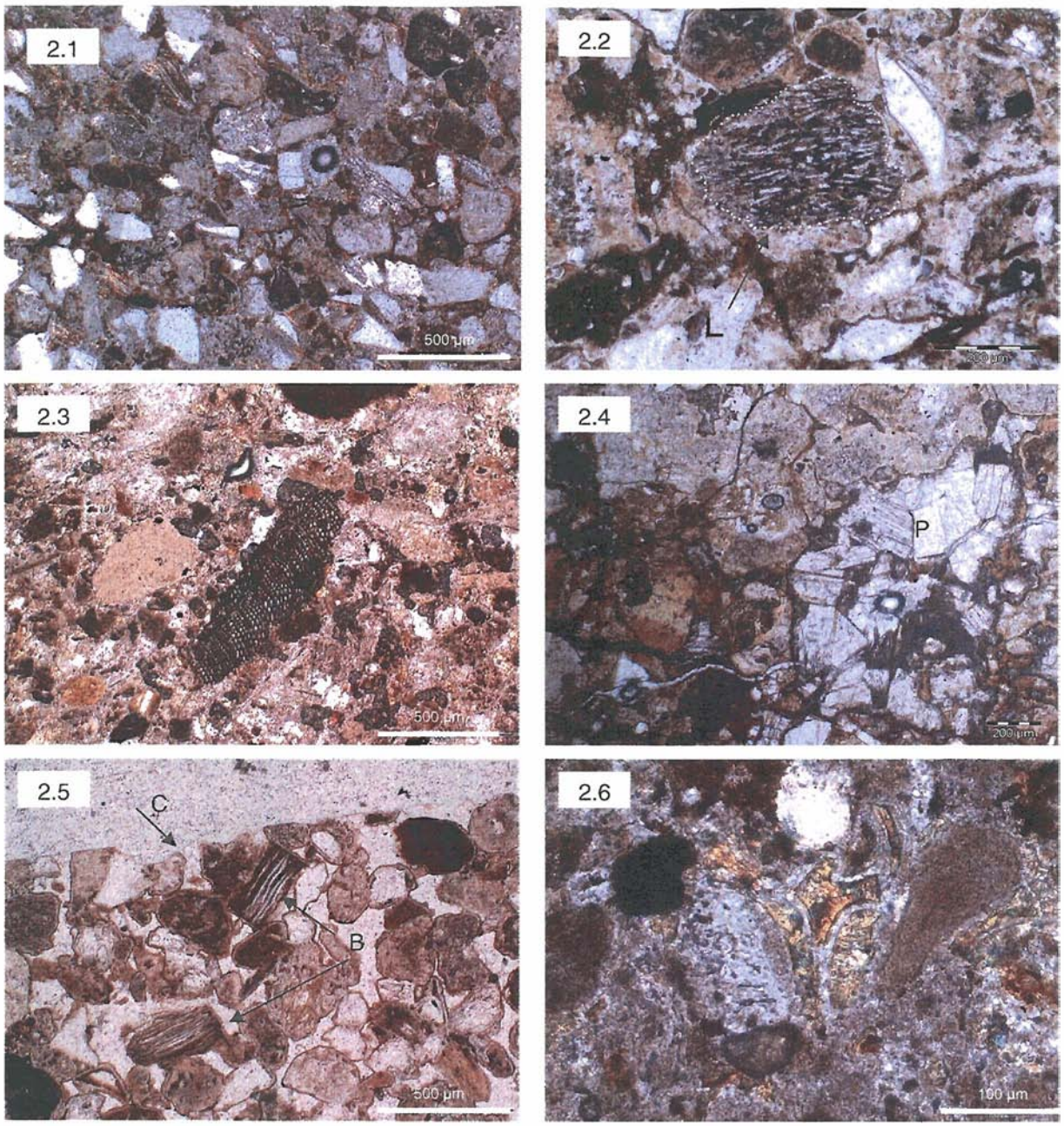

Plate 2.1. Micrograph of the volcanilithic sandstone (UTGD 154334), showing angular, immature quartz crystals with distinct curviplanar margins. Also shows abundant lithic clasts. **Plate 2.2.** Micrograph of mafic lithic clast (UTGD 154334), with feldspathic microlathes. **Plate 2.3.** Organic, charcoalified intraclast with structure intact. Smaller clasts of mineralised organic material, probably peat, appear in the matrix (UTGD 154335). **Plate 2.4.** "P" indicates clusters of plagioclase crystals among lithic clasts in the sandstone (UTGD 154334). **Plate** 2.5. Arrows indicate decrepitated biotite with chlorite alteration, occurring amongst lithic clasts (UTGD 154335). Note the sharp contact between the sandstone and the associated ash deposit. **Plate 2.6.** Glassy bubble wall shards between clasts (UTGD 154335).

Provenance

The unit has components from both mafic and felsic provenances. Many of the rounded lithic clasts are mafic. The hornblende crystals have an Mg # ranging from 56-68 (Appendix 3). Hornblende with low Mg # (56) is magnesio-hornblende (sensu stricto). It often results from primary crystallisation of intermediate melts (Deer et al. 1998). Microprobe analysis of some of the singular plagioclase crystals from the sandstone indicates that these also derived from an intermediate source. These proved to be labradorite, An # 54-56, which is often an abundant mineral in intermediate lavas (Deer at al., 1998).

Glass from between the clasts has been completely recrystallised and was of no value for analysis to determine its composition or source. The devitrification of the volcanic glass may have resulted from raised temperatures either due to burial or magmatic intrusion. However, groundwater movement can also act to devitrify glass, and accounts for the in filling of secondary quartz cement between clasts.

The quartz and the clumps of feldspars are felsic indicators, although they probably have different origins. Curviplanar immature quartz with straight extinction is typical of crystals liberated from explosive, phreatic eruptions (Hanson and Elliot (1996). These and the isolated angular potassium feldspars are probably pyroclasts. The bubble wall shards are also a product of explosive volcanism.

The clumps of feldspar crystals however, derive from a crystalline granitoid source, most likely to be the underlying S-type Devonian granitic basement rocks in the region. The garnet and biotite crystals probably share the same source, although they may result from contact metamorphism of the Tyennan sediments and Adamsfield Trough sediments into which the granitoids intruded. Alternatively, the garnet and biotite may have been released from the metamorphic terrane of the South Tasman Rise, where granitic gneiss has been dredged (Berry et al. 1997). The polygonal, strained quartz crystals support a strained metamorphic provenance typical of gneiss, rather than a contact metamorphic provenance.

Volcanic ash deposits

These are very fine-grained, pale grey, silicified sediments with lenses and blebs of fine to very fine grained quartz sandstone, reworked mudstone clasts, lithic and glass fragments and euhedral black FeTiOx. Montrnorillonite crystals up to *2* mm occur in pockets 1-2 cm in diameter, within the sediment. It is thinly laminated in places and shows no evidence of ripple or current lamination at the site although these features may occur elsewhere. The contacts between the tops of the ash beds and the bottom of the coarse bed above are knife-sharp (refer to Plate *2.5).* Iron staining occurs on some fracture surfaces and most surfaces are coated with a yellow powder, which was established to be *60* % nontronite, a yellow, powdery, iron rich smectite, and *30* % magnesium clay. Plant fragments are common, with a mean size ranging from *0.5-5.0* cm, although many examples are much larger. Carbonaceous fragments *2-5* mm in length are common. This sediment is the host rock in which the silicified fossils occur and is texturally variable throughout the site. In thin section, it is fine-very fine grained, well-sorted, glassy and diffusely laminated. Infrequent bubble wall shards, often with alteration halos (Plate 3.1), and rare angular quartz crystals occur within the matrix. The glass fragments and bubble-wall shards, as well as the angular quartz and lithic components, indicate that this unit is a fine tuff, derived from a volcanic ash.

When compared with the Middle to Late Triassic Upper Parmeener Supergroup (Table 1), both the sandstone and the ash-derived sediments from Lune River are mature and depleted in TiO, Al_2O_3 and Na_2O. They have low concentrations of Sr, Cr, and CaO relative to the Triassic sediments. However, they are rich in Rb, Ba and K_2O, which are fluid mobile elements and likely reflect the alteration of the sediments to clay. The total abundances of Zr and Nb are much lower in the Jurassic sediments but the ratios of these elements are similar in both groups. Both samples from Lune River appear geochemically related to the Parmeener sediments; however, the movement of hydrothermal fluids has likely altered them.

Table 1. Raw geochemical data comparing the sediments from Lune River, UTGD 1543 and UTGD 154333 with data from Grapes et al. (1996), showing elemental ranges in the Triassic sediments of the Upper Parmeener Supergroup, from northern, northeast, and southern Tasmania.

	UTGD 154342	UTGD 154333	Trss Range
Sio2	80.57	76.29	65.04-89.31
TiO2	0.25	0.35	0.34-0.79
Al2O3	6.83	9.02	4.15-16.24
Fe2O3	4.47	4.39	n.d.
MnO	0.02	0.02	0.04-0.15
MgO	1.1	1.11	0.11-1.47
CaO	0.27	0.3	0.4-1.35
Na2O	0.16	0.16	0.03-3.87
K2O	3.81	4.83	0.49-3
P2O5	0.04	0.03	0.01-0.18
Loss	2.58	2.87	2.86-6.74
Total	99.65	99.77	
Nb	4.8	4.1	8.0-13
Zr	92.7	83.7	148-296
Sr	26.8	44	34-373
Cr	13.4	13.6	13-63
Ba	687.2	1204.6	129-737
Y	19.66	16.67	8.0-30
Rb	111.1	141.5	4.0-92
Zr/Nb	19.31	20.41	13.38-29.6
Zr/Y	4.72	5.02	6.33-21.75
Rb/Ba	0.16	0.12	0.12-0.21
Ti/V	40.18	34.5	35.26-81.53
Ti/Sc	168.4	247.56	317.38-1019
Sr/Ba	0.04	0.04	0.12-0.51
Cr/Sc	1.51	1.6	3.71-6.50

Pb-U dating using zircons

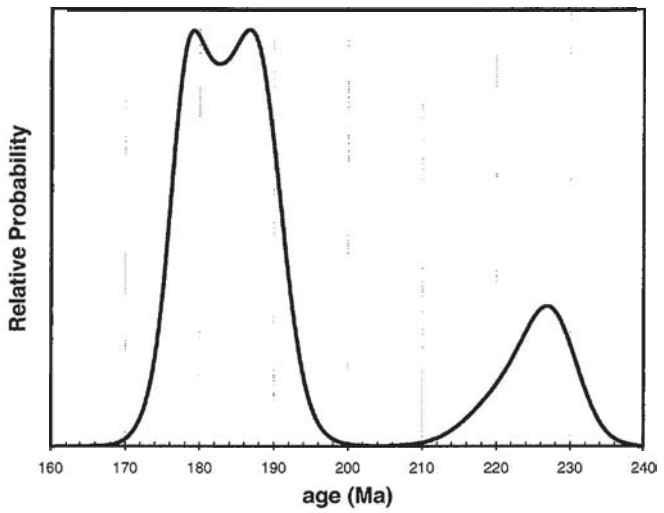

Figure 12. Probability versus age distribution of zircon ages derived from both the sandstone and the volcanic ash

Zircons from both the sandstone and the volcanic ash deposits demonstrated a semi-bimodal age distribution (Figure 12). In the tuff, the zircons are predominantly small and rounded, indicative of reworked sediment. Many are zoned. Overall, the volcanic sandstone contains larger, euhedral, zircons (appendix 1A), which have not been extensively reworked. These crystals are also zoned. However, both sedimentary units contain both forms. The rounded zircons give a middle Triassic age of 226 +/- 2My. The euhedral examples are younger, and give an age of 182 My +/- 4 My, coincident with the Toarcian stage of the early mid-Jurassic. The Jurassic zircons probably derive from the same volcanism responsible for the inclusion of curviplanar unstrained quartz crystals found in the sandstone.

Basalt

Basalt from the Lune River site has MgO 5.4-5.6 wt % and SiO_2 55.1-55.5-wt %. It is quenched, sparsely plagioclase-phyric, weakly vesicular basaltic lava. The groundmass is texturally variable, from dendritic crystallites in glass associated with quench crystallisation to glass itself, now completely altered to brown clay. Relict phenocrysts of plagioclase occur in the glass in multi-crystal clots (Plate 3.2). Larger clinopyroxene phenocrysts occur, although many have altered to smectite (Plate 3.3). Abundant altered tiny FeTiOx crystals are scattered in the groundmass.

Fresh basalt outcrops proximal to the site (Figure 13). This comprises plagioclase and clinopyroxene phases in a groundmass composed of acicular elongate plagioclase needles in black altered glass (Plate 3.4). Local spots of yellow-red smectite overprinting of the glass occur

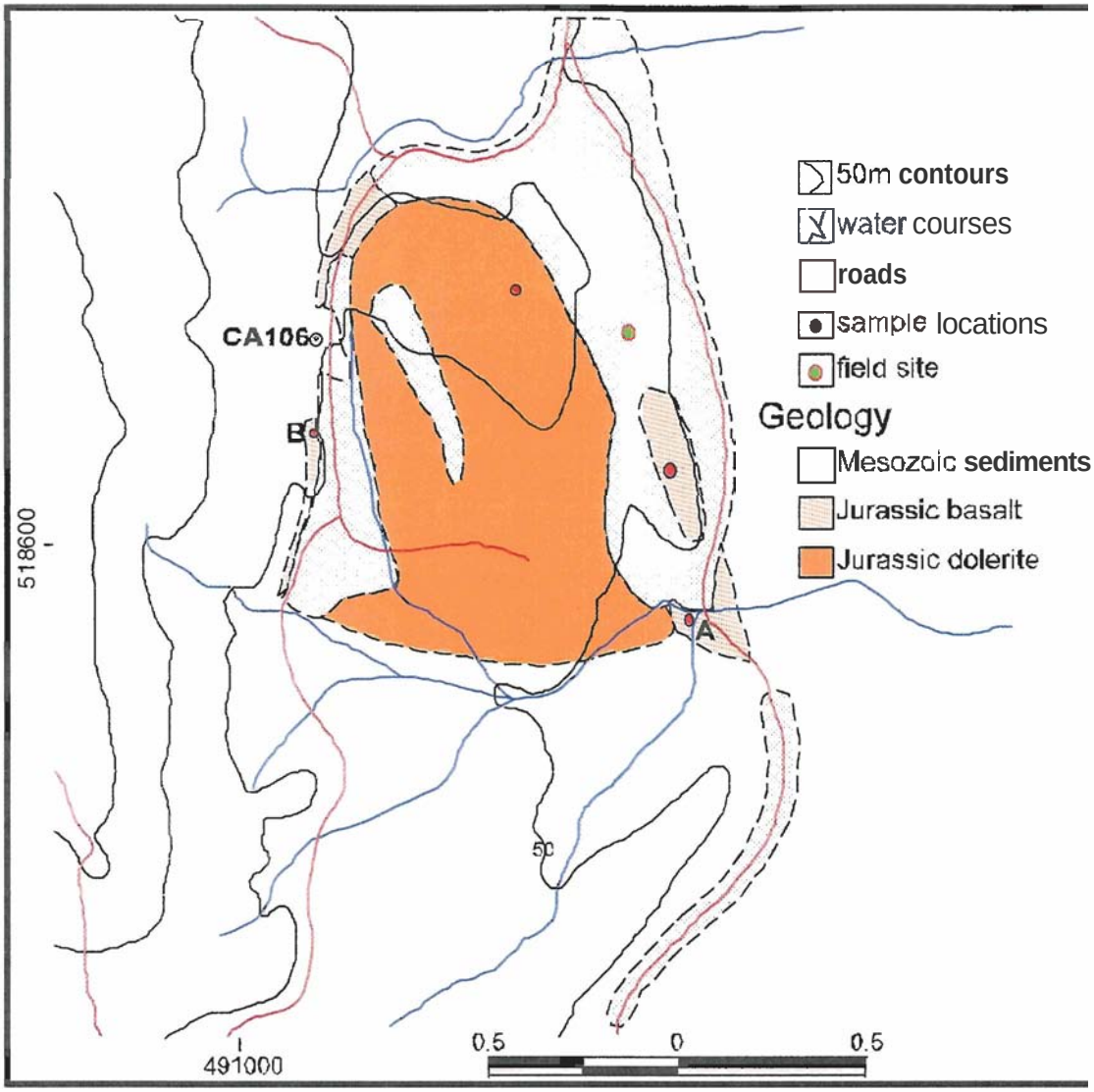

Figure 13. Map of the immediate region surrounding the Lune River fossil site. Adapted from unpublished work by C. Sharples. A and B indicate outcropping pillow basalt.

Figure 13 also shows two locations, marked (A) and (B), at which pillow basalts outcrop near the site. At location (A), (Plate 3.5), the basalt exhibits classical radial joints, which define polygonal pillow structures. These pillows are in-filled with very fine grained, laminated volcanic ash (Plate 3.6). The ash has been disturbed by the emplacement of the basalt (Plate 4.1), demonstrating that the ash was present prior to the emplacement of the basalt. However, laminations in the ash above the pillow rims indicate that deposition continued following the emplacement of the magma. At location (B), weathered, altered basaltic pillows outcrop. Here the fractures between the pillows acted as conduits for groundwater movement, and quartz veins have replaced the inter-pillow spaces (Plate 4.2). Rare, thin veins of pure montmorillonite also occur (Plate 4.3).

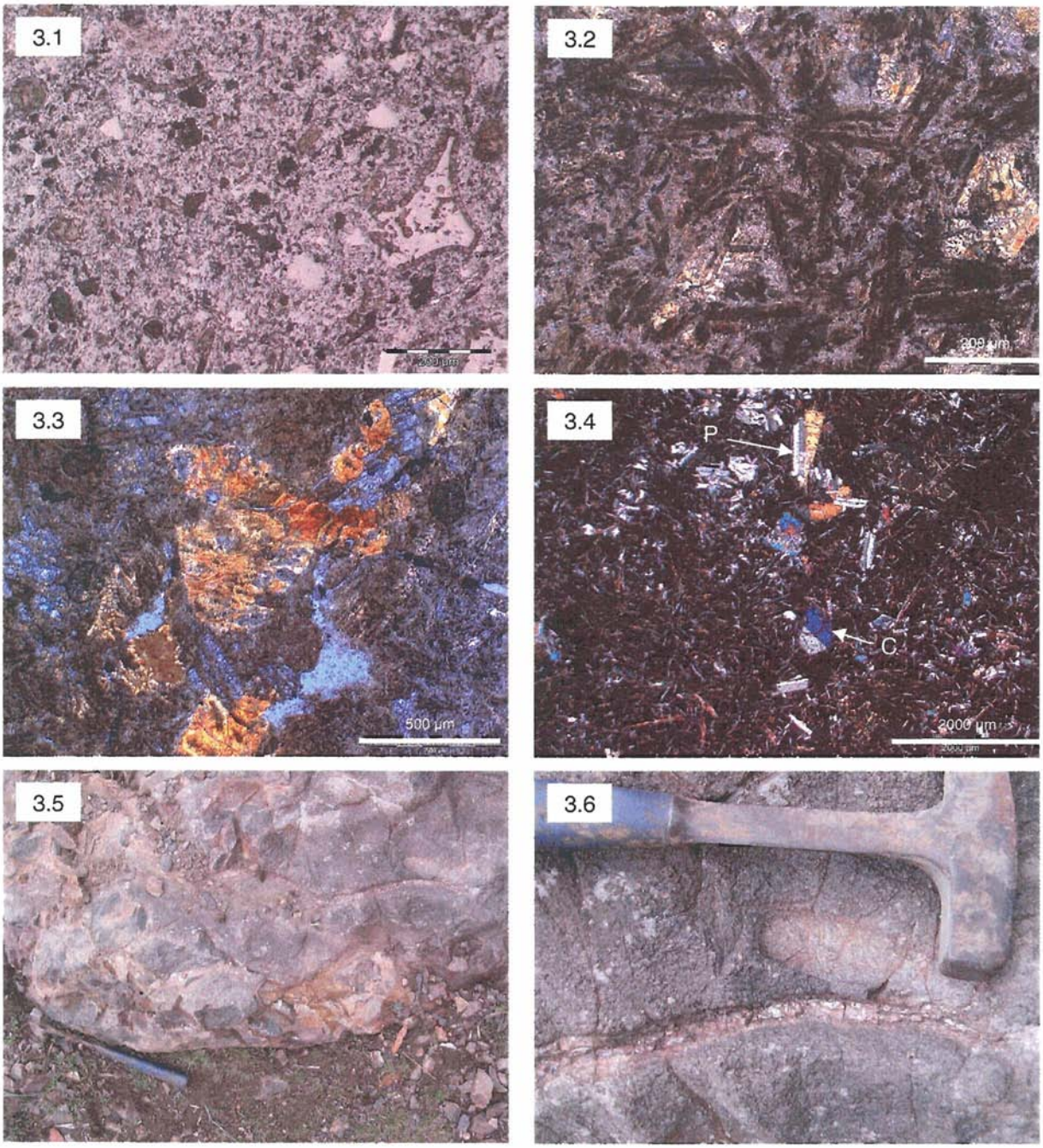

Plate 3.1. Volcanic ash (UTGD 154351) photographed using reflected light, with a rare bubble-wall shard surrounded by an alteration halo. **Plate 3.2.** Clay derived from the weathering of basalt (UTGD 154336). Relict plagioclase needles show up clearly in reflected light, and unaltered clinopyroxene crystals are present. **Plate 3.3.** Alteration of clinopyroxene in basalt to smectite, (cross-polarised light) (UTGD 154336). **Plate 3.4.** Fresh basalt (UTGD 154337) with plagioclase needles and clinopyroxene phenocrysts in a glassy groundmass, (cross-polarised light). **Plate 3.5.** Polygonal form created by radial joints in pillow basalt at Site '' A , Lune River. **Plate 3.6.** Fine grained inter-pillow sediments in basalts at Site ''A'', Lune River.

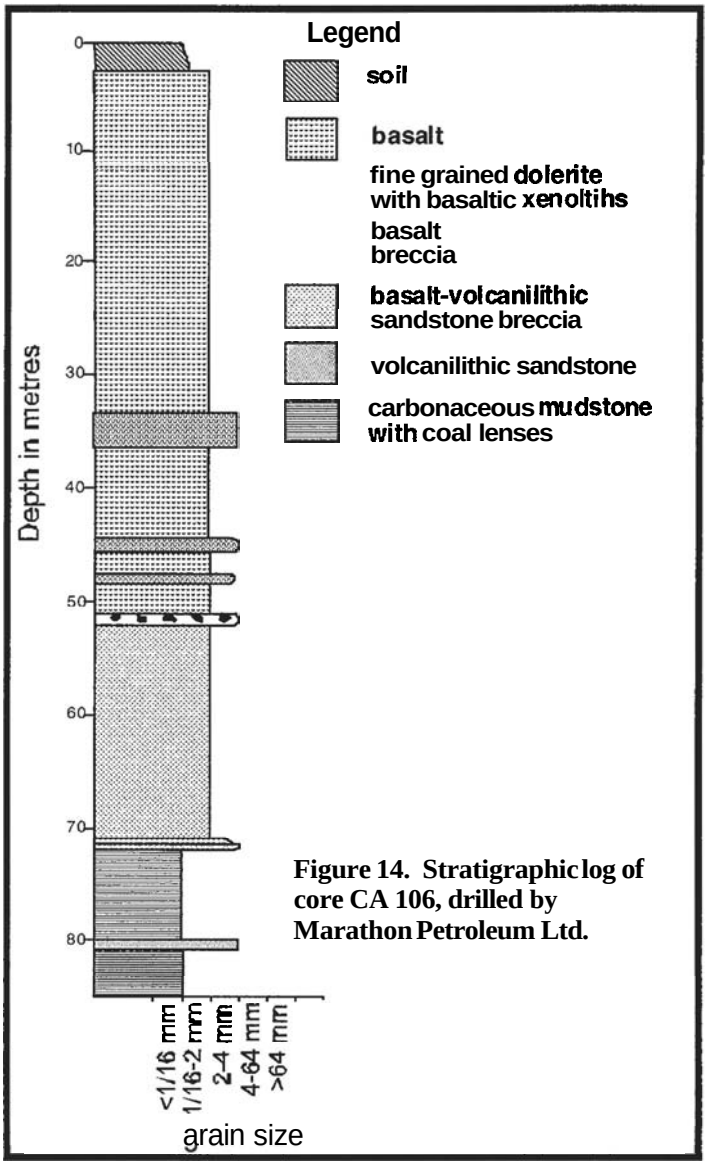

Figure 14. Stratigraphic log of core CA 106, drilled by Marathon Petroleum Ltd.

In 1980, Marathon Petroleum Australia ltd. drilled exploratory wells in search of Triassic coal deposits and the cores are now stored at MRT. One of these wells, CA 106, lies close to the Lune River fossil site. The stratigraphic log from this core (Figure 14) has carbonaceous mudstone from 70 metres to the base of the core. Two thin beds of quartz and crystal-rich volcanilithic sandstone overlay this, and above these, a thick bed of jigsaw-fit texture, intrusive, basalt breccia with a sedimentary matrix occurs, where the basalt intruded into wet volcanilithic sediment. This unit is an intrusive basalt hyaloclastite. The basalt clasts show both thready and curviplanar margins, resulting from quenching of the basalt as it interacted with the wet sediment. A thin bed of basaltic breccia with minimal sedimentary matrix overlies the hyaloclastite. The upper part of the core is basalt, intruded in at least three places by a very fine-grained to glassy basic, igneous rock with no vesicles. The intruding magma is interpreted to be dolerite. Five-ten centimetres of red, basalt-derived soil caps the core. The basalt hyaloclastite proved important in providing geochronological constraints for the timing of the basalt in relation to the volcaniclastic deposits found at the site. Between 51 meters and 71 metres, the volcanilithic matrix of the hyaloclastite (Plate 4.4) is very similar in petrographically and texturally to the sandstone sampled at the fossil site, demonstrating that the basalt erupted into unconsolidated, wet sediment.

The geometry of the basalt flows is similar to that seen in the Tertiary Basalts, especially in northern Tasmania, where they are mostly found along rifts and faults and also in the southeast of the state where they infill parallel graben separated by complex horst structures (Sutherland 1989). In the Lune River region, the basalt is confined to the floor of the graben and is associated with the fault bounding the western side. However, the geochemistry of the basalt is not similar to the Tertiary basalts and is very similar to that of the Jurassic dolerite common in the state. From figure 15, it is clear that the Lune River basalts have an affinity with both the Tasmanian Jurassic dolerite and to the Kirkpatrick Basalts fi-om Victoria Land, Antarctica. They have an arc signature, with low Nb and high Zr abundances, resulting in a high Zr/Nb, while the Tertiary basalts have an intra-plate geochemical signature (Sutherland, 1989) with low Zr/Nb and high Ti/V. The plot axes in figure 15 are fluid immobile element ratios and their values do not reflect changes in abundance resulting fi-om hydrothermal alteration (Pearce and Norry 1979); (Shervais 1982). Furthermore, their immobile nature is supported by the position of the clay derived from the basalt, which still plots within the Kirkpatrick Basalt field.

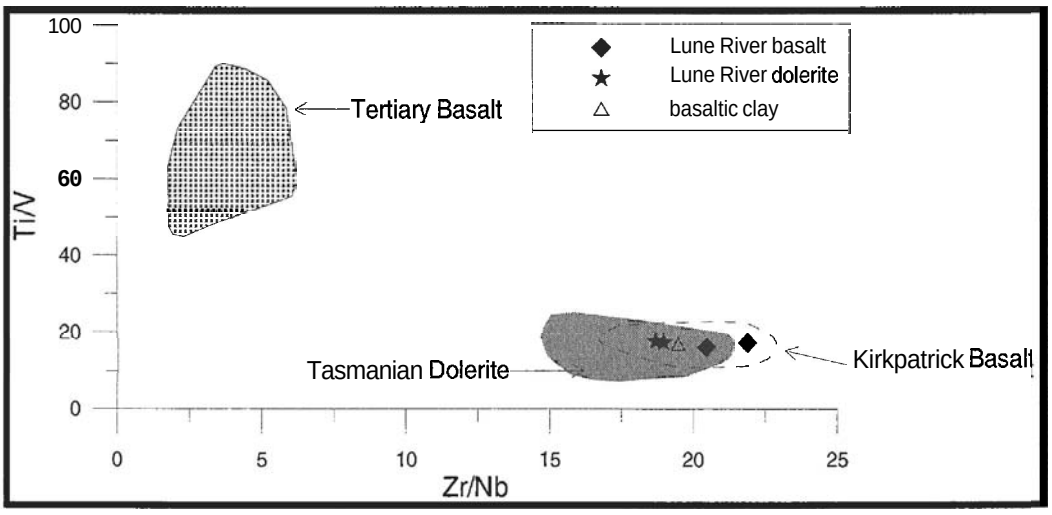

Figure 15. Ti/V versus Zr/Nb plot showing the Tasmanian Dolerite field adapted from Everard, (1987), the Tertiary Basalt field adapted from Sutherland (1989), and the Kirkpatrich Basalt field adapted from Siders and Elliot (1985). The igneous rocks from Lune River, and the clay derived from the weathering of basalt capping the site; clearly lie in the Kirkpatrick Basalt/Tasmanian Dolerite fields.

Clay

The fossils and their host rock underlie three to four metres of fine-grained yellow clay with variable quantities of quartz crystals, some of which are angular, up to lmm, while others are rounded and range in size from 0.5 mm to 2 mm. In hand specimen, it was difficult to determine whether this clay derived from the alteration of ash fall deposits or basalt. However, in thin section, the clay clearly falls into two subgroups, basalt, and volcanic ash examples.

The clay is in two populations; montmorillonite and halloysite, and nontronite and montmorillonite (Figure 16). (Reference spectra for halloysite, nontronite and montmorillonite, as well as an average spectrum for the samples composed of montmorillonite and nontronite, are presented in appendix 9). The top three samples in Figure 16, (UTGD 154347, UTGD 154348 and UTGD 154349), from the top down, represent montrnorillonite with halloysite in roughly an 8:1 ratio. The lower four lines, represent different aspects of samples UTGD 154351 and UTGD 154350, and are composed of montrnorillonite and nontronite, in a 2:1 ratio.

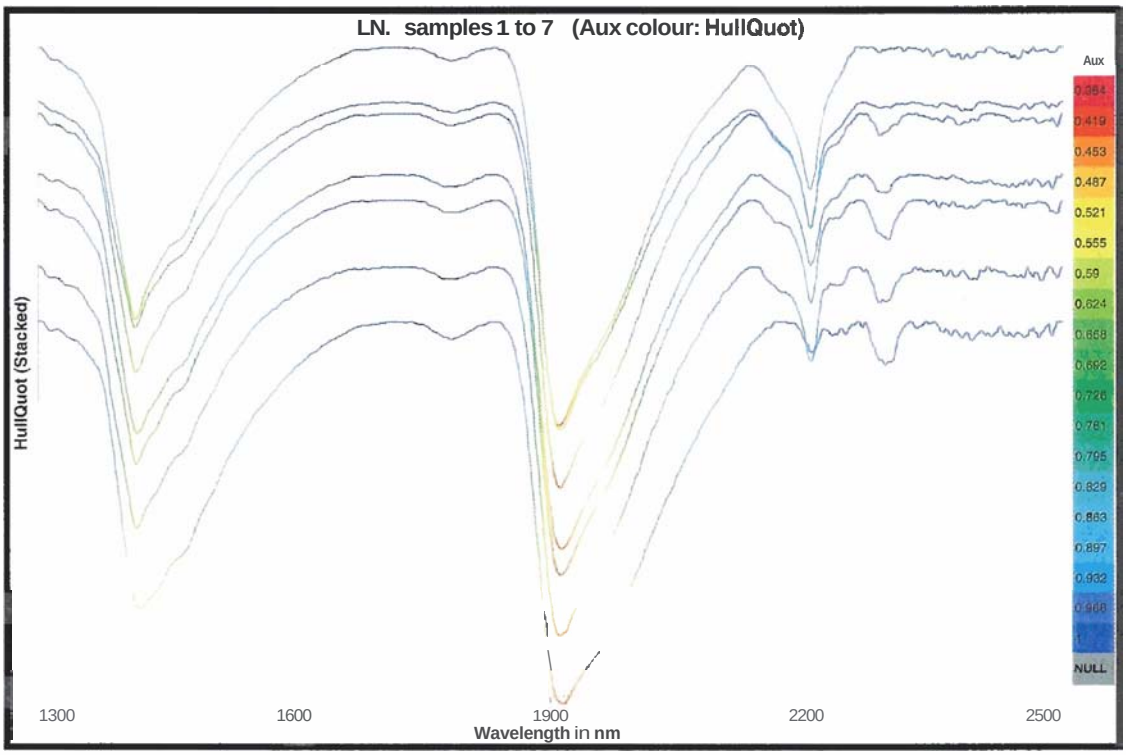

Figure 16. Short wave infrared spectra of seven samples of clay removed from the Lune River fossil site, showing the alteration products resulting from weathering of the original sediments.

Montmorillonite forms by the alteration of eruptive volcanic rocks, usually tuffs and volcanic ash, and by the weathering of basic igneous rocks (Deer et al. 1998). Nontronite also derives from the weathering of basalts and ultra-basics.

Halloysite is a low temperature, hydrated equivalent of kaolinite. It results from the low temperature hydrothermal alteration of feldspars, muscovite, and other Al-rich silicates usually in acid rocks such as granite, rhyolite, and quartz diorite (Deer et al. 1998). Its derivation from feldspar is expressed as:

$$2KAlSi_3O_8 + 3H_2O \rightarrow Al_2Si_2O_5(OH)_4 + 4SiO_2 + 2K(OH) \qquad 1$$

The population of clays containing halloysite and montmorillonite, was derived from the breakdown of the volcaniclastic deposit found at the site, which is rich in feldspars and lithic fragments derived from acidic rocks. The subgroup composed of montmorillonite and nontronite was derived from the breakdown of basalts overlying the site. Samples correlate spatially with this supposition. Those taken from lower in the stratigraphic log have altered to halloysite while those from higher in the column have relict basaltic textures, including iron-filled vesicles (Plate 4.5), and are altered to nontronite.

Dolerite

Although dolerite does not occur at the fossil site except as float, it outcrops adjacent to the site, and forms the hill flanking the site. It is holocrystalline and fine to medium grained, with platy jointing. Tabular feldspar crystals, with some decrepitated cores in a few examples, and clinopyroxene, dominate composition. There is no evidence at the site of a contact aureole around the dolerite where it intruded the volcanilithic sediments underlying the basalt. However, the stratigraphic log for core CA 106 shows that the dolerite intruded the basalt. The dolerite at the contact between the two is very fine-grained, and glassy. Margins of the basalt show embayrnent by intruding magma, and angular rip-up clasts of basalt lie within the chilled, dolerite (Plate 4.6). The basalt itself has a baked margin 7-10 mm wide.

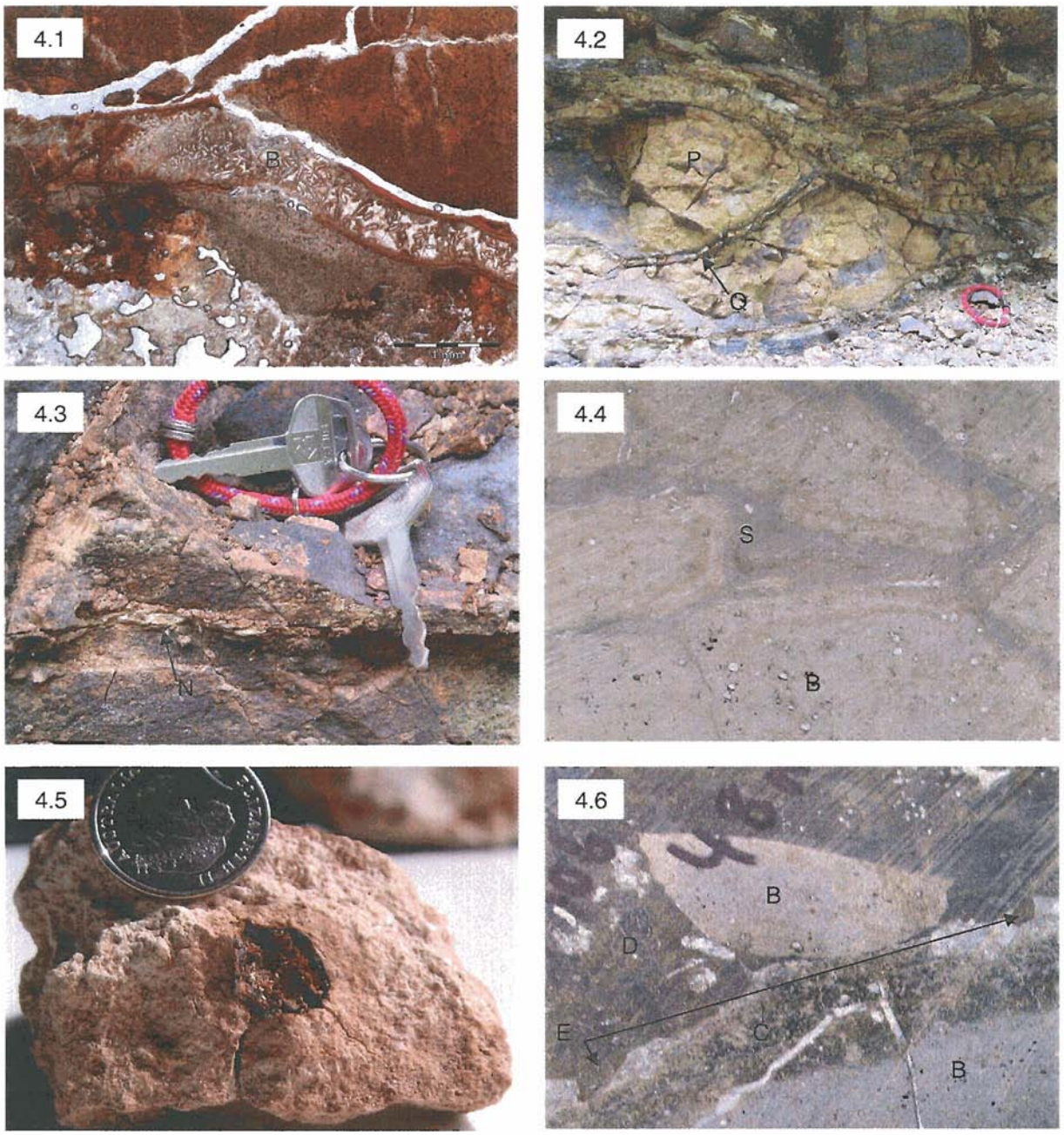

Plate 4.1. Micrograph showing the disturbance of ash by the emplacement of the pillow basalt (UTGD 154338), Site "A", Lune River, (cross-polarised light). **Plate 4.2.** Quartz veins replacing the inter-pillow sediments at Site "B", Lune River. Key for scale. **Plate 4.3.** Montmorillonite veins replacing inter-pillow sediments at Site "B", Lune River. Key for scale. **Plate** 4.4. Hyaloclastic texture resulting fi-om the interaction between erupting basalt and the wet sediments. From drill core CA106 (UTGD 154340). B indicates basalt, S indicates sandstone. **Plate** 4.5. Relict vesicle, now lined with iron oxides, fi-om clay derived fi-om the weathering of basalt. **Plate** 4.6. Dolerite intruding basalt. Note the basaltic rip-up clast (BC) included in the chilled dolerite (D), and the embayed margin (E) of the basalt (B). From drill core CA 106 (UTGD 154341).

Discussion

The volcaniclastic deposits from Lune River show remarkable similarities to the pyroclastic deposits of the Hanson Formation, Trans-Antarctic Mountains, Antarctica. Both contain felsic, immature volcanic crystals, 50-60 % accidental lithic fragments, and grains derived from the underlying strata; the basement rocks and Triassic sediments (Hanson and Elliot, 1996). Characteristics of the volcanigenic deposit indicate derivation from a hydrovolcanic eruption. The zircons and the volcanic quartz in the sediments likely derive from this eruption, and the age of the zircons (182 +/- 4 Ma) may record the timing of this event.

The Lune River basalt correlates geochemically with the Kirkpatrick Basalts, Antarctica. It shares the distinct arc-like signatures of these Jurassic flood basalts. Even after alteration, it still lies within the Kirkpatrick Basalt field defined by plotting ZR/Ni versus Ti/V. It erupted through the volcanilithic sandstone, creating a hyaloclastite texture, and leaving an imprint of its geochemical signature, as it interacted with the wet sediment. Contact with the basalt may account for the baked, cherty, fine-grained ash that occurs between the sediments and the basalt at the site. Much of the basalt erupted directly into water, creating pillow textures. Where these are associated with ash deposits, it is clear that the ash was deposited prior to the eruption of the basalt. Field evidence, i.e. the basaltic rip-up clast included in the glassy dolerite margin, and the embayment along the margin of the basalt, suggests that the basalt was in place prior to the intrusion of the dolerite or that these events were geologically contemporaneous

Recent weathering has produced the deep clay profile evident at Lune River, and iron oxides on the rims of clasts. The sand grains in the volcanilithic sandstone have quartz overgrowths that have some similarities with the sub-Tertiary basalt silicified sands (silcretes) mentioned by Sharples (1996). The latter feature results in part from the movement of siliceous hydrothermal fluids. The source of the silica may be the basaltic cap leaching during weathering. However, it may also derive from the weathering of the volcanigenic sediments. It is likely that in the future, some of the sediment and rock on the floor of the Lune River Graben will be recognised as resulting from an early mid-Jurassic phreatic event.

Source rocks

Potential source rocks at Lune River are the fossiliferous, fine-grained volcanic ash associated with many of the fossils, and the medium-grained volcanilithic sandstone. Samples of both were sent to independent laboratories for analysis of vitrinite reflectance and maceral description. Samples of the volcanic ash removed from directly adjacent to the fossil tree were analysed for total organic carbon. Both the VR and maceral data contained herein must be treated with a degree of caution. Statistically, the data are weak due to the extremely low amount of organic matter.

Thermal Alteration Index

Thermal Alteration Index (TAI) defines the organic material, typically palynomorphs, based on physical appearance, into four categories. The percentages of the various types can be calibrated with the colour scale ranging from 1-5 (Figure 17). A TAI of 2.5-3 means that kerogen is at the oil generation stage, or within the oil window.

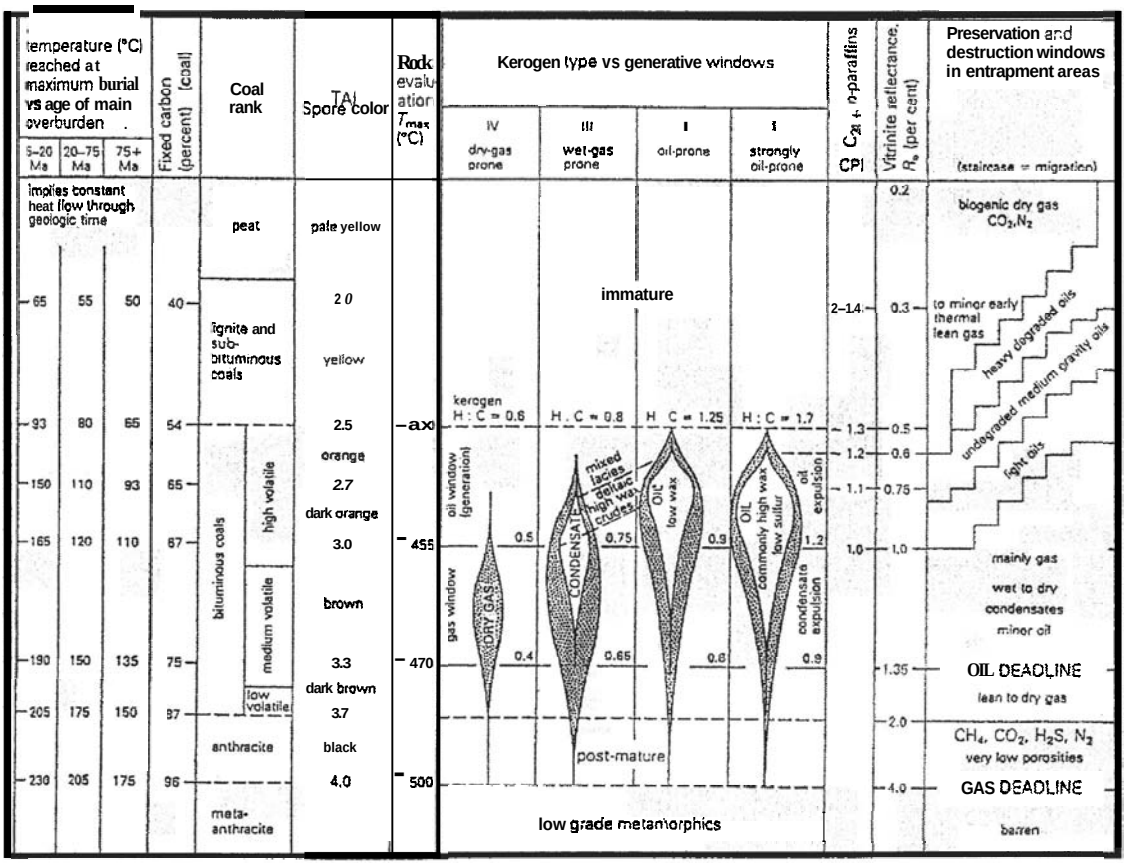

Figure 17. Maturation range chart. From North, 1984

The only palynomorph from Lune River reliably identified as Jurassic came from sample UTGD 154353. It is brown to dark brown, and has a TAI of 3-3.3. This indicates that the sediments passed through the oil window and are over-mature for oil generation. However, based on this test, organic components of the sediments may still be within the gas window.

Total Organic Carbon

Total Organic Carbon reflects the level of organic material present in the rock. Two samples, UTGD 154343 and UTGD 154342, sent for analysis came back with negative results.

UTGD 154343	%N-ND	%C-ND	%H-1.36	%S-ND
UTGD 154342	%N - 0.01	%C - 0.05	%H - 0.34	%S - 0.06

ND is not detected or below 0.01%

However, samples sent to Alan Cook, from Keiraville Consultants, proved to have a variable amount of organic carbon, from very little to 20 %. The normal TOC required for oil and gas generation is 1 % but potential source rocks typically contain 1-5 % organic carbon.

Maceral Description

The original organic-rich lithologies contained telovitrinite and cutinite. In general, the organic matter was mainly diffuse and structureless, with very low amounts of vitrinitic, inertinite and algal matter. Two occurrences of textinite, a brown coal maceral, were noted in sample UTGD 154353 (Plate 5.1). The maceral is dark brown-black and the cell structure is still intact.

The intraclasts contain some relatively large phytoclasts. The vitrinite illustrated in Plates 5.2 and 5.3, is present as telovitrinite and shows transition to mineralised vitrinite at the margins. Liptinite is sometimes associated with the vitrinite. Some occurrences show well-preserved morphologies (Plate 5.4, upper part). Other occurrences are less distinct but appear to represent cutinite. In the lower part of Plate 5.4, some of the entities could represent sporinite.

(Maceral percentages and charts of organic matter are provided in Appendix 4).

UV Fluorescence

Vitrinite and associated cutinite fluorescence intensity is relatively low and the fluorescence colour is dull orange (Plate 5.5). However, two samples, UTGD 154354 and UTGD 154353, contain very rare occurrences of algal bodies. These fluoresced with a dull yellow colour suggesting a maturity of VR/e 0.43-0.65 (Plate 5.6). In some samples, the vitrinite is associated with dull orange fluorescing liptinite some of which is cutinite. The vitrinite also occurs in smaller intraclasts, not associated with liptinite. The liptinite shows dull orange fluorescence colours and low fluorescence intensity in relation to the vitrinite reflectance values obtained.

Vitrinite Reflectance

Vitrinite reflectance, VR, is the most widely used method of determining the maturity of sediments, thus indicating the potential of the sediments for oil and gas production. Vitrinite is a maceral, or component, of carbonaceous material that is highly reflective. Analysis of vitrinite reflectance defines the level of maturity of a sample, and displays a strong depth, rather than time dependency. Reflectance ranges from 0.2-4.0 % R_O and the oil window lies between 0.6-1.3 % R_O (Figure 18).

Initial examination of the samples showed what appeared to be carbonaceous flecks. However, closer inspection showed these to be composed mainly of diffuse, amorphous organic matter and not vitrinitic material. The quality of the rare amount of vitrinite was poor and difficult to identify due to very small particle size and oxidation features. One sample, UTGD 154353, had ten vitrinite reflectance measurements based on telocollinite, with a lower identifiable population based on low reflecting vitrinite (desmocollinite). Vitrinite measured in sample UTGD 154355 exhibited heavy oxidation features. (See appendix 4 for raw data and histograms).

Data from samples UTGD 154354 and UTGD 154353 gave the most reliable VR data and furthermore, agree with fluorescence colours observed from algae. The maturity of the volcanolithic sandstone, sample UTGD 154353 (VR/m 0.54-0.64), is slightly

lower than the maturity of the underlying volcanic ash, UTGD 154354 (VR/m 0.63-0.77)[1].

Reservoir and Seal

A possible reservoir rock at Lune River may be the volcanilithic sandstone. However, while this immature sandstone may have had a high primary porosity, it now has a clay matrix dominated by montmorillonite from the alteration of volcanic components. Sorting is variable and secondary quartz in fills much of the remaining pore space, reducing the overall porosity and permeability of the unit. This rock type makes only a poor to moderate reservoir. However, the fine grained, non-vesicular basalt overlying the sandstone would provide an excellent seal.

[1] Keiraville Consultants provided the upper R_O range in both samples, while Mirror Image provided the more conservative R_O estimate.

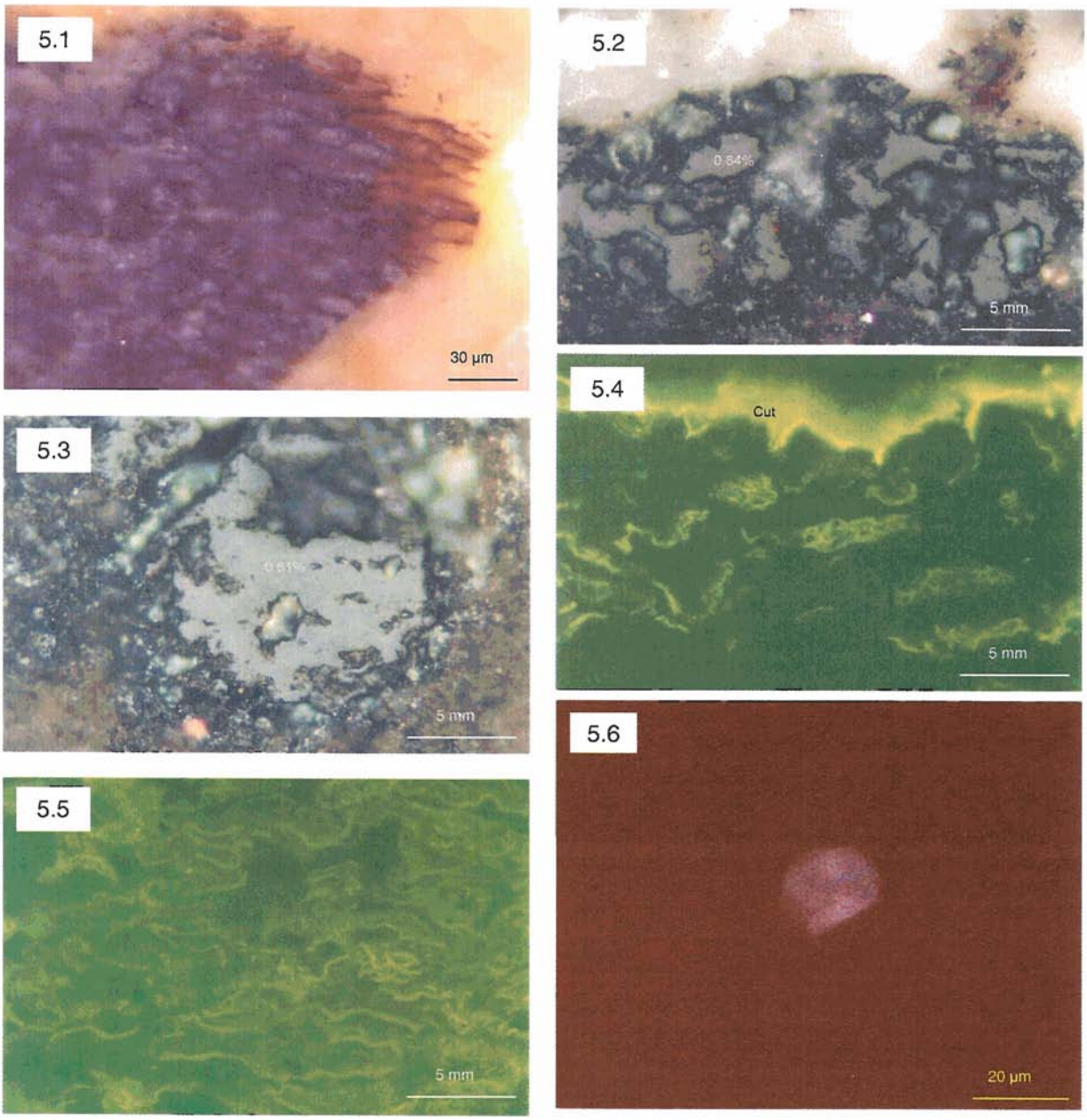

Plate 5.1. Textinite, a brown coal maceral (UTGD 154353). Note that the structure is not flattened. **Plate 5.2.** Vitrinite present as telovitrinite (UTGD 154333), with halo of mineralised vitrinite. $R_O = 0.54$. **Plate 5.3.** Large telovitrinite maceral with alteration halo of mineralised vitrinite (UTGD 154355). RO=0.51. **Plate 5.4.** (UTGD 154333). The upper section of the micrograph illustrates well preserved liptinite associated with vitrinite, and some examples of cutinite (Cut), while the lower section of the micrograph contains examples of sporinite. **Plate 5.5.** Vitrinite and cutinite identified by their dull orange florescence under ultra-violet light (UTGD 154333). **Plate** 5.6. One of the rare algal bodies (UTGD 154354), which fluoresce to a dull yellow colour.

Plate 5.1-5.5 curtesy of Dr. Allan Cook. Kieraville Konsultants, 2004. Plate 5.6 curtesy of Wayne Knowles, Mirror lmage, 2004

Discussion

The ranges of vitrinite reflectance found are relatively high. This is partly due to a number of low values that were measured on small vitrinite grains. These represent more strongly mineralised tissues. The variation in values is probably associated with the proportion of low values found, and a mean ranging from 0.54 % to 0.77 % is representative of the site.

If the maturation resulted from regional coalification associated with deep burial, a maximum cover of about 2000 m can be inferred assuming average geothermal gradients. This inference implies that deposition of Jurassic sediments was originally much more widespread than the graben within which they are now preserved. It also has implications for the extent of post-Jurassic uplift and erosion. However, contact alteration from nearby intrusions is a likely cause of the high vitrinite reflectance. A range of temperature and time combinations could produce the coalification found. An episode of mild contact alteration is consistent with the weak fluorescence intensity and red shift found for the liptinite (Cook, written communication).

The TAI and the R_O of the sediments both indicate that they reached a maturation level within the zone of oil generation. However, the TAI, at 3-3.3, indicates that organic material is approaching the transition from mature for oil, to over-mature, and metamorphosed, while the R_O, between 0.54-0.77, indicates that the organic material is just entering the oil window. It is probable that the coalification level is largely due to contact alteration. If the maturation is due to regional coalification resulting from burial, a large part of the sedimentary overburden has eroded, taking with it any organic material required for oil generation

Due to silicification of organic material, the TOC is variable to very low. The site is therefore unlikely be a potential hydrocarbon source. The site has a good seal in the overlying basalt, but lacks a trap. Reactivation of regional faults in the Tertiary means any gas generated since the Jurassic may have escaped. Alternative locations in the Tasmania Basin, where the source rock has not been silicified, and where a likely trap has developed and been maintained, may potentially retain hydrocarbons.

Chapter 5 Description, Identification and Interpretation of the Plants Found at Lune River

The plants discussed in this chapter were preserved via cellular replacement by microcrystalline quartz. The assemblage includes a diverse range of plants, from a fallen Araucarian tree, to a number of gymnosperms and pteridophytes, which were found closely associated with it. The fossils are immediately encased in fine-grained fossiliferous tuff, and are generally confined to the unit of weathered, volcanilithic sandstone. Phylogenetic relationships amongst some species of the Lune River assemblage led Tidwell et al. (1987) to interpret the age of the fossil site to be Late Jurassic-Early Cretaceous. The location of each of the fossils at the site has been carefully surveyed (Appendix 5) and their identification is presented in Table 2, and discussed below.

Table 2. Classification of plant fossils removed from the fossil site at Lune River

Division	Class	Order	Family	Genus	Species
Pinophyta	Pinopsida	Pinales	Araucariaceae	*Agathis*	
Pinophyta		Pteridospermales		***Pachypteris***	**cf. *indica***
Pinophyta	Cycadopsida	Bennettitales	Bennettitaceae	*Otozamites*	
Pteridophyta	Polypodiopsida	Osmundales	Guaireaceae	*Lunea*	*jonesii*
Pteridophyta	Polypodiopsida	Osmundales	Osmundaceae	*Osmundacaulis*	*pruchnickii*
Pteridophyta	Polypodiopsida	Osmundales	Osmundaceae	*Osmundacaulis*	*nerii*
Pteridophyta	Polypodiopsida	Filicales (Polypodiales)	Matoniaceae	*Tasmanopteris*	*richmondii*
Pteridophyta	Polypodiopsida	Filicales (Polypodiales)		*Cladophebis*	*indica*
Pteridophyta	Equisetopsida	Equisetales	Equisetaceae		

Description and Identification

Division Pinophyta

Araucariaceae

Material UTGD 154358, UTGD 154357, UTGD 154356, UTGD 154359.
The trunk of the tree lies down-slope, with roots pointing skywards (Plate 6.1), suggesting it fell before it was preserved, and is not in growth position.

The base of the tree has a radius in excess of 120 cm. The buttress of the trunk and adjacent roots are lobed. Annual rings are clearly visible on the trunk, which extends for 7 metres before it crowns, or begins to branch. The exposed section of tree reaches 12 metres, but continues under ground beyond that, so the full length of the tree is unknown. The trunk is fragmented into segments (Plate 6.2). The branches appear to be paired and have a "Y"-shaped form; the angle of bifurcation is 12°. Where the roots are exposed in cross section, large fractures, in filled with opaline silica are clear (Plate 6.3). The outside of the trunk has trace amounts of bark intact and is texturally smooth with minor evidence of abrasion.

In radial longitudinal section, the rays are visible in a "brick-like" arrangement, with axial tracheids and uniseriate pit apertures (Plate 6.4). The axial tracheids are ~ 40 µm wide. The pit apertures are 20 pm across and 25 µm high. The rays are 30-40 µm wide. Alignment of the pit apertures relative to wall of the axial tracheids is 45-50" (Plate 6.5). Pits occur in rows of two but sometimes three.

Relative thickening of tracheids leads to the appearance of annual rings in trees. In cross section, distinct banding is visible (Plate 7.1). Earlywood, produced early in a growing season is relatively wide, 40-50 µm, with minimal lignin in the cell walls, which appear hexagonal in transverse section. In latewood, produced near the end of a growing season, the tracheids are narrower, 20-30 pm, and have thicker walls. Earlywood cells have collapsed where they occur adjacent to previous season's latewood cells.

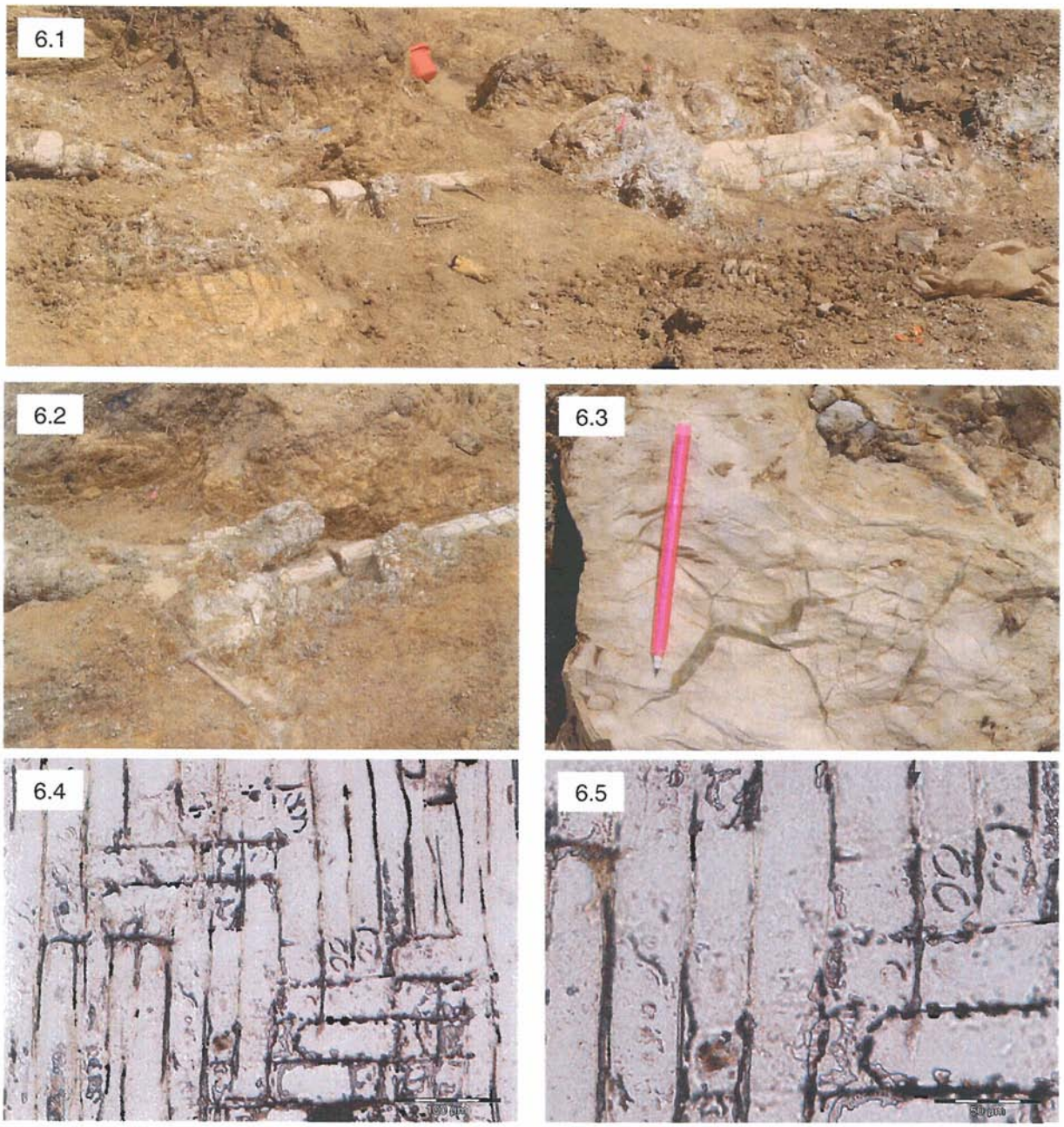

Plate 6.1. The Lune River fossil site with the *Agathis* sp. dominating the view. Note the root bundle to the right of the field of view. Branching begins left of centre and the branches continue beyond the left margin of the picture. Glove in foreground for scale. **Plate 6.2.** Fractures perpendicular to the grain of the *Agathis* trunk. Pick for scale. **Plate 6.3.** Fractures parallel to the grain of the trunk, in-filled with opaline silica. **Plate** 6.4. Radial longitudinal section of the *Agathis* trunk (UTGD 154356) (x 20). The rays are visible in a "brick-like" arrangement, with axial tracheids and uniseriate pit apertures, in groups of two and three. **Plate** 6.5. Radial longitudinal section of the *Agathis* trunk (UTGD 154356) (x 40). Alignment of pit apertures relative to the tracheid walls is 45-50°.

The width of a single ring is variable, from 0.5 mm up to 20 mm. The ratio of earlywood to whole ring is on average 9:1. While many rings are homogenous and wide, with regular tightly packed earlywood cells, others are narrow, with a higher ratio of latewood to earlywood, sometimes 1:4, or 3:7. These denser rings demonstrate a higher occurrence of false rings[2], and the fragmentation of cellular structure gives them a ragged appearance.

In transverse section, tracheids, approximately 40 μm wide are packed longitudinally with rays 20 μm by 40 pm, stacked in rows of 5-10 but usually six (Plate 7.2). Annular rings are preserved on some tracheids.

A thin branch from the site has a spongy parenchymatous medulla, or pith, which is 10 mm in diameter (Plate 7.3). Fibre bundles are scattered throughout the pith, although they are concentrated near the endodermis. Uniseriate rays radiate from pith towards margin. Two-three minor growth rings are present before rays interdigitate into cambium. Only part of the mantle and cambium are still present. The presence of ray tracheids and the proportionally large pith relative to the width of the stem indicates that this is an araucarian branch from the silicified tree found at the site. It represents two–three years of growth.

[2] False rings form in response to adverse environmental conditions, particularly when water supply is limited. Cell expansion is prevented and a band of very small cells results, which mimics a normal end-of-season boundary (Creber & Chaloner, 1984)

The most reliable method of wood identification is the arrangement of axial tracheids[3] and rays seen in radial longitudinal section. The arrangement of tracheids and rays in the Lune River tree are distinct. When compared with Figure 18, the tree is assignable to the family Araucariaceae.

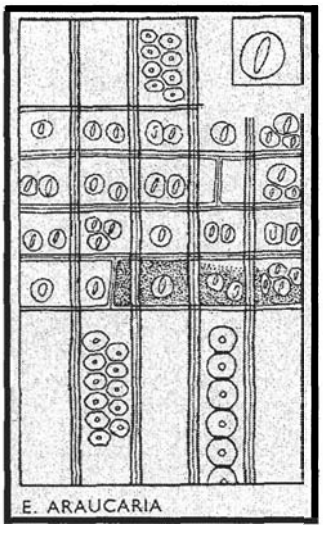

There are two major genera within the family, *Araucaria* and *Agathis*. They are not easily distinguishable from each other, but they differ from other softwoods in that they have alternately arranged pitting of their axial tracheids[4]. In *Agathis* these are sometimes in up to four rows, but more usually, in both genera, they occur in not more than two or three rows.

Figure 18. Pit aperture characteristics of Araucaria. This example is A. *angustifolia*, but the arrangement is typical of the entire family. From Wilson and White (1986).

In terms of form and size of the tree, a modern analogue may be similar to *Agathis australis* (Plate 7.4). The Lune River tree is therefore assigned to this genus. *Agathis jurassica* was a common species of the genus during the Jurassic, and foliage assigned to this species has been recovered from New South Wales (White 1981). Assignment to species level is impossible based on evidence preserved at Lune River, so assignment to this species is based tentatively on ancient distribution.

[3] **A** tracheid is an elongate conductive cell with moderately lignified walls, and pitted side and end walls. When mature, the protoplast breaks down and only non-living cell wall remains (Wilson and White, 1986). Tracheids dominate axial elements in conifers and most other gymnosperms.

[4] Pits in tracheids form the major pathway for water and solutes from one cell to another. They occur in the region known as the primary pit field, where the primary wall of the cell is thinner than usual, and the secondary wall is absent. **A** cavity therefore develops in the secondary wall. Pits are usually opposite to a pit in an adjacent cell so that only a thin membrane, formed by the middle lamella and the thin primary cell walls, divides the two cells.

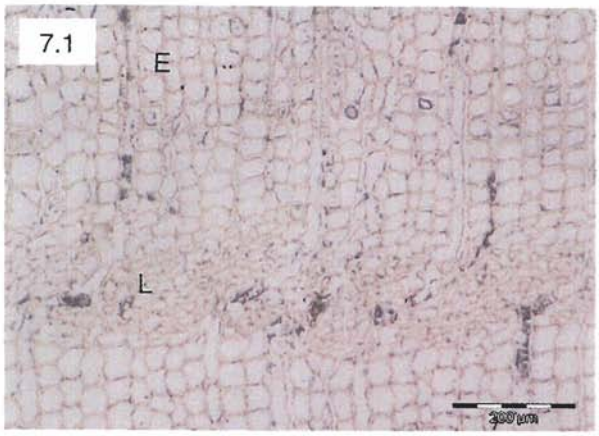

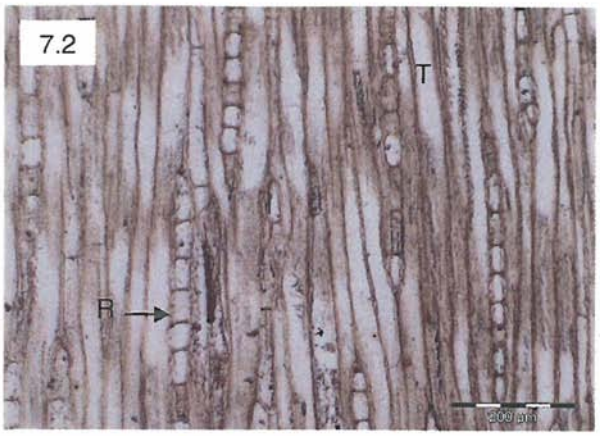

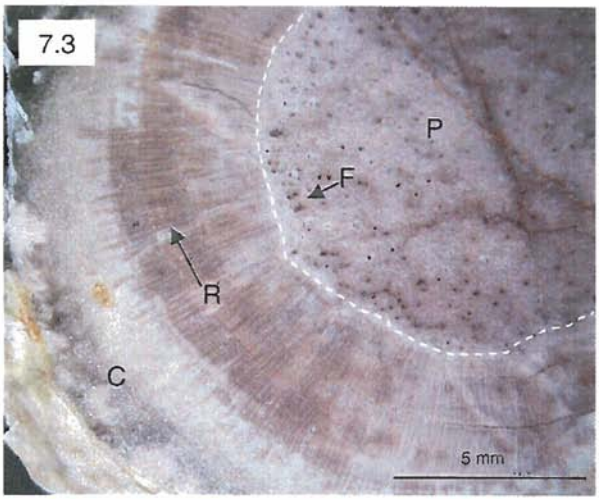

Plate 7.1. Cross-section of the ***Agathis*** trunk, with early season growth (E) top and bottom of the micrograph, and late season growth (L) in the bottom third of the picture. Plane polarised light. **Plate 7.2.** Transverse section of the trunk. Ray cells (R) in stacks of 5-10 cells, but typically occur in stacks of 6. Tracheids indicated **Plate 7.3.** ***Agathis*** branch ***(UTGD*** 154359). P=pith, F=fibre bundles, R=uniseriate ray cells, C=cambium. Note the "stars" of silica in the outer cambium. **Plate 7.4.** *Agathis* ***australis,*** the New Zealand Kauri, is a likely modern analogue for the tree found at Line River in terms of size, growth morphology and habitat.

Other gymnosperms

Description *Pachypteris* sp. cf. *indica*. (Tidwell et al. 1987).
Material UTGD 154360.
The example of P. cf. *indica* has a fertile, bipinnate macrophyll (leaf), with a thick rachis, lmm wide, and a very faint median groove (Plate 8.1). The pinnules are short-oblanceolate, or ovate in outline; 10-15 mm long and 5-7 mm wide. They arise from the rachis at 55°. The pinnule apices are blunt to obtuse. Simple or once forked veins arise from the pinnule midrib.

Cuticular and epidermal features are not preserved and no stomata were observed. Due to the incomplete nature of the specimen, it is difficult to identify the species of this leaf. However, it is sufficiently similar to the samples described by (Tidwell et al. 1987) to assign it to *Pachypteris* sp. cf *indica.*

Description *Otozamites* sp. (Tidwell, Kim et al. 1987).
Material UTGD 154361.
The sterile pinnules in this specimen are broadly falcate, 5 x 3 mm, with an expanded acroscopic (facing the side toward the apex) basal angle (Plate 8.2). The upper margins are concave, while the lower margins are convex. The apex of each pinnule is obtuse-subacute. Pinnules overlap and are sub-alternate. They are attached to a rachis, which is 0.5-1 mm wide, by the lower portion of the inner edge of the pinna base, at a right angle. The upper portion of pinna base is fi-ee. Five veins originate from the basal attachment; the inner three fork twice, then radiate towards the acroscopic angle and margins; the outer two fork twice and end at the distal basiscopic margin.

One specimen was used for identification, and consists of an isolated fragment of frond with pinnules, but the apex and base of the frond are absent. Cuticular and epidermal features are not preserved. Stomata were not observed on either surface of the leaf. The species is characterised by typical 'gull-wing' shaped pinnae and a well-defined fi-ee acroscopic angle (Tidwell, Kim et al. 1987), making it possible to assign it to *Otozamites* sp.

Incertae sedis

Material UTGD 154362.

No pith is present and there are four growth rings (Plate 8.3). Uniseriate rays are present. The mantle is 10 mm in diameter. A cambium is present, with a hypodermis beneath it. There are two-three layers of large parenchyma cells between the mantle and the hypodermis.

The description is based on one gymnosperm fragment, 16 mm in diameter and 45 mm long, set in very fine-grained silicified, fossiliferous volcanic ash, with abundant pteridophytic debris present. Only a partial cambium is preserved. Assignment to generic gymnosperm (probably conifer) is based on the organised cell structure. All the tree ferns have complex trunks (caudices), while this example has tracheids arranged in perfect radial pattern, with symmetrical rays.

Incertae sedis Parallel-veined foliage

Material UTGD 154363.

The leaf is ~10mm wide. Length is unknown as the base and apex are unavailable. The leaf tapers slightly, possibly towards apex. The margin is entire. Venation is parallel (Plate 8.4), possibly dichotomous (forking to produce two veins of the same size). Indistinct linear striations occur between veins.

The specimen may resemble detached cycadalean or bennettitalean pinnules (McLoughlin and Drinnan 1995), which are common components in laterally equivalent strata in other locations, both in Australia and globally.

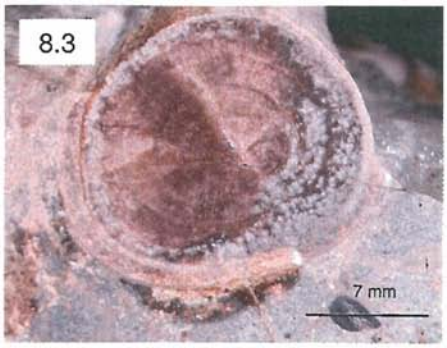

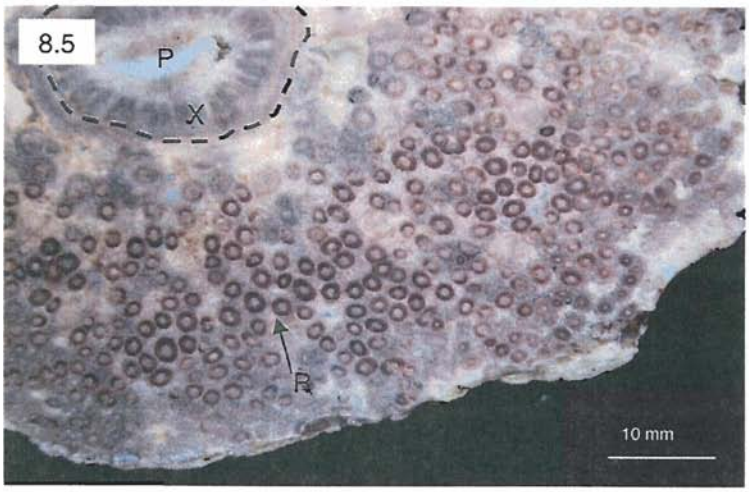

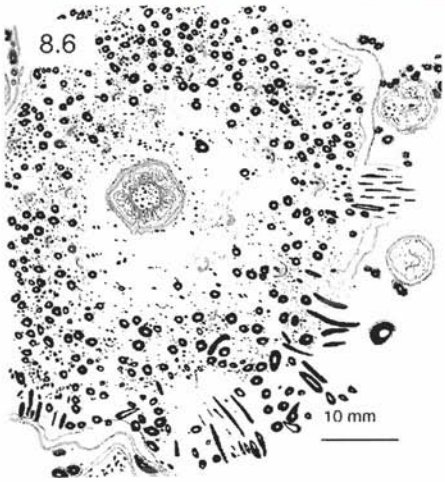

Plate 8.1. Fertile macrophyll of *Pacypteris* cf *indica*. **Plate 8.2.** Sterile macrophyll of *Otozamites* sp. **Plate 8.3.** Branch from a gymnosperm with uncertain affinities. Note the lack of pith, and the remnant of the cambium on the left hand side of the specimen. **Plate 8.4.** Parallel veins foliage impression of uncertain affinity. It may represent cycadalean or bennettitalean foliage. **Plate 8.5.** Transverse section of *Lunea jonesii*. P=pith, now replaced by opaline silica. X= concentrically arranged xylem strands. R=root traces. **Plate** 8.6. Transverse section of ***Lunea jonesii*** stem, roots and petioles. Stippled area=cells around pith and in cortex. Black rings and elongate zones=roots. Dark areas=sclerenchyma. Double lines mark epidermis. From Tidwell (1991).

Division Pteridophyta

Description *Lunea jonesii* (Tidwell 1991).

Material UTGD 154364, UTGD 154365, UTGD 154356.

Both a cortex and mantle are present. The inner cortex is a rounded–oval, dictyostele[5], 12 mm across, containing pith parenchyma, and surrounded by concentrically arranged xylem cylinders interspersed with packages of parenchymatous tissue (Plate 8.5). The phloem and pericycle form the outer rim of the circle of vascular tissue. An endodermis with an outer layer of thick walled cells, 130 µm across, encloses the stele. The outer cortex contains polygonal cells of rounded fibre bundles, and root traces. Two to three layers of cells comprise the epidermis, marking the boundary between the cortex and the mantle. Indistinct petioles or leaf traces occur in the mantle, with a partial Ω shape evident. Roots occur throughout both the cortex and the mantle. These are typically 1 mm in diameter, and contain a central protostele of parenchyma cells, and sclerotic outer cortex.

Characteristic anatomical features include abundant, small vertical roots throughout the cortex and mantle (Plate 8.6), and a homogenous outer cortex. Leaf traces are typically characterised by distinctive Ω shape (Tidwell 1991), but these are not well enough preserved for identification based on this character. Assignment to species level is based on form and abundance of root traces

Description *Osmundacaulis nerii* (Tidwell and Jones 1987)

Material UTGD 154368

The stem is 25 mm in diameter, surrounded by a mantle of adhering, overlapping adventitious roots (Plate 9.1). The stele is ectophloic[6] and dictyostelic, and is 15 mm across. The xylem cylinder has 30 xylem strands. The pith is 2 mm wide and contains thin-walled parenchyma cells, although sclerenchyma occurs in the outer pith region, bordering the root traces and leaf gaps. Leaf traces are "C"-shaped, with recurved tips, and are associated with sclerenchymatous stipular wings.

---

[5] Stele refers to the arrangement of vascular tissue in a stem, and a dictyostele is a stele in which leaf gaps are present and occur frequently enough to overlap (Sporne, K. R. (1966). The morphology of Pteridophytes. London, Hutchinson & Co Ltd.

[6] An ectoploic stele has phloem external to the circumference of the stele.

Pith and mantle are both preserved well enough to enable diagnosis based on the number of xylem strands in the xylem cylinder, size and homogeneity of the pith (Plate 9.2), and the overlapping petiole traces (Tidwell and Pigg 1993).

Description *Osmundacaulis pruchnikii* (Tidwell and Pigg 1993)
Material UTGD 154367.
The stem is surrounded by stipulated petiole bases and adventitious roots (Plate 9.3). The stele is dictyostelic, and 15 x 17 mm. The xylem cylinder contains 55 fused and single xylem strands. The pith is 7 mm across, and mostly parenchymatous, although small clusters of sclerenchyma and tracheids are present. Phloem is both internal and external to the central stele. An inner and outer endodermis and epidermis are present. The inner cortex contains parenchyma and sclerenchyma, while the outer cortex is homogenous, with only sclerenchymatous cells. The cortex contains "C"-shaped leaf traces that expand near their tips and are thinner in the middle. No sclerenchyma occurs in the leaf gaps.

Diagnostic features include the number of xylem strands in the xylem cylinder, and the lack of sclerenchymatous stipular wings on the petioles (Plate 9.4). These characters, defined by Tidwell and Jones (1987), make it possible to assign the specimen to the species *Osmundacaulis neriii.*

Description *Tasmanopteris richmondii* (Tidwell and Skog 1992).
Material UTGD 154369.
The specimen has a polycyclic siphonostele, consisting of four annular steles surrounding a central core, and with pith at its centre (Plate 9.5). Each annular stele is separated by parenchymatous ground tissue. The central core and stele is 0.15 mm in diameter (Plate 9.6), with xylem forming from a central point outwards. Xylem in the inner ring is has metaxylem developed both internal and external to the protoxylem. Xylem in the outer rings formed from the periphery towards the centre. The pericycle and endodermis enclose each ring of the xylem. Secretory cells occur in the parenchyma tissue of the cortices outside the outer annular steles, but are not associated with the innermost stele or protostele. These cells are hollow, ~170 μm in diameter, and encircled by 1-2 layers of thin walled cells.

The outermost portion of stem is not preserved, so the actual number of annular steles is unknown. Local flattening of cells is apparent in the outer annular stele. The purpose of secretory cells and the nature of the substances they may have secreted are unknown (Tidwell and Skog 1992). The characteristic polycyclic siphonostele and the presence of the secretory cells make this sample sufficiently similar to the holotype held at the Tasmanian Museum and Art Gallery, and described by Tidwell and Skog (1992) (Figure 19), to assign it to *Tasmanoptevis richmondii.*

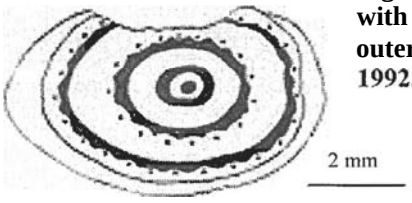

Figure 19. *Tasmanopteris richmondii* rhizome in transverse section, with four annular steles. Note the secretory cells associated with outer steles but not the inner two. Modified from Tidwell and Skog 1992.

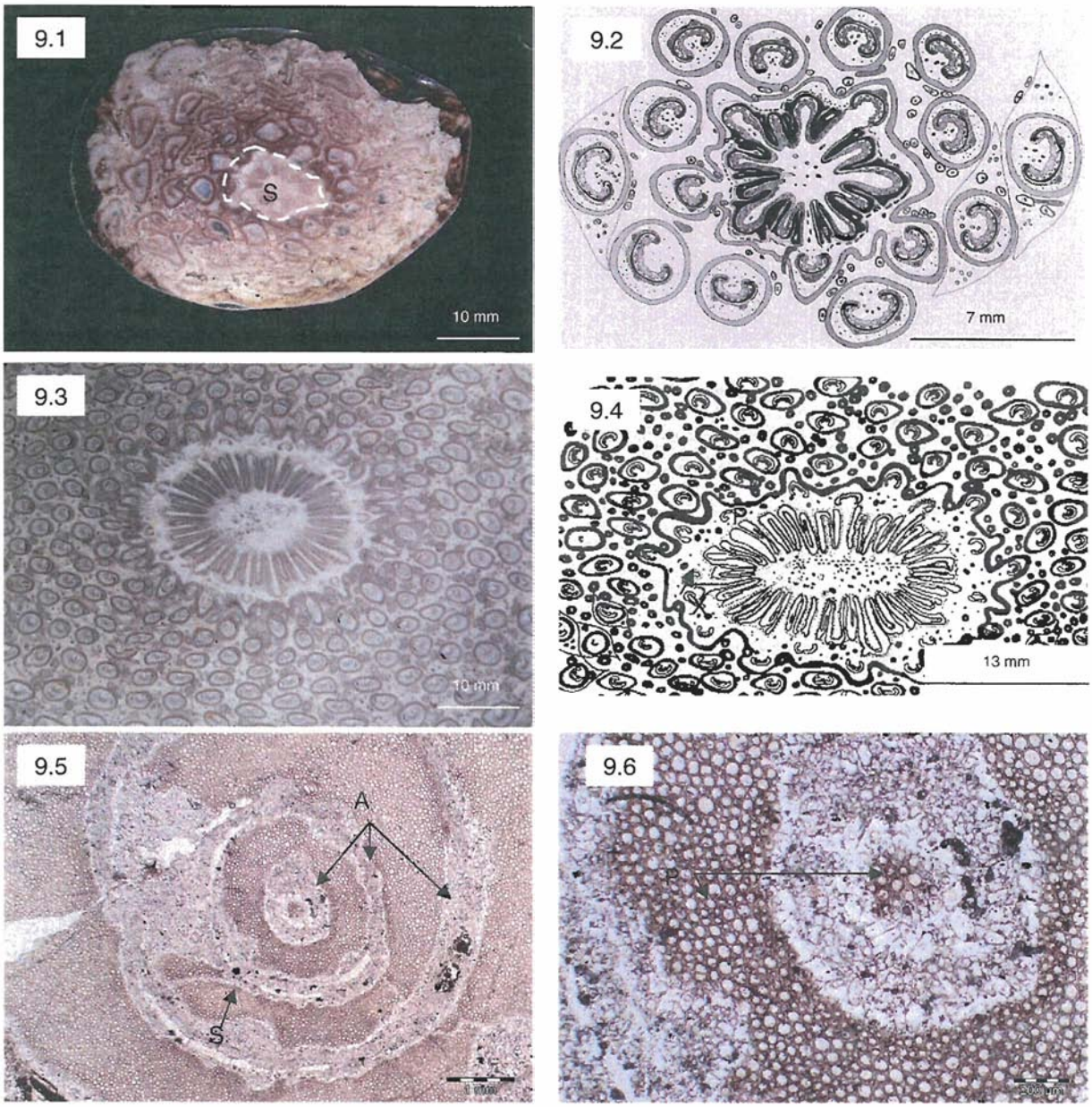

Plate 9.1. Transverse section through O. ***nerii.*** Dashed lines delimit the stele (S). **Plate 9.2.** Transverse section of O. nerii stem and adjacent petiole traces. Xylem black, sclerenchyma light stipple, outer cortex and sclerotic ring of trace darker stipple, external to xylem, dashed lines delimit endodermis and phloem and internally they indicate xylem sheath. (From Tidwell and Jones 1987). **Plate 9.3.** Transverse section through *O. pruchnickii.* **Plate *9.4.*** Dotted/dashed lines=endodermis. Solid black= sclerenchyma. (From Tidwell and Pigg 1993). **Plate** 9.5. Transverse section through *T.* ***richmondii*** (x 20). AS=annular stele. SC=secretory cells. **Plate 9.6.** Transverse section through *T.* ***richmondii*** (x ***40).*** P=parenchyma cells forming in the inner protostele and between older annular steles.

Description *Cladophlebis indica* (Tidwell et al. 1987).

Material UTGD 154372, UTGD 154370, UTGD 154371.

The macrophyll is bipinnate with a 2 mm wide rachis. Sterile pinnae are alternate to sub-opposite, with stout pinna axes (Plate 10.1). Pinnae diverge from the rachis at 65-70°. Pinnules are sub-opposite, and falcate-deltoid in outline, tapering towards the apex. They are typically 10 mm long and 3 mm wide, although they are 4-5 mm wide at the base. Apices are subacute. The margins are slightly recurved, and entire or pseudo-serriate. The midrib is distinct, 1 mm wide, and extends towards the apex. Lateral veins fork once, and occur in 9-10 pairs.

Specimens used for identification contained isolated fragments of fern fronds, with pinna and pinnules present. Cuticular and epidermal features are not preserved. No stomata were observed. Despite the incomplete nature of the specimens, the venation is well enough preserved to assign them to Cladophlebis indica based on this character (Retallack 1980).

Description *Equisitites* sp.

Material UTGD 154360, UTGD 154374, UTGD 154373.

Examples have slender, hollow (Plate 10.2), jointed (Plate 10.3), ovate stems, approximately 3 mm x 2 mm. The stem is ridged and grooved. Eight to ten whorls of reduced leaves occur as rings of minute, pointed-triangular scales, and form at each node on the stem. There appears to be one leaflet for each ridge on the stem.

Modern Equisetum is a small, easily recognized, and highly distinctive genus of vascular plants (Plate 10.4, Plate 10.5). The characteristic whorled leaves and ridged stem makes it possible to assign the Lune River samples to the family Equisetaceae; fossil members of this family are typically Equisitites, while extant members are Equisetum. All members of the family are now extinct in Australia. Fossils assigned to Equisitites date back to the Triassic, with possible records extending to the Carboniferous.

Plate 10.1. *Cladophlebis indica.* **Plate 10.2.** Transverse section of *Equisitites* sp. Pencil for scale. **Plate 10.3.** Longitudinal view of *Equisitites* sp. Pencil nib for scale. **Plate 10.4.** Extant member of the family Equisetaceae, *Equisetum laevigatum*. **Plate 10.5.** Extant member of the family Equisetaceae, *Equisetum* sp.

Palynology

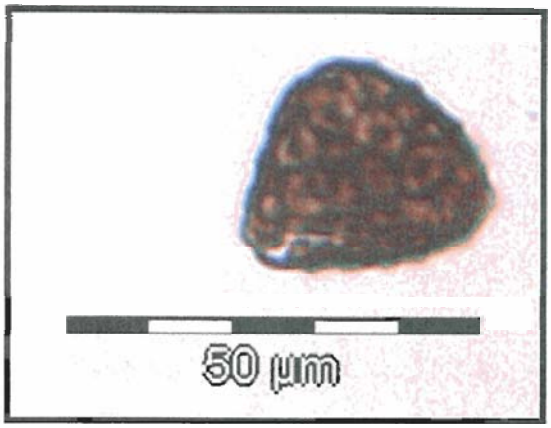

Figure 20. Trilete reticulate spore possibly cf. *Retitriletes*

The only possible specimen that could be Jurassic (Playford, pers. comm.) is a trilete reticulate spore referable to *Retitriletes* (Figure 20). Species of *Retitriletes* can be correlated to extant Lycopodiaceae (Mohr and Gee 1992) and the common Palaeozoic order is Lepidodendrales. Preservation is not good enough to enable assignment to a particular species. Figure 21 shows the range of species within the genus prominent in the palynoflora of eastern Australia. The slides from the subsurface sample taken fi-om CA 106, (@ 51.5 m) include occasional, badly corroded palynomorphs. A few of these appear to represent trilete spores and bisaccate pollen grains, but very poor preservation does not permit taxonomic identification.

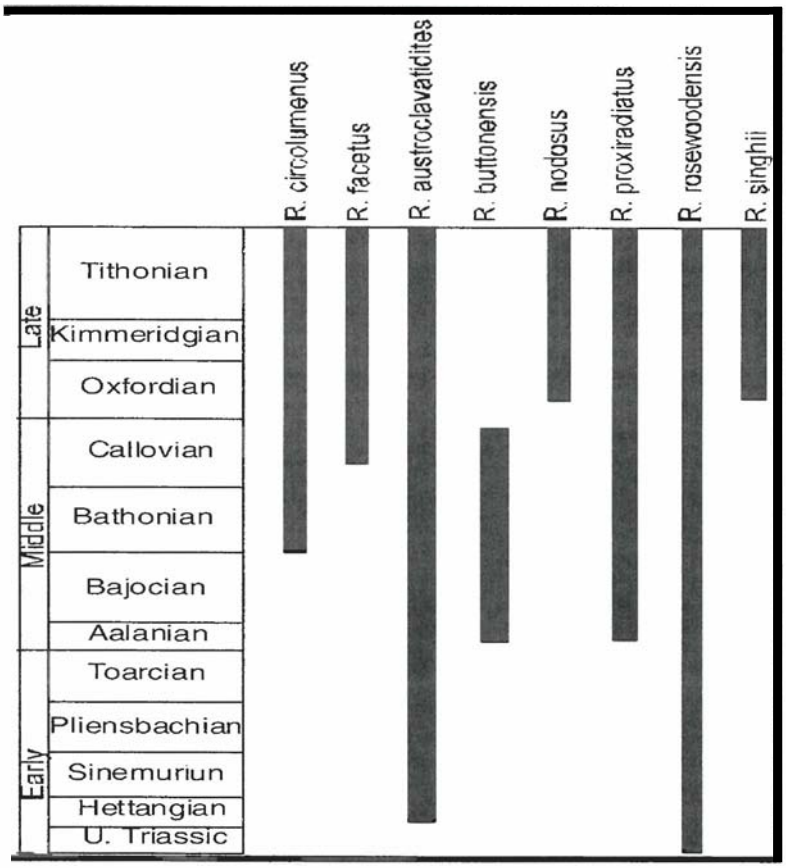

Figure 21. Biostratigraphic ranges of eight species of *Retitriletes* found in eastern Australia in the Jurassic. Adapted from Sarjeant (1992), and Sajjadi and Playford (2002).

Charcoal fragments

Fossil charcoal fragments removed from the volcaniclastic sandstone (UTGD 15435) at the Lune River fossil site have had their internal ultrastructure destroyed and replaced by smooth, homogenous cell walls (Plate 11.1, Plate 11.2). Under experimental conditions, the same result occurs when wood is subjected to 240° C for one hour (Scott and Jones 1991). Despite overall homogenisation, the fragments show no evidence of compression of cellular structures, and preservation of pit apertures is perfect in many cases (Plate 11.3). Some fragments show evidence of shrinkage cracks on their outer surfaces (Plate 11.4).

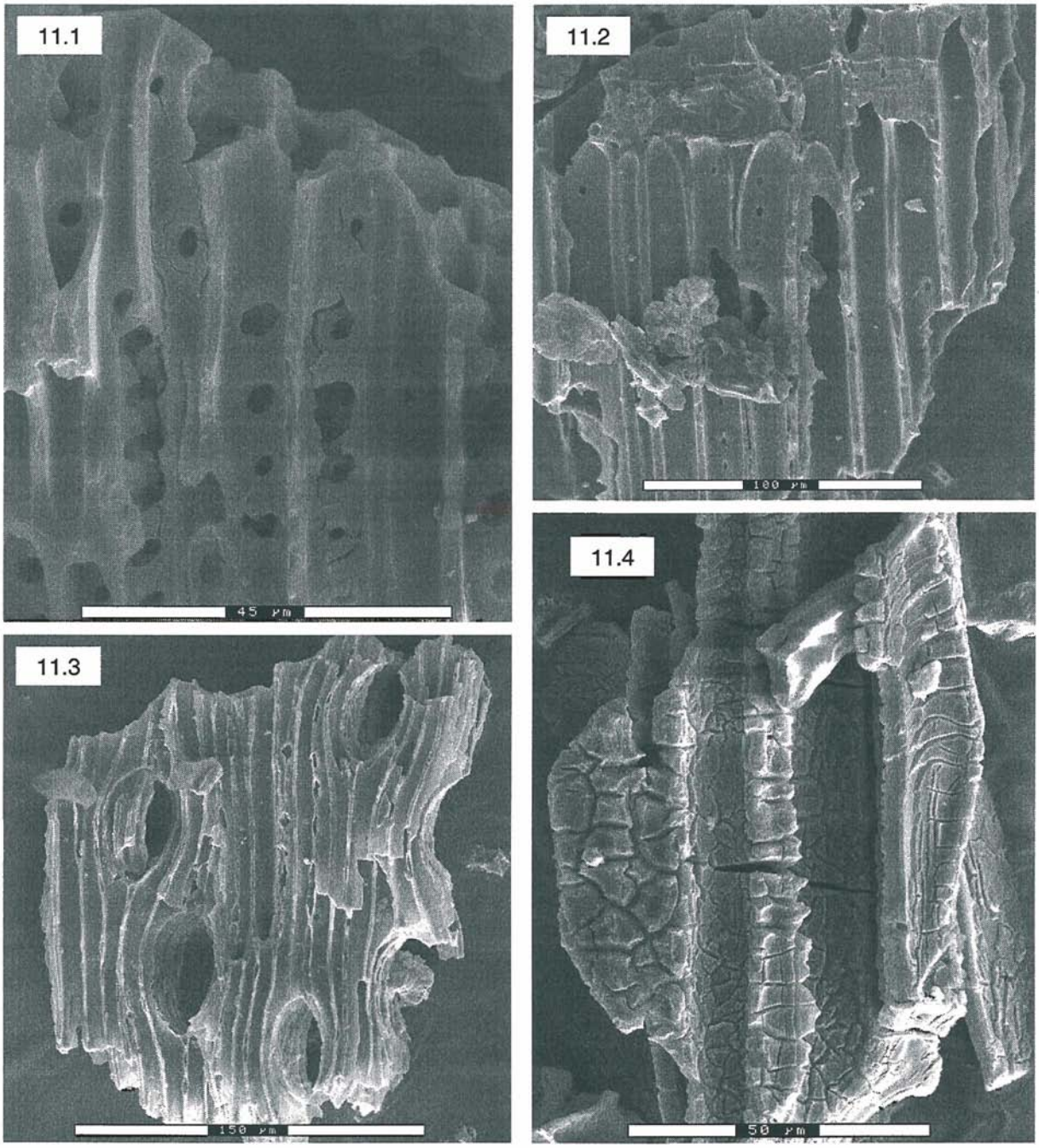

Plate 11.1. Scanning electron micrograph of charcoal fragment demonstrating the lack of internal cell structure. **Plate 11.2.** Scanning electron micrograph showing homogenous cell structure. **Plate 11.3.** Scanning electron micrograph showing that the charcoal has retained cell shape despite homogenisation, and there is no evidence of cellular compaction.
Plate 11.4. Scanning electron micrograph showing shrinkage cracks on the outer surface of organic, charcoalified fragments.

Discussion

There are three distinct phases to taphonomy. The first, necrology, involves the death or loss of a part of the organism. Biostratinomy then includes any biological processes that act to modify the remains, such as microbial decay of cell structure, response to transport, and the length of time an organism stays in the environment before burial. Burial and diagenesis play an important role in preservation of organic matter. Very specific chemical and physical conditions must exist in the burial environment to allow preservation of the organism in a recognisable form. Diagenesis involves all the processes responsible for lithification of the sediment and chemical interactions with waters residing between clasts (Meyen 1987).

The fossils show features of two stages of taphonomy. There are numerous indications that the plants had began to degrade prior to burial and silicification. The cracks seen in cross section of the roots and trunk, in-filled with opaline silica, are a product of wood shrinkage prior to preservation. Many of the fossil wood samples collected from the site have a spongy texture, particularly in their cores, and were not suitable for sectioning or polishing. The lack of bark preserved on the trunk and branches indicates that the tree travelled some way before burial. The abrasions on the surface of the trunk indicate that it was transported through water. In the five-class decay system of Robison & Beschta (1990), (Table 3), the fossils fit between

Table 3. A five-class system of evaluating decay of coniferous woody debris. From Robison and Beschta 1990.

Decay class	Bark	Twigs (3 cm; 1.18 in)	Texture	Shape	Wood color
I	Intact	Present	Intact	Round	Original color
II	Intact	Absent	Intact	Round	Original color
III	Trace	Absent	Smooth; some surface abrasion	Round	Origial color; darkening
IV	Absent	Absent	Abrasion; some holes and openings	Round to oval	Dark
V	Absent	Absent	Vesicular; many holes and openings	Irregular	Dark

decay class III and IV. The problem with wood in water is that environmental conditions can dictate the decay rate as much, or more, than time. For instance, if the wood is partially submerged then dried each year, it will decay much faster than if it remains fully submerged. Water temperature also affects decay rates; decay occurs much slower in cold water. Finally, decay rates can vary between species. For these reasons, Robison and Beschta (1990) did not attempt to tie a length of time to each decay class.

Local flattening of parenchyma in the outer rings of *Tasmanopteris* richmondii, and the collapsed cells in the Araucariaceae annual rings, resulted from pressure during diagenesis. Silicification, either in the form of cellular replacement, or as the opaline silica infilling the cracks within the trunk and roots of the tree, also occurred during this process. The fragmentations seen in the trunk of the tree represent brittle fractures, and are a result of ground movements after the tree silicified.

Had there been a Jurassic palynoflora preserved in situ *(sensu* stricto), abundant pollen should be present. Preservation of the few palynomorphs found at the site was so poor that only one was identifiable in any of the slides examined. It is difficult therefore to say whether they were never preserved in abundance, or if they were destroyed during silicification or contact-metamorphism of the site. Retitriletes species whose ranges are shown, extend back to the Early Jurassic and in some cases, to the Late Triassic, so without consignment of the sporomorph to species level, it is impossible to constrain the age of the sediments at the site beyond the date provided by the zircons.

The homogenisation of the cell structure of the charcoal fragments found in the volcanilithic sandstone is typically the result of pyrolysis[7] (Scott and Jones 1991), and a proportion of organic macerals present at the site charred during this process. However, fast moving forest fires can also produce these textures, where wood is exposed to high temperatures for short periods, or where internal wood structures are protected from extreme heat by the outer cells, and heat remains in the structure for long periods. The shrinkage cracks shown in Plate 10.4 imply charcoalification

[7] The thermal decomposition of organic material through the application of heat greater than 200° C, in the absence of oxygen.

occurred as a result of fire, rather than pyrolysis, which homogenises cell structure without causing shrinkage cracks to develop. The same degree of charcoalification can also result from heat generated by an intruding magma body but again, fracture cracks do not occur. Whether any of the charcoalified fragments derived from fires resulting from volcanic activity in the region is impossible to tell. It is possible that there are two populations of charcoalified fragments present; those with fractures, which were charred by passing fires, and those with homogenous cell structure and no fractures, which were unaffected by fire prior to deposition, and were later charred by pyrolysis.

By far the most important fact that came from studying these plant fossils is the size of the tracheids in the araucarian tree. Trachieds are typically 5-10 μm wide. In the specimen from Lune River, the tracheids are between 30 and 50 pm, with most averaging 40 μm in width. Large tracheids means high water conductance per unit volume, which in turn means high transpiration. (Brodribb and Feild 2000) demonstrated the link between water conductance and photosysnthesis, such that it is clear that any plant with sustainable, high hydraulic supply has a high photosynthetic capacity. Given the width, 1-2 cm, of the annual growth rings in the tree from Lune River, this particular tree had extremely high photosynthetic rates. There are modem analogues with tracheids this size; Agathis *australis*, (the giant Kauri of New Zealand), has tracheids 30 μm +/- 5, and some *Pinus* spp. also have tracheids 35-40 μm (Silvester, written communication).

Chapter 6 Interpretation and Environmental Reconstruction

One hundred and eighty-two million years ago, at the boundary between the Toarcian and Pliensbachian stages of the Jurassic, Tasmania was at 75-82' south (Figure 22). It has been proposed that the inclination of Earth's rotational axis may have been substantially different during the Mesozoic than it is today. At high latitudes this would have resulted in warmer climates and a more even day length throughout the year (Douglas and Williams 1982). In contrast, theoretical investigations suggest that except for the regular and well-understood variation of a few degrees that takes place on the scale of tens of thousands of years, the inclination of the Earth axis has remained the same relative to the plane of the ecliptic (Rich et al. 2002). In the latter case, biota would have contended with the same extremes of day length throughout the year that characterize similar latitudes today. Mean annual temperature on the other hand, may have been substantially different at polar locations than at comparable latitudes today. Hallam (1998) proposed a broad temperate belt ranging from the poles to 30° north and south.

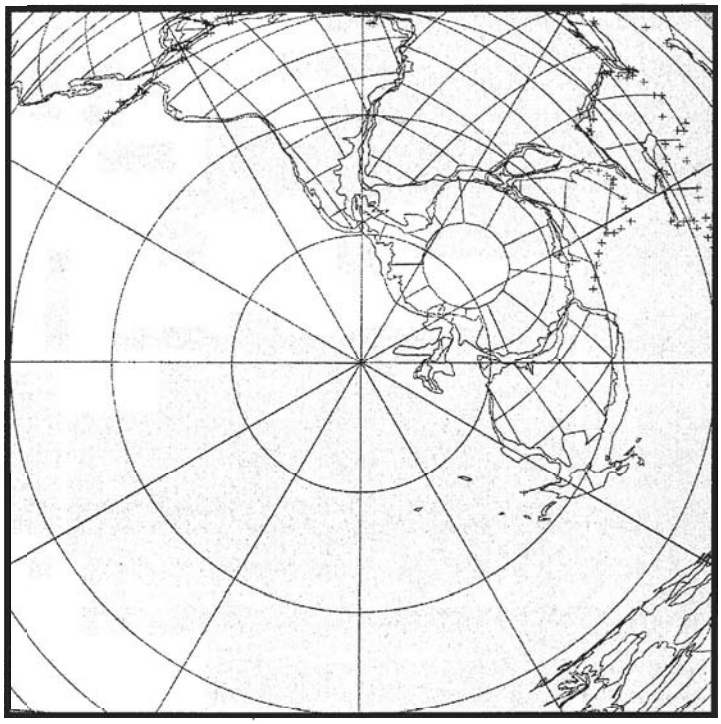

Figure 22. Palaeomagnetic reconstruction of the configuration of continents 180 Ma. Shows Tasmania lying 80° south From Smith et al. (1981)

The plants found at Lune River support the higher mean annual temperatures proposed by Rich et al. (2002), and the temperate climate proposed by Hallam (1998). Osmundaceae has an extensive Mesozoic record, with petrified stems well known globally (van Konijnenburg-van Cittert 2002). They probably preferred warm, humid conditions, either along riverbanks, or in fresh water marshes. Cladophlebis spp. also

preferred freshwater marshes, although they favoured those that were filling up with clastic material.

The ecology of Matoniaceae, however, varied. Some Jurassic species were large and inhabited riverbanks, or grew in humid environments as forest understorey. Others were stress-adapted. In Yorkshire and Scotland, one species, found in deltaic sediments as charcoal fragments, lived in inland heath environments, and was preserved during fire and flood events (van Konijnenburg-van Cittert 2002). It is therefore impossible to use the Lune River member of the family, *Tasmanopteris* richmondii, to interpret the Jurassic environment, without evidence of leaf structure, stomatal arrangement, and stomatal density, associated with the petrified stems found at the site.

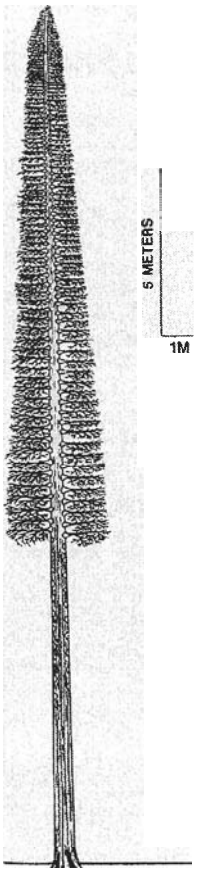

Figure 23. Jurassic lycopod possibly similar in form to adult *Retitriletes*.

In the Jurassic, many Lycopodales, the order to which Retitriletes belongs, were large, arborescent plants (Figure 23). Some species grew up to 40 metres tall. They dominated the forest canopy in many floral communities. They occupied a specific range, preferring swamp environments, analogous to modern tropical peat forming environments, transitional between domination by clastic processes and peat accumulation (Wnuk 1989). Many species were tolerant of periodic episodes of drought.

Though they are often among the larger plants in their environment, cycadopsids are no longer abundant or dominant components of the world's flora. Today they occur on every continent except Europe and Antarctica, but are restricted to the tropics and subtropics. Cycadopsids occupy a number of different habitats, from understorey in both rainforests and seasonally dry forests, or occasionally as members of the forest canopy. At Lune River, they are represented by Otozamites *sp.*

Modem examples of Equisetum have a cosmopolitan distribution. Only Australia, New Zealand, and Antarctica lack endemic representatives. Most species occur at latitudes between 40 and 60° N, and are confined to seasonally wet ground, including

standing waters of shallow ponds and ditches, marshy areas, and moist woods. They live along riverbanks, lakeshores, ditches, seepage areas, meadows, marshes, and wet woodlands (Kelber and van Konijnenburg-van Cittert 1998). The order Equisitales has undergone a dramatic range restriction since the Jurassic. Equisetites were very similar to present day Equisetum and there is some controversy as to whether they may actually have been congeneric with present day Equisetum. If Equisetites actually is Equisetum, then Equisetum has existed since the Palaeozoic, and may be the oldest vascular plant genus (Hauke 1963). Some Jurassic Equisetites were significantly larger than present day Equisetum, reaching 8 to 14 cm in diameter (Stewart and Rothwell 1993). However, the examples from Lune River appear to have a stem diameter similar to extant Equisetum.

The vertical root structure of Lunea fossils indicates they had an erect, possibly arborescent, growth habit. Proposed areal roots may have had an absorptive function, but it is also likely they had the ability to photosynthesise when exposed to light (Tidwell 1991). This increase in photosynthetic ability may have maximised light use during the daylight months, helping store energy for the months of darkness.

Seed ferns (Pteridospermales) were prolific in the Mesozoic, although they are now extinct. They probably formed dense shrub-lands. Some of these plants resembled modem tree ferns, with upright trunks bearing fern-like leaves. Others had a more scrambling habit, resembling modern rainforest vines (Taylor 1981). They were r-selected[8], and produced large quantities of small seeds. These plants were dominant in non-swamp habitats, and formed a significant component of forest understorey flora.

The size of the tracheids observed in the Agathis, indicate that Lune River must have been subject to high annual rainfall. Banding on the trunk and branches indicates a seasonal climate regime operated during the early Middle-Jurassic. During the growing season, the tree added 2-4 cm to its diameter. The false rings between

[8] For r-selected species, "r" refers to the growth rate term in the logistic population growth model. For these species, population sizes and mortality tend to be variable and unpredictable. Since populations frequently are far from carrying capacity ("K"), intraspecific competition often is weak. Selection tends to favour individuals with rapid development, high and early reproduction that is not repeated, small body sizes, high resource requirements, and short lives. Populations of r-selected species tend to be large (Pianka, E. (1970). "On r- and K selection." American Naturalist 104: 592-597.

growth rings indicate changes within seasons, i.e. drought, altered rainfall, or defoliation by insects (Creber and Chaloner 1984). The size of tracheids and the width of the rings indicate that the tree grew rapidly each year, using the months of light to photosynthesise efficiently.

The Modern distribution of *Agathis*

Araucarians are almost entirely restricted to rainforest or, in modem terms, the boundaries of rainforests composed of more complex forest types. They are therefore useful in interpretation of the extent of rainforest regions. They have a distinct emergent habit, which exposes them to the atmosphere above the forest and makes them ideal in studies of region climatic conditions (Kershaw and Wagstaff 2001).

The genus *Agathis* grows in montane tropical forests of the western Pacific, including Australia, Papua New Guinea, and New Caledonia. It reaches its southern limit in New Zealand, where latitude 38° S marks the southern limit of *A. australis.* Until recently, *Agathis* was widespread in Australia, and was recorded in Quaternary sand-rock near Evans Head, New South Wales,(Bamber and McGarity 1956). As Australia became drier, it retreated. Today it only grows wild in confined remnant rainforests. There are approximately 21 species of *Agathis;* however, it is no longer a prominent feature of the landscape, as it was during the Mesozoic.

Three extant species of *Agathis* occur in Australia, in Queensland. *A. palmerstonii* and *A. microstycha* grow in rainforests on ranges and tablelands on well-drained, granite-derived soils. They usually occur at altitudes of 600 metres or more, but may follow rivers down to 75 metres. *A. robusta,* which of the three, is most similar in form to the Lune River tree, occurs in rainforest growing on deep, porous, sandy, well-drained soils between dunes, within a few kilometres of the sea. The roots of all three species are able to penetrate deep down to the water table and none grows where free water occurs on the surface of the ground (Bamber and McGarity 1956).

Modem *A. australis* has tracheids the same size and a form similar to the tree found at Lune River. Its modem range is restricted to the North Island of New Zealand, where it occurs as a canopy emergent tree, dominating relict rainforest stands growing in areas with a mean annual rainfall of between 2272-2555 mm. The mean solar

radiation required for growth of this species is 124-137 M joules/m^2/day, and the mean annual temperature ranges from 10-14° C (Ogden et al. 1993).

Fossil Record of Araucariaceae

The family Araucariaceae, along with Podocarpaceae and some genera of Cupressaceae make up a group of southern conifers that have a history extending back into the Mesozoic. Araucarians have a well-documented fossil record. Both macro- and microfossils are common, with pollen usually abundant in association with parent plants, and not usually dispersed widely beyond the source of vegetation (Kershaw and Wagstaff 2001). In ancient environments, they indicate the presence of environments suitable for rainforest development prior to the evolution of angiosperms. However, the fact they require disturbance in order to regenerate, means their distribution in the fossil record may not reflect their true climatic range. There has been a long-term decline in all the southern conifers since the emergence of angiosperms in the Early Cretaceous. Araucarian populations have become increasingly isolated. However, the decline in the extent and range of this family has not been matched by an overall decrease in diversity (Lidgard and Crane 1990).

Silicification

The fossils are petrified, meaning the cell walls and the cell voids have been mineralised. The cell walls have been replaced by microcrystalline quartz and the intercellular spaces have been in filled with chalcedony. In saturated or near saturated solutions, silicon exists as hydrated molecules of H_4SiO_4, which link together and exclude the water, forming SiO_2 (Martin 1999). Sources of silica are variable, and can include volcanigenic, hydrothermal, detrital, and biogenic sources. Volcanic ash and lava weather easily and provide monosilicic acid, the primary form of soluble silica in nature. The pH of monosilicic acid is neutral to slightly acidic, and it bonds via hydrogen bonds to the hydroxyl group in plant tissues. As the concentration of silicic acid rises in the plant, polymerisation of the silicic acid occurs.

A small degree of decay is required before silicification can take place, so that the hydroxyl molecules can bond easily with the monosilicic acid molecules (Allison and Briggs 1991). In some instances, silica rich fluids invade the outer cells and petrify them, acting as a seal, and preventing fluids from penetrating into the core of the

plant. The inner core then decays further before being preserved. This process explains why the centres of some of the larger petrified Lune River fossils are spongy and poorly preserved. Silicification of vascular plants and in particular, fragile leaves must occur quickly to prevent decay of the entire structure. In some instances, it can be very rapid, with onset of silicification occurring after only a few hours. In other instances, the full process of petrification can take thousands of years, even in high silica environments (Allison and Briggs 1991).

Cell preservation at Lune River is of moderate to good quality, and there are indications that the plants began to degrade prior to silicification. The fossil tree has shrinkage cracks in the centre of the trunk, filled with chalcedony, and in places, it has a poorly defined cellular structure. The fragment of the branch from the *Agathis* shown in Plate 7.3, and the gymnosperm fragment seen in Plate 8.3 show "stars", where silica replaced parts of the outer cambium cells that were already losing their structure. This is probably a result of submersion in water before silicification occurred.

Discussion

The interesting question arising from the interpretation of the plants from Lune River is why the *Agathis* sp. became extinct considering that it had such large tracheids and grew so efficiently. However, it needed a large sustainable water supply and high light levels in order to use the large tracheids effectively. Small tracheids offer resistance to embolism[g] and cavitation caused by freezing. The benefit of small tracheids is that if cavitation occurs, the loss of one small tracheid does not affect the overall efficiency of the tree. Plants with large tracheids are greatly affected by the loss of productivity of a single cell. In order to adopt large tracheids as an evolutionary strategy, the advantages have to out way the dangers of freezing, drought or other environmental stresses. These advantages include up to eighteen times the water transport efficiency compared to plants employing large numbers of small tracheids (Jordan pers com). This huge potential for transpiration means that during the growth season, this tree photosynthesised up to eighteen times faster than many

[9] Embolisms are air bubbles that form in the vessels that transport water taken up from the soil towards the aboveground parts of the tree, and they have serious consequences due to the risk that leaves will no longer be supplied with water and will dry out irreversibly. Drought and frost are the two climatic factors than can cause embolism.

modern conifers with tracheids 5–10 μm wide, providing it with enough energy to endure the months of darkness.

This in part explains how the tree can have been so prolific, given the months of reduced light at latitude 80° S. Coniferous forests, composed of families other than Araucariaceae, do not extend today past –60" to the south, although in the northern hemisphere, in the Taymir region of northern Siberia for example, they extend as far as 75" N (Jacoby et al. 2000). In order for large, arborescent forests to grow at high palaeolatitudes in the Jurassic, the global mean temperature and incipient insolation must have been high enough such that plants were able to maintain sufficient cambial growth during the summer months to compensate for an extended season of reduced light. Furthermore, the postulated increase in global atmospheric CO_2 (McElwain et al. 1999), would have enhanced photosynthetic productivity (Creber and Chaloner 1984).

Other plants that make up the floral assemblage of Lune River adopted r-selection as a reproduction strategy. This increases the survival rate in communities exposed to months of darkness. Plants using this strategy develop rapidly after germination and flourish quickly, analogous to modern angiosperm annuals. They have high fecundity rates, and abundant *Pactypteris* seeds would have been dormant during the dark months. This strategy maximises efficiency during the months of light, and reduces energy wasted when photosynthesis is impossible.

The plants fiom Lune River indicate that the environment during the Jurassic was humid, seasonal, and temperate, with an annual rainfall of over 2000 mm. The temperature never reached fieezing point, otherwise the large tracheids would have been a disadvantage, and using *Agathis australis* as an analogue, it was usually above 10° C. Most of the species identified prefer wet or seasonally wet habitats, and the osmunaceous plants definitively indicate that the temperature was warmer than at present. Lune River in modern times expects a mean annual rainfall of between 800-1000 mm (www.bom.gov.au/cgi-bin/climate/cgi_bin_scripts/annual_rnfall.cgi). A forest with an araucarian and lycopod-emergent canopy grew close to a marshy area or swamp, or along a riverbank. The area may have experienced episodic droughts, although these could never have been severe enough to stop the aruacarians from

being able to access the water table. Despite months with extended hours of darkness, the mean annual solar radiation, mean annual temperature, and atmospheric CO_2 provided enough resources during the growing months to support this floristic community at high latitudes.

Chapter 7 Synthesis and Conclusions

Palaeoenvironment

Sedimentary features within the volcanic sandstone indicate that deposition occurred in an aqueous setting, probably a meandering river system. These sedimentary features include laminated volcanic ash, and siltstone facies, combined with normal graded beds and erosional scouring in-filled with pebble conglomerate. The single subordinate reverse-graded bed represents a change in the ambient current regime and an increase in flow velocity. The stratigraphy of the Lune River fossil site correlates with a small section of the ideal meandering river system (Figure 24). It represents the normal graded beds that overlie fine-grained sediments in the upper section of the abandoned channel. The fine grained, laminated ash deposits and the erosional scours in-filled with coarse sand to pebble sized clasts represent a facies association that indicates a meandering fluvial system was active in the region at the time of deposition. Desiccation cracks, seen in the palaeosurface at Lune River, are typical features of floodplain deposits in meandering systems, confirming this as the environment of deposition.

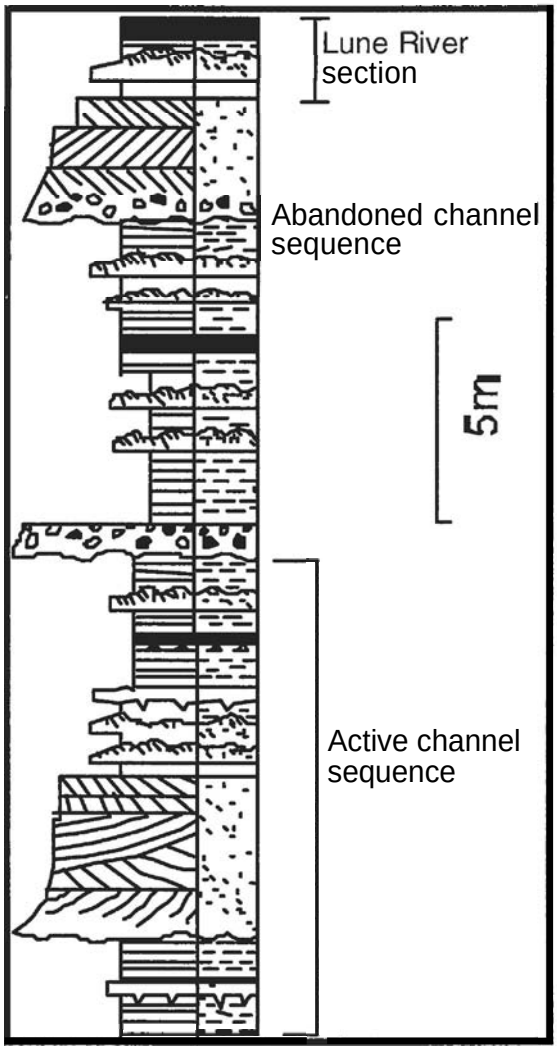

Figure 24. Typical vertical stratigraphy of a meandering fluvial deposit showing both the active channel and abandoned channel deposits. Modified from Prothero and Schwab (1996).

In the Jurassic, the plants in the Lune River region were growing in a seasonally dry rainforest with large araucarian trees and possibly emergent lycopods, and a dense understorey of seed ferns. The forest grew proximal to a meandering river edged by hydrophilic vegetation, including a variety of tree ferns and horsetails (Equisetites

spp.). Figure 25 depicts the likely Jurassic palaeoenvironment, where a forest of *Agathis* sp. and lycopods grew in the drier, up-slope regions of a valley catchment area, while the riparian community was associated with the valley adjacent to the river.

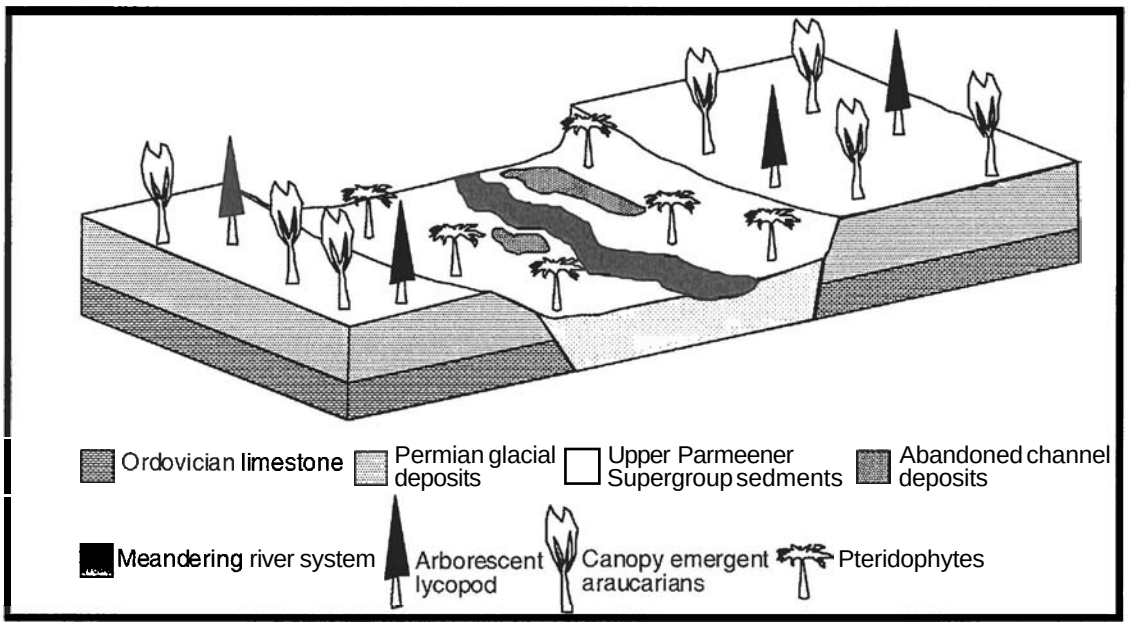

Figure 25. Jurassic forest community up-slope from a meandering river system bordered by hydrophilic plant species in a riparian community.

In meandering fluvial systems, the energy generated in fast-moving braided systems transferres from incising up-stream channels, to cutting the deep, down-stream meandering river channels sideways (Prothero and Schwab 1996). As the river hits the opposite bank, it scours out a section of bank. In time, this undermines the bank, releasing a "raft" of vegetation including trees, understorey, and riverbank vegetation. River bank undercutting is a major contributor of fresh vegetation into aquatic systems (Allison and Briggs 1991). Oxbows and abandoned channels capture this debris as they fill up with fine sediment. Consequently, they tend to reflect the floral composition of local biota (Martin 1999). However, tree trunks are durable and can be reworked a number of times before final deposition, so the *Agathis* specimen may represent the regional, upslope flora, rather than local vegetation. Leaves on the other hand have little reworking potential, and decay rapidly. Accordingly, their preservation is a function of rapid burial, and they therefore reflect the local flora (Martin 1999).

During over-bank erosion by rivers, vegetation is subject to different buoyancy and down stream transport. While logs may remain afloat for many years, leaves need to preserve rapidly, before they can decompose. The lack of coniferous leaves preserved at the site implies that the tree travelled further than the pteridophytic vegetation. The leaves from the tree abraded from the branches prior to its final deposition. The pteridophytic leaves show no evidence of natural decay, i.e. embayed margins or holes in the leaf surface caused by microbial action. Minor angular breaks and tears from limited fluvial transport resulted in their fragmentation. As decay is typically rapid in warm humid environments, assuming these conditions prevailed during the Mesozoic, their excellent preservation supports rapid burial.

Deposition of the pteridophytic vegetation at Lune River occurred in what Benke et al. (1985) referred to as a snag habitat, where small stems snagged on the riverbed, causing a build up of debris. Robison and Beschta (1990) regarded plant debris as grouped where each piece touched another piece. Thus, the fossils are in a grouped snag deposit.

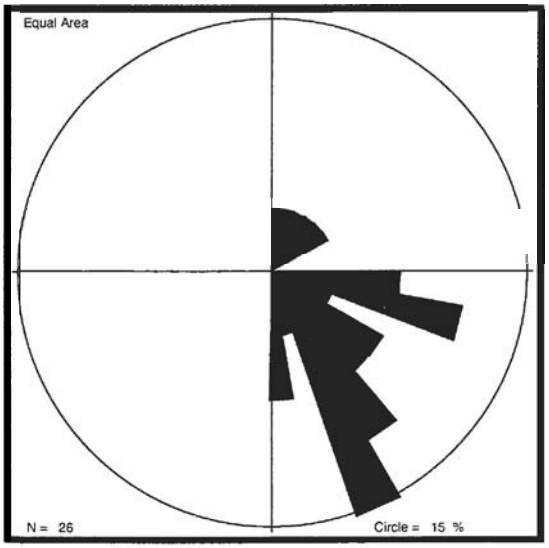

Figure 26. Rose diagram depicting orientation of pteridophytic stems calculated using dip direction.

According to Robison and Beschta (1990), at least 1/3rd of coarse woody debris will lie perpendicular to the directional force of the stream that deposits them. Thus, it is possible to estimate the probable flow direction of a stream or river, from the orientation of stems found within the river, or from fossil stems. Stable debris tends to be oriented perpendicular or slanted to the direction of flow, while unstable debris tends to parallel flow direction. The *Agathis* at Lune River can be considered stable or unmovable, while the smaller pteridophytic stems constitute unstable debris. Ninety percent of the stems preserved at the fossil site have a south-southeast dip direction (Figure 26), and were probably imbricated in the direction of flow, while the *Agathis* sp. lies west to east. Flow

direction was therefore likely to have been perpendicular, or oblique, to the latter, i.e. from the south-southeast to the north-northwest.

Since there is greater potential for debris movement in larger, swifter streams, and given the size of the tree, it is likely that any river capable of depositing it in the snag-debris load, must have had a high flow velocity The tree may have been moved in a flood episode, which might also have accounted for the episode of reverse grading seen at the site, overlying the position of the tree relative to the stratigraphy. Accordingly, the pteridophytes may then have built up around the stranded log after the floods subsided, with the tree acting as the snag catalyst.

The still water environment in the abandoned channel, required for the burial and preservation of the leaf material is difficult to reconcile with the lack of palynological material was preserved. Araucariaceaea is usually associated with abundant pollen, and the notable lack of preserved pollen at Lune River implies that the tree moved out of the source area prior to preservation. However, the lack of pollen may be also be a result of silicification and the movement of hydrothermal fluids, rather than a reflection on the original quantities of pollen deposited at the site. The presence of sporinite in the samples sent for vitrinite analysis indicates that spores were present at the time of deposition. In addition, the presence of rare, undifferentiated algal cells identified during vitrinite reflectance analysis, provides further support that the sediments were deposited in an aqueous environment. Abandoned river channels or an oxbow lakes filling with fine clastic debris, are typically good sources of preserved vegetation.

Geological History

The facies associations at Lune River, which include pyroclastic and lithic rich sediments capped with arc-like tholeiitic basalt, can be correlated with the early Jurassic Hanson Formation, which along with the Prebble Formation, forms the upper section of the Beacon Supergroup, in the Trans-Antarctic Mountains. The lithic rich sediments of both, have clast textures typical of phreatomagmatic eruptions i.e. curviplanar quartz margins. They both contain felsic ash units and volcanigenic sandstone. Furthermore, according to Collinson et al. (1990) sediments from the Hanson Formation were also deposited in a meandering fluvial system.

At Lune River, the sediments petrographically and geochemically resemble the sediments fi-om the Upper Parmeener Supergroup. Given the immaturity of the sediments, and the fact that many of the clasts have retained their angularity, the deposit was not extensively fluvially reworked after eruption, and was deposited proximal to its volcanic source.

If the Lune River sediments are chronostratigraphic and lithostratigraphic correlatives of the Hanson Formation, then they imply a large-scale tectonic control related to the early break-up of Gondwana. Volcanism occurred in a rift setting associated with an extensional tectonic regime (Hanson and Elliot 1996). Several authors e.g. Elliot (1992); Elliot and Larsen (1993), suggested that the onset of extension might have been contemporaneous with the felsic volcanism in the Transantartic Mountains.

Other correlative features between Lune River and the Hanson Formation include the capping of felsic sediments by tholeiitic basalt (Figure 27). The stratigraphic section of Transantarctic Mountains shows a basaltic, lahar deposit, the Prebble Formation, between the early Jurassic Hanson Formation and the middle Jurassic Kirkpatrick Basalt (Elliot 1996). While laharic deposits were not evident at the small site studied at Lune River, their existence at other locations within the Lune River Graben

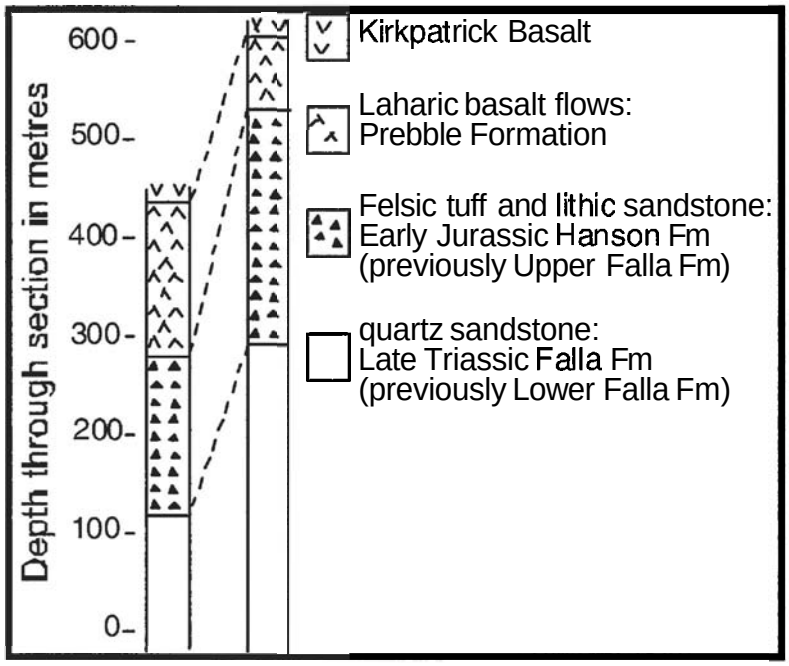

Figure 27. Representation of stratigraphy of the Transantarctic Mountains, Antarctica. Left column is from Mt. Kirkpatrick. The right column is from Mt Falla. Modified from Elliot, 1996.

cannot be ruled out. Unfortunately, the thickness of the Jurassic sediments in Tasmania is unknown, so a schematic representation of the correlative features is difficult to establish.

Sediments comprising the Beacon Supergroup and the Upper Parmeener Supergroup were deposited in a large intracratonic basin extending landward into the Victoria Land portion of east Antarctica (Figure 28). The East Antarctic Craton bound the basin to the west (Collinson et al. 1990). During the onset of rifting, a plume began welling up underneath the Victoria sub-basin (Riley and Knight 2001). The up-welling plume heated crustal rocks and initiated bimodal felsic and mafic volcanism within the new rift valley. The volcainclastic sediments, basalt and dolerite associated with this event all show arc-like trace element geochemistry. This presumably resulted from interaction between the plume and the sub-continental lithosphere that likely contained components related to subduction along the Pacific margin of Gondwana, which had been active at least since the Devonian (Duncan 1987).

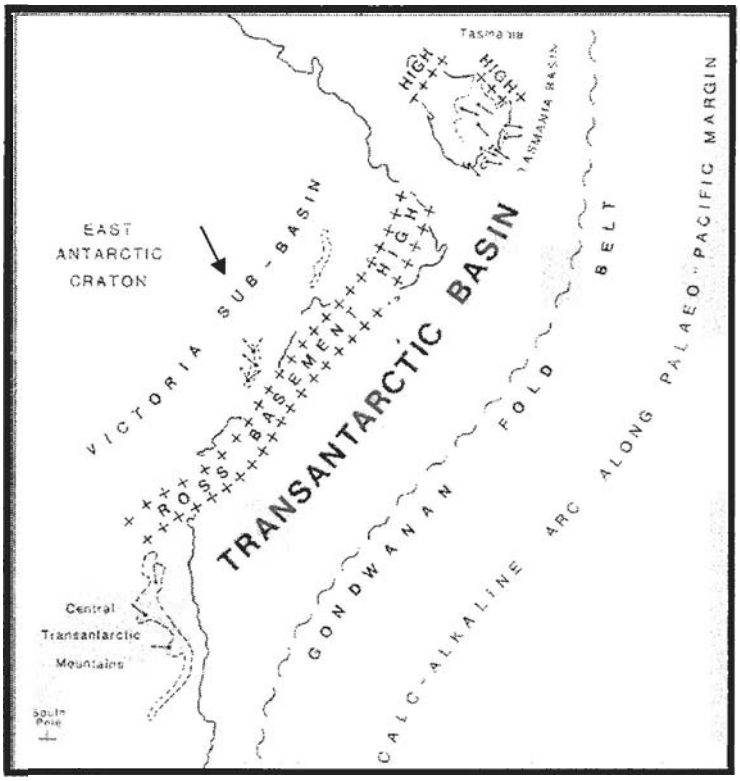

Figure 28. Late Triassic (–205Ma) Palaeo-Pacific margin of the Gondwanan supercontinent including the Ross Sea coastline of East Antarctica and Tasmania. Arrow highlights the location of the Victoria sub-basin. From Colliinson et al. 1990.

A proportion of the lithic fragments included in the sandstone at Lune River appear to derive from regional basement rocks. This indicates that the volcanism responsible for their deposition must have been located close to southeast Tasmania. This idea is not new, and Collinson et al. (1990) proposed a felsic volcanic source for late Triassic sediments in Tasmania, east of the state. The abundant lithic clasts, particularly those

with granitic compositions i.e. the clumps of sodic plagioclase, or metamorphic textures i.e. polygonal strained quartz, derived from the regional basement rocks; became incorporated into the felsic magma on ascent during eruption.

Hanson and Elliot (1996) believed that the mafic volcanism associated with the outpouring of the Kirkpatrick continental flood basalts post-dated the felsic volcanism and the onset of the rifting of Gondwana. These flood basalts erupted from fissures rather than vent volcanoes (Wilson 1989). At Lune River, the basalt interacted with the wet, volcaniclastic sediment, evidenced by the intrusive basalt hyalclastite seen in drill core CA 106. Locally it erupted under or through water and formed the basaltic pillows seen near the fossil site. At the site itself, the basalt is very heavily weathered, but lobed and polygonal forms are still present, indicating that as the basalt erupted, it interacted with the fossiliferous ash and lapilli tuff. It eventually capped the site, encasing both the sediments and the plants.

The small, rounded zircons removed from the sediment samples derived from a Triassic volcanic event –226 Ma, and have been reworked into the Lune River sediments. However, the large euhedral zircons found in the sediments probably record the timing of the mafic volcanic event, 182+/- 4 Ma.

Secondary quartz in-filling pore-space and quartz over-growths on many of the grains within the volcanilithic sandstone indicate movement of siliceous fluids through the site post deposition. This fluid may have resulted from silica-rich hydrothermal fluids associated with active extension. The replacement of inter-pillow sediments with quartz veins and montrnorillonite at pillow-basalt outcrops proximal to the fossil site, are further indication of the movement of siliceous hydrothermal fluids after the site was preserved. However, it is impossible to determine whether the plants recovered from the fossil site silicified prior to the emplacement of the basalt, or whether the later movement of hydrothermal fluids silicified them.

Sedimentary overburden

The vitrinite analyses on macerals in the Lune River sediments indicate that an overburden of between two and four kilometres existed at the time of dolerite emplacement. Wayne Knowles, from Mirror Image estimated that 3-4 kilometres of

sediments burying the site would account for the reflectance seen in the organic macerals. Alan Cook, from Kieraville Konsultants, provided a smaller estimate of up to two kilometres of sedimentary overburden, based on the degree of maceral coalification recorded. However, as the R_O value for macerals is dependent on thermal gradient rather than pressure, the influence of contact metamorphism at Lune River has acted to increase the R_O value of macerals and the colour alteration index of palynomorphs, such that the depth of burial appears greater than it probably was.

To create the degree of coalification seen in macerals at the site, an upper temperature limit of about 200° C is inferred because char textures are absent using VR analysis techniques. However, the charcoal fragments described using the SEM did reveal char textures and a temperature limit of ~240° C is therefore inferred. Discrepancies between the TAI and R_O may be diminished if more palynomorphs could be found, showing a broader range of TAI values.

Dolerite as a feeder to the Basalt

The question of overburden can be addressed by considering that basalt at the site erupted subareally onto the Jurassic surface. From intrusives relations observed in drill core CA 106, where rip-up clasts of basalt occur within the dolerite, it is inferred that the basalt and the dolerite were coeval. Given that they share the same geochemical signatures, and that they are contemporaneous in geological time, the dolerite may have resulted from cooling of magma in a feeder dyke venting pulses of basaltic magma. This explanation eliminates the need for an extensive sedimentary overburden in the region. The Lune River dolerite clearly postdates extrusion of the basalt; the dolerite may have cooled under the basalt cap, leading to the fine-medium grain size and platy jointing seen at Lune River exposures. In short, there was no significant sedimentary overburden at Lune River.

Conclusion

The most important result of this study has been to finally constrain the age of the fossil plants at Lune River. They are preserved in the volcanic sandstone, which contains early mid-Jurassic zircons, from the Toarcian stage of the era. These sediments are clearly overlain by basalt. From the clasts of basalt in glassy, fine-grained dolerite, and the embayed, baked margins of basalt, the basalt predates, or is

coeval with the intrusion of the Tasmanian dolerite, between 184-175 Ma. The sediments and the plants they contain can therefore be confidently dated at between 182-175 Ma. This result redates the interpretation of Tidwell et al. (1987), and makes the plants significantly older than previously thought.

Recommendations

In view of the presence of the reptile Tasmaniosaurus, a primitive group fiom which the dinosaurs are thought to have evolved, in Tasmania in the Early Triassic (Banks et al. 1978), added to the excellent preservation of the fossils described within this thesis, it is likely vertebrate fossils exist at Lune River and will be discovered in the future.

The presence of Araucariaceaea at the site is important. Members of this family are specific climatic indicators, and are excellent in regional climate studies. Future studies should include tree-ring analysis of the tree to determine early-Mid Jurassic seasonal climate fluctuations. The results would be comparable to modem climate fluctuations studied using the dendrochronology of Agathis *australis*, the New Zealand Kauri. The tree will need to be unearthed again, but a section of the trunk could be polished in position in order to protect the geo-significance of the site. A full study of the trunk section could be made using a portable field microscope.

Radiometric dating of the basalt would fully constrain the age of the Lune River deposit, and should be undertaken as soon as practicable. The occurrence in Tasmania, of correlatives of the Kirkpatrick Basalt, is profound. Although I firmly believe that this link is demonstrated herein, the extent of the basalt at Lune River should be determined, and a full geochemical analysis made. I understand that John Everard from MRT is beginning to undertake this study, and his results will be very interesting.

The full extent of the Lune River protected site itself should be established. At this point, we know that fossil vegetation extends at least 12 by 5 metres, but while doing fieldwork, it was obvious that fossilised patches went beyond the boundaries of our exploration. The lateral extent of the site itself would be useful to tie in with the regional occurrences of fossils fiom southeast Tasmania. The Coal Hill example

implies that other trees are present in the region and if these could be located, some may be found in growth position, and a full study of Tasmania's Jurassic forests could be undertaken. Further, establishing the extent of the deposit may help to ascertain whether the form of the river flowing in the Jurassic, and responsible for the transport and deposition of the macrofossils, was controlled by local faults. In light of the above, I recommend that the fossil site be re-opened for further study in the near future.

References

www.bom.gov.au/cgi-bin/climate/cgi_bin_scripts/annual_rnfall.cgi. 2004.

Allison, P. A. and D. E. G. Briggs (1991). Taphonomy: releasing the data locked in the fossil record. New York, Plenum Press.

Bacon, C. A., C. R. Calver, C. J. Boreham, D. E. Leaman, K. C. Morrison, A. T. Revill and J. K. Volkman (2000). The petroleum potential of onshore Tasmania: a review. Geological Survey Bulletin, Mineral Resources of Tasmania. 71.

Baillie (1989). Jurassic-Cainozoic. Geolonv and mineral resources of Tasmania. C. F. Burrett and E. L. Martin, Geological Society of Australia. 15: 339-341.

Bamber, K. and J. W. McGarity (1956). "A note on the identification of plant remains in sandrock near Evans Head, N.S.W." Proceedings of the Linnean Society of New South Wales **81**(1): 59-61.

Banks, M. R. (1990). Unpublished report to Forestry Commision of Tasmania.

Banks, M. R., J. W. Cosgriff and N. R. Kemp (1978). "A Tasmanian Triassic stream community." Australian Natural History **19**(5): 150-157.

Banks, M. R., D. H. Green, J. M. Hergt and I. McDougall (1989). Igneous Rocks. Geology and Mineral Resources of Tasmania. C. F. Burrett and E. L. Martin. Brisbane, Geological Society of Australia. 15: 375-378.

Banks, M. R., D. H. Green, I. McDougall, S. F. Eggins, J. M. Hergt, H. M. Seitz and S. H. Stephens "Basalts comagmatic with the Jurassic dolerite, southern Tasmania." unpublished article.

Benke, A. C., R. L. Henry, D. M. Gillespie and R. J. Hunter (1985). "Importance of snag habitat for animal production in southeastern streams." Fisheries **10**(5): 8-13.

Berry, R. F. and M. R. Banks (1985). "Striations on minor faults and the structure of the Parmeener Super-Group near Hobart, Tasmania." Papers and Proceedings of the Roval Society of Tasmania 119: 23-29.

Berry, R. F., S. Meffre and H. Kreuzer (1997). "Metamorphic rocks from the southern margin of Tasmania and their tectonic significance." Australian Journal of Earth Sciences 44: 609-619.

Brodribb, T. J. and T. S. Feild (2000). "Stem hydraulic supply is linked to leaf photosynthetic capacity: evidence from New Caledonian and Tasmanian rainforests." Plant. Cell and Environment 23: 1381-1388.

Burnham, R. J. (1989). "Relationships between standing vegetation and leaf litter in a paratropica forest: implications for palaeobotany." Review of Palaeobotany and Palynology 58: 5-32.

Burnham, R. J., S. L. Wing and G. G. Parker (1992). "The reflection of deciduous forest communities in leaf litter: implications for autochthonous litter assemblages from the fossil record." Paleobiology **18**(1): 30-49.

Collinson, J. W., J. T. Eggart and N. R. Kemp (1990). "Triassic sandstone petrology of Tasmania: evidence for a Tasmania-Transantartic basin." Papers and Proceedings of the Royal Society of Tasmania **124**(1): 61-75.

Compston, W., I. McDougall and K. S. Heier (1968). "Geochemical comparison of the Mesozoic basaltic rocks of Antarctica, South Africa, South America and Tasmania." Geochimica et Cosmochimica Acta **32**(2): 129-149.

Corbet, K. D. and N. J. Turner (1989). Early Palaeozoic deformation and tectonics. Geology and Mineral Resources of Tasmania. C. F. Burrett and E. L. Martin. Brisbane, Geological Society of Australia. 15: 154-181.

Creber, G. T. and W. G. Chaloner (1984). "Influence of environmental factors on the wood structure of living and fossil trees." The Botanical Review **50**(4): 357-448.

Cuneo, N. R., E. L. Taylor, T. N. Taylor and M. Krings (2003). "In situ fossil forest from the upper Fremouw Formation (Triassic) of Antarctica: paleoenvironmental setting and paleoclimate analysis." Palaegeography, Palaeoclimatology, Palaeoecoloav 197: 239-261.

Deer, W. A., R. A. Howe and J. Zussman (1998). An introduction to the rock-forming minerals. Essex, Longman.

Douglas, J. G. and G. E. Williams (1982). "Southern polar forests; the early Cretaceous floras of Victoria and their palaeoclimatic significance." Palaeogeography, Palaeoclimatology, Palaeoecoloav **39**(3-4): 171-185.

Duncan, A. R. (1987). "The Karoo igneous province- a problem area for inferring tectonic setting from basalt geochemistry." Journal of Volcanology and Geothermal Research 32: 13-34.

Elliot, D. H. (1992). Jurassic magmatism and tectonism associated with Gondwanaland break-up: an Antarctic perspective. Magmatism and the causes of continental break-up. B. C. Storey, T. Alabaster and R. J. Pankhurst, Geological Society of London Special Publication. 68: 165-184.

Elliot, D. H. (1996). "The Hanson Formation: a new stratigraphic unit in the Transantarctic Mountains, Antarctica." Antarctic Science **8**(4): 389-394.

Elliot, D. H. and D. Larsen (1993). Mesozoic volcanism in the central Transantarctic Mountains, Antarctica: depositional environments and tectonic setting. Gondwana Eight: assembly. evolution and dispersal. R. H. Findlay, R. Unrug, M. R. Banks and J. J. Veevers. Rotterdam, Balkema. 397-410.

Everard, J. L. (1987). Petrology of the Jurassic dolerite. Geological Survey Explanatow Report, St. Marvs. N. J. Turner and C. R. Calver. Hobart, Tasmanian Department of Mines. **sheet** 49: 124-148.

Farmer, N. (1985). Kingborough. Geological Survey explanatory report; Geological atlas 1:50 000 series. Rosney Park, Tasmanian Department of Mines.

Forsyth, S. M. (1989a). Upper Parmeener Supergroup. Geology and Mineral Resources of Tasmania. C. F. Burrett and E. L. Martin. Brisbane, Geological Society of Australia. 15: 309-333.

Forsyth, S. M. (1989b). Interlaken. Geological Survev Explanatory Report. Hobart, Tasmanian Department of Mines: 1-93.

Forsyth, S. M., B. Clarke, C. R. Calver, M. P. McClenaghan and K. D. Corbet (1995). Geology of Southeast Tasmania. Geological Atlas 1:250,000 digital series, Tasmanian Geological Survey.

Gould, R. E. (1971). "*Cibotium tasmanense* sp. nov., A fossil tree-fern from the Tertiary of Tasmania." Australian Journal of Botany 20: 119-126.

Grant-Mackie, J. A., Y. Aita, B. E. Balme, H. J. Campbell, A. B. Challinor, D. A. B. MacFarlan, R. E. Molnar, G. R. Stevens and R. A. Thulborne (2000). "Jurassic palaeobiogeography of Australia." Memoir of the Association of Australian Palaeontologists **23:** 311-353.

Grapes, R., D. Smale, G. Gibson, C. Landis, Y. Kawachi, H. J. Campbell, N. Mortimer, K. Palmer and D. Ren (1996). "X-Ray fluorescence and electron microprobe analysis of western province Permian and Triassic sediments and associated intrusives, northwest South Island of New Zealand and Tasmania." Analytical Facility Publication 18: 1-49.

Gunn, P. J., T. E. Mackey, A. N. Yeates, R. G. Richardson, D. B. Seymour, M. P. McClenaghan, C. R. Calver and M. J. Roach (1997). "The basement elements of Tasmania." Exvloration Geophysics 28: 225-231.

Hallam, A. (1998). "The determination of Jurassic environments using palaeoecological methods." Bulletin of the Geological Societv of France **169**(5): 681-687.

Hanson, R. E. and D. H. Elliot (1996). "Rift-related Jurassic basaltic phreatomagmatic volcanism in the central Transantarctic Mountains: precursory stage to flood basalt effusion." Bulletin of Volcanolgy 58: 327-347.

Hauke, R. L. (1963). "A taxonomic monograph of the genus Equisetum subgenus Hippochaete." Nova Hedwigia 8: 1-123.

Jacoby, G. C., N. V. Lovelius, O. I. Shumilov, O. M. Raspopov, J. M. Karbainov and D. C. Frank (2000). "Long-term temperature trends and tree growth in the Taymir region of northern Siberia." Quaternary Research **53**(3): 312-318.

Jones, T. P. and N. P. Rowe (1999). Fossil Plants and Spores:modern techniques. Cambridge, UK, Geological Society London.

Kelber, K. P. and J. H. A. van Konijnenburg-van Cittert (1998). "***Equisetites arenaceus*** from the Upper Triassic of Germany with evidence for reproductive strategies." Review of Palaeobotanv and Palynology **100**(1-2): 1-26.

Kershaw, P. and B. Wagstaff (2001). "The southern conifer family Araucariaceae: history, status and value for paleoenvironmental reconstruction." Annual Review of Ecological Systems 32: 397-414.

Langford, R. P. (1992). Permian coal and palaeogeography of Gondwana. Canberra, Bureau of Mineral Resources.

Leaman, D. E. (1975). "Form, mechanism, and control of dolerite intrusion near Hobart, Tasmania." Journal of the Geological Societv of Australia **22**(2): 175-186.

Leaman, D. E. (1995). "Mechanics of sill emplacement: comments on the Tasmanian dolerites." Australian Journal of Earth Sciences 42: 151-155.

Lidgard, S. and P. R. Crane (1990). "Angiosperm diversification and Cretaceous floristic trends: a comparison of palynofloras and leaf macrofloras." Palaeobiolonv 16: 77-93.

Martin, R. E. (1999). Taphonomy: A process approach. Cambridge, Cambridge University Press.

McClenaghan, M. P. (1989). Mid-Palaeozoic deformation, granitoids and ore deposits. Brisbane, Geological Society of Australia.

McDougall, I. (1962). "Differentiation of the Tasmanian dolerites: Red Hill dolerite-granophyre association." Geolonical Societv of America Bulletin **73**(3): 279-315.

McElwain, J. C., D. J. Beerling and F. I. Woodward (1999). "Fossil plants and global warming at the Triassic-Jurassicboundary." Science 285: 1386-1389.

McLoughlin, S. and A. N. Drinnan (1995). "**A** Middle Jurassic flora from the Walloon Coal Measures, Mutdapilly, Queensland, Australia." Memoirs of the Queensland Museum 38: 257-272.

Meffre, S., R. J. Scott, G. R.A and S. R.J ((in prep)). "Re-evaluation of contact relationships between Ordovician volcanic belts and the quartz-rich turbidites of the Lachlan Orogen." Australian Journal of Earth Sciences.

Meyen, S. V. (1987). Fundamentals of valaeobotanv. London, Chapman & Hall.

Minor, D. R. and S. B. Mukasa (1997). "Zircon U-Pb and hornblende 40 Argon-39Argon ages fro the Dufek layered mafic intrusion, Antarctica: Implications

for the age of the Ferrar large igneous province." Geochimica et Cosmochimica Acta 61: 2497-2504.
Mohr, B. A. R. and C. T. Gee (1992). "An early Albian palynoflora from the Kerguelen Plateau, southern Indian Ocean (Leg 120)." Proceedings of ODP Scientific Results 120: 255-271.
Niklas, K. J. (1994). "Predicting the height of fossil plant remains: an allometric approach to an old problem." American Journal of Botany **81**(10): 1235-1242.
North, F. K. (1984). Petroleum Geology, Allen and Unwin.
Ogden, J., R. M. Newnhamk, J. G. Palmer, G. R. Serra and N. D. Mitchell (1993). "Climatic implications of macro- and microfossil assemblages from Late Pleistocene deposits in northern New Zealand." Quaternary Research 39: 107-119.
Osborne, C. P. and D. J. Beerling (2002). "Sensitivity of tree growth to a high CO_2 environment: consequences for interpreting the characteristics of fossil woods from ancient 'greenhouse' worlds." Palaegeography, Palaeoclimatolonv, Palaeoecoloav 182: 15-29.
Pearce, J. A. and M. J. Norry (1979). "Petrogenic implications of Ti, Zr,Y and Nb variations in volcanic rocks." Contributions to Mineralogy and Petrology 69: 33-47.
Pianka, E. (1970). "On r- and K selection." American Naturalist 104: 592-597.
Prothero, D. R. and F. Schwab (1996). Sedimentary Geology. New York, W.H. Freeman and Company.
Reid, C. M., S. M. Forsyth and M. J. Clarke (2004). "Geology of Tasmania." Geological Society of Australia Special Publication: 1-25.
Reid, C. M., S. M. Forsyth and M. J. Clarke (in prep). "Geology of Tasmania." Geological Society of Australia Special Publication: 1-25.
Retallack, G. J. (1980). "Middle Triassic megafossil plants and trace fossils from Tank Gully, Canterbury, New Zealand." Journal of the Roval Societv of New Zealand **10**(1): 31-63.
Rich, T. H., P. Vickers-Rich and R. A. Gangloff (2002). "Polar Dinosaurs." Science **295**(5557): 979-980.
Riley, T. R. and K. B. Knight (2001). "Age of pre-break-up Gondwana magrnatism." Antarctic Science **13**(2): 99-110.
Robison, E. G. and R. L. Beschta (1990). "Characteristics of coarse woody debris for several coastal streams of southeast Alaska, USA." Canadian Journal of Fisheries and Aquatic Science 47: 1684-1693.
Sajjadi, F. and G. Playford (2002). "Systematic and stratigraphic palynology of Late-Jurassic-earliest Cretaceous strata of the Eromanga Basin, Queensland, Australia: Part One." Palaeontographica Abt. B **261**: 1-97.
Sarjeant, W. A. S., W. Volkheimer and W. P. Zhang (1992). Jurassic palynomorphs of the Circum-Pacific region.
Scott, A. C. and T. P. Jones (1991). "Microscopical observations of recent and fossil charcoal." Microscopy and Analvsis: 13-15.
Seymour, D. B. and C. R. Calver (1998). Space-Time diagram of Tasmania. V. NGMA TasGO Project, Mineral Resources of Tasmania.
Sharples, C. (1996). A reconnaissance of landforms and geological sites of geoconsewation significance in the Murchison Forest district. A report to Forestry Tasmania. 2: 1-120.
Shervais, J. W. (1982). "Ti-V plots and the petrogenesis of modern ophiolite lavas." Earth and Planetary Science Letters 59: 101-118.

Siders, M. A. and D. H. Elliot (1985). "Major and trace element geochemistry of the Kirkpatrick Basalt, Mesa Range, Antarctica." Earth and Planetory Science Letters 72: 54-64.
Smith, A. G., A. M. Hurley and J. C. Briden (1981). Phanerozoic paleocontinental world maps. London,, Cambridge University Press.
Sporne, K. R. (1966). The morphology of Pteridophytes. London, Hutchinson & Co Ltd.
Stacey, A. R. and R. F. Berry (2004). "The structural history of Tasmania: a review for petroleum explorers." PESA Eastern Australian Basins Symposium 2.
Stewart, W. N. and G. W. Rothwell (1993). Paleobotany and the evolution of plants. Cambridge, Cambridge University Press.
Sutherland, F. L. (1989). Tasmania and Bass Strait. Intraplate Volcanism in eastern Australia and New Zealand. R. W. Johnson. Melbourne, Press Syndicate of the University of Cambridge.
Taylor, T. N. (1981). "Current concepts of Paleozoic seed ferns." Review of Palaeobotany and Palynology 32: 1-3.
Thorne, V. (2001). "Vegetation communities of a high palaeolatitude Middle Jurassic forest in New Zealand." Palaegeography, Palaeoclimatology, Palaeoecology **168**: 273-289.
Tidwell, W. D. (1987). "A new species of Osmundacaulis (*O. jonesii* sp. nov.) from Tasmania, Australia." Review of Palaeobotany and Palynology **52**(2-3): 205-216.
Tidwell, W. D. (1991). " *Lunea jonesii* gen. et sp. nov., A new member of Guareaceae from the Mid-Mesozoic of Tasmania, Australia." Palaeontographica 223: 81-90.
Tidwell, W. D. and R. Jones (1987). "*Osmundacaulis nerii*, A new Osmundaceous species from Tasmania, Australia." Palaeontographica 204: 181-191.
Tidwell, W. D., J. H. Kim and T. Kimura (1987). " Mid-Mesozoic leaves from near Ida Bay, southern Tasmania, Australia." Papers and Proceedings of the Royal Society of Tasmania 121: 159-170.
Tidwell, W. D., G. E. Munzig and M. R. Banks (1991). "*Millerocaulis* species (Osmundaceae) from Tasmania, Australia." Palaeontographica 223: 91-105.
Tidwell, W. D. and K. B. Pigg (1993). "New species of *Osmundacaulis* emend. from Tasmania, Australia." Palaeontomaphica Abt. B 230: 141-158.
Tidwell, W. D. and J. E. Skog (1992). "Two new fossil matoniaceous stem genera from Tasmania, Australia." Review of Palaeobotany and Palynology 70: 263-277.
Turner, N. J. (1989). Precambrian. Geology and Mineral Resources of Tasmania. C. F. Burrett and E. L. Martin. Brisbane, Geological Society of Australia. 15: 5-46.
van Konijnenburg-van Cittert, J. H. A. (2002). "Ecology of some Late Triassic to Early Cretaceous ferns in Eurasia." Review of Palaeobotany and Palynology 119: 113-124.
White, M. E. (1981). "Revision of the Talbragar Fish Bed flora (Jurassic) of New South Wales." Records of the Australian Museum **33**(15): 695-721.
White, M. E. (1986). The greening of Gondwana. Frenchs Forest, N.S.W., Australia, Reed Books.
Williams, E. (1989). Summary and Synthesis. Geology and Mineral Resources of Tasmania. C. F. Burrett and E. L. Martin. Brisbane, Geological Society of Australia. 15: 468-499.

Wilson, K. and D. J. B. White (1986). The anatomy of wood: its diversitv and variabilitv. London, Stobart & Son Ltd.

Wilson, M. (1989). Igneous petrogenesis. London, Chapman & Hall.

Wilson, T. J. (1993). Jurassic faulting and magmatism in the Transantarctic Mountains: Implications for Gondwana breakup. Gondwana Eight: Assembly, evolution and dispersal. R. H. Findlay, R. Unrug, M. R. Banks and J. J. Veevers. Rotterdam, Balkema: 563-572.

Wnuk, C. (1989). "Ontogeny and paleoecology of the middle Pennsylvanian arborescent lycopod Bothrodendron *punctatum*, Bothrodendraceae." American Journal of Botany **76**(7): 966-980.

Appendices

Apendix 1. Separation and analysis of zircons

modified from Meffre et al. in prep.

150 g of rock from each sample was repeatedly sieved and crushed to a grain size of <180 micron. Crushing was performed in a Cr-steel ring mill. Heavy minerals were then separated using a combination of a mechanised panning device (superpan) and a hand pan. The heavy mineral residue was then dried. Magnetic and paramagnetic minerals were separated using a hand magnet and a Franz magnetic separator. Zircons and garnets were picked from the non-magnetic heavy mineral separate using a single hair from a fine artist's paint brush, and mounted on double sided sticky tape. Epoxy glue was then poured into a 2.5 cm diameter mould on top of the zircons. The mount was dried for 12 hours and polished using clean sandpaper and a clean polishing lap. The samples were then washed in distilled water in an ultrasonic bath.

Analyses were performed two hours after ignition of the mass spectrometer to enable the machine to stabilise. Four primary (Temora standard of Black et al. 2003) and two secondary standards (91500 standard of Wiendenbeck et al. 1995) were analysed at the beginning of the session and again roughly every hour. Each analysis began with a 30 second blank gas measurement followed by a further 30 seconds of analysis time when the laser was switched on. Zircons were sampled on 30-micron spots using the laser at 5 Hz and a density of approximately 12 mJ/cm^2. A flow of He carrier gas at a rate of 0.7 litres/minute carried particles ablated by the laser out of the chamber to be mixed with Ar gas and carried to the plasma torch. Elements measured include ^{96}Zr, ^{146}Nd, ^{178}Hf, ^{202}Hg, ^{204}Pb, ^{206}Pb, ^{207}Pb, ^{208}Pb, ^{232}Th and ^{238}U with each element being measured sequentially every 0.2 s.

The data reduction method used was based on the method outlined in detail by Hams *et al.* (2004), modified to suit the ICPMS and laser at the University of Tasmania. The average of the background count rates were subtracted from each isotope. Pb and U isotopic ratios were then calculated for each 0.2 s measurement. These ratios were filtered to exclude the top and bottom 1% to eliminate spikes and spurious data. Filtered ratios were then corrected for machine drift, down hole fractionation, and mass bias. The machine drift correction was calculated by fitting a line to the primary

standard data measured every 12 analysis throughout the day. Machine drift was also checked by examining the secondary standard data. The downhole fractionation and mass bias correction factors were calculated by averaging the drift corrected ratios on each 0.2 s primary standard measurements (relative to the start of the analysis), fitting a line to the data and then dividing it by the recommended value for the primary standard. A set of correction factors was generated for each 0.2 s intervals and for each isotopic ratio.

After the corrections were applied to the ratios, radiometric ages were calculated for each 0.2 s measurement and the age data for each analysis was plotted against the analysis time. An integration interval was then chosen for the most stable portion of the analysis, to exclude parts with contamination from inclusions. The standard errors quoted were based on the standard error of the measurements within the integration intervals and the errors on the measurement of the standards.

Element abundances were calculated using the method outlined by Kosler (2001) using Zr as the internal standard element, assuming stoichiometric proportions and using the secondary standard 91500 to correct for mass bias.

Appendix 1A. Morphology of zircons removed from volcanilithic ash (UTGD 154352)

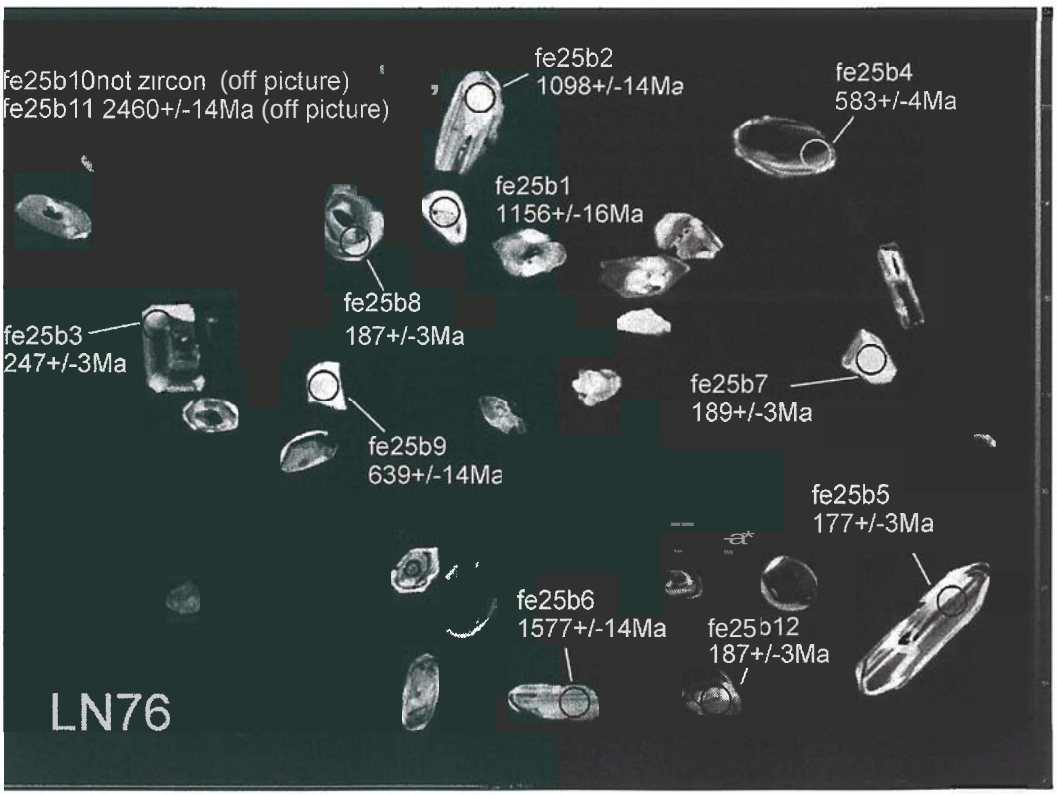

Morphology of zircons removed from volcanilithic sandstone (UTGD 154333).

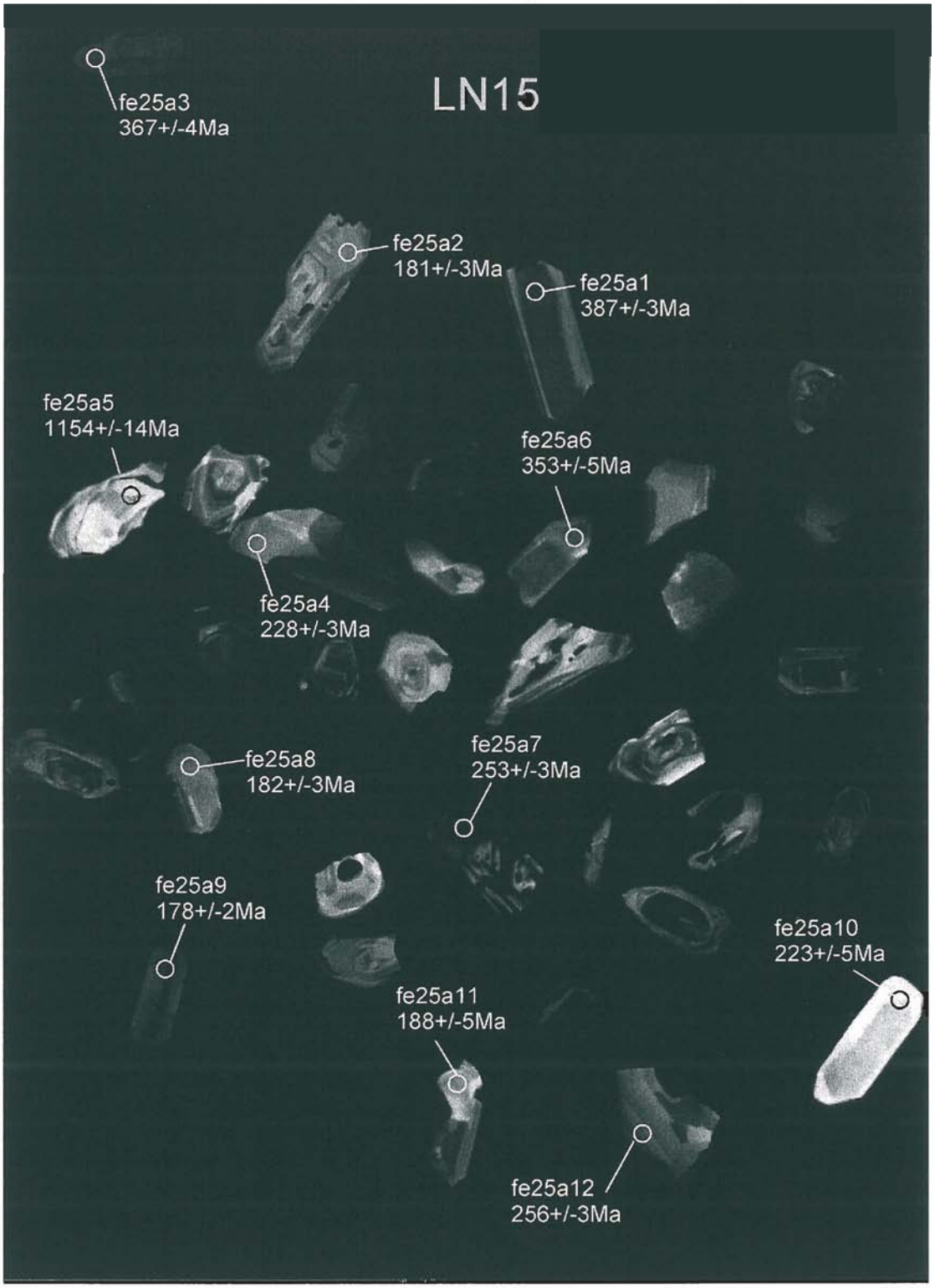

For raw data see data disk folder 'Kate Bromfield Fe25 results"

Appendix 2. Summary of XRF Analysis (X-Ray Fluorescence Analysis)

(Phil Robinson, in prep).

Instrument	Philips PW1480 X-Ray Spectrometer
X-Ray Tubes	3kW max. ScMo anode side window.
	Elements analysed Majors, S and Y, Rb, U, Th, Cu, Pb, Zn, Ni, As, Bi, Co, Ga, Tl, Se, W, Br
	3kW max. Au anode side window.
	Elements analysed; Nb, Zr, Sr, Ba, Cr, V, Sc, La, Ce, Nd, Sb, Sn
	3kW max. Rh anode side window.
	Elements analysed: Mo, occasionally Nb
Crystals:	LiF 200, LiF 220, PX-1 (for Na and Mg), PE002, Ge111
Collimators:	Coarse (0.7mm) and fine (0.3mm) with auxiliary (0.14mm)
Detectors:	Gas flow proportional counter with P10 gas (10% methane in argon) and Scintillation Counter.
Sample Changer:	Philips 30 position sample holder

Sample Preparation

Major Elements:	Fusion discs prepared at 1100 degreesC in 5%Au/95% Pt crucibles
	0.77g sample, 4.125g Norrish Flux (Lithium borates/La2O3 mix), 0.055g LiNO3 for silicates.Platinum/gold moulds used for cooling.
Trace Elements	Pressed powder pills (3.5 tonnes/cm^{-2}) with 10 grams sample.
	Binder used; PVP-MC.

Corrections

Corrections for mass absorption calculated using Philips X40 software with De Jongh's calibration model and Philips (or CSIRO) alpha coefficients. Compton scattering also used for many trace elements.

Calibration

Pure element oxide mixes in pure silica, along with international and Tasmanian standard rocks used. Numerous checks of standard rocks and pure silica blanks ran with each program.

Appendix 2A. XRF raw data

XRF ANALYSES — SES-CODES, University of Tasmania

Analyst: Phil Robinson

Philips PW1480 XRF

XRF sample **preparation:Katie McGoldrick**

International and Tasmanian Standard Rocks analysed.

Rock Crushing in tungsten carbide mill by Kate Brom.

MAJORS program (ScMo X-ray tube) with fusion discs

Ident	Si02	Ti02	Al2O3	Fe2O3	MnO	MgO	CaO	Na2O	K2O	P2O5	1000deg. Loss	Total	S
BLANK(1/3/04)	99.69	0.00	0.01	0.00	0.00	0.01	0.00	<0.03	0.00	0.00	0.00	99.70	<0.01
BLANK (expected)	100.00	0.00	0.00	0.00	0.00	0.00	0.00	0.00	0.00	0.00	0.00	100.00	0
TASBAS(1/3)KM	44.52	2.32	14.11	12.68	0.17	8.27	7.85	5.31	1.94	0.95	1.56	99.67	0.04
TASBAS expected	44.55	2.32	14.15	12.65	0.17	8.29	7.84	5.37	1.93	0.94	1.56	99.77	0.04
LN54	55.20	0.74	**14.36**	**10.20**	**0.1**7	**5.57**	9.99	**1.97**	**0.44**	**0.13**	0.90	99.66	**0.04**
LN55	55.52	0.73	**14.30**	**10.36**	0.19	**5.66**	**10.14**	**1.89**	**0.48**	**0.12**	0.77	100.16	**0.03**
LN67	51.46	0.96	**19.40**	**7.29**	0.06	**3.61**	0.67	**1.36**	**3.16**	**0.04**	11.81	99.82	**<0.01**
LN94	54.95	0.76	**14.42**	**10.99**	**0.1**8	**5.67**	9.26	**1.87**	**0.98**	**0.11**	0.66	99.86	**<0.01**
LN107	55.11	0.74	**14.34**	**10.42**	**0.17**	**5.42**	9.89	**1.93**	**0.77**	**0.13**	0.70	99.61	**0.04**
LN118	80.57	0.25	**6.38**	**4.47**	**0.02**	**1.10**	0.27	**0.16**	**3.81**	**0.04**	2.58	99.65	**<0.01**
LNX15	76.29	0.35	**9.02**	**4.39**	**0.02**	**1.11**	0.30	**0.57**	**4.83**	**0.03**	2.87	99.77	**<0.01**
TASGRAN14(1/3)KM	72.88	0.29	13.70	2.21	0.04	0.69	1.84	2.74	4.51	0.12	0.73	99.75	<0.01
TASGRAN1(14) expected	72.78	0.283	13.72	2.21	0.040	0.70	1.85	2.76	4.51	0.116	0.73	99.70	*0.01*

GOLD1 program (Au X-ray tube) with pressed powder pills

ppm	**Nb**	**Zr**	**Sr**	**Cr**	Ba	**Sc**	**V** (not requested)
AWQUARTZ	<1	<1	<1	1.1	<4	<2	**<1.5**
TASBAS	54	254	993	179	194	14.9	157
TASBAS expected	54.5	259	1008	181	186.5 ANU	14-14.7	**156**
LN54	**5.5**	**120**	**145**	**64**	298	**41**	258
LN55	**6.4**	**120**	**162**	**60**	276	**40**	249
LN67	**8.5**	**166**	**72**	**82**	1457	**54**	343
LN94	**5.5**	**113**	**124**	**79**	266	**41**	286
LN107	**6.4**	**122**	**137**	**58**	255	**41**	257
LN118	**4.8**	**93**	**27**	**13**	687	**9**	37
LNX.15	**4.1**	**84**	**44**	**14**	**1205**	**9**	61
AGV-1	14.5	236	653	8.8	1199	14.5	119.8
AGVI expected	13.6,14.4TAS	232	662	10.1	1227, 1196	12.2,13.9	121, 118
TASGRAN1(10)	14.0	163	147	8.5	446	6.6	25
TASGRAN1(10) expect.	14	163	147	8.2	445	7	25
RSES	<1	12	141	55	46	45	318
RSES(Tafahi)expected	0.456	12.1	139	53	40.3	45.5	298,315(XRF)
BIR-1	1.4	15	110	395	6.5	38	309
BIR-1 (expected)	0.6	14.5	110, 108	382, 389	6.4	44, 38	313
detection **limit(ppm)**	**1**	**1**	**1**	**1**	4	**2**	1.5

Note:- Sr required to correct the Zr analysis. (overlapping line)

mean

MOCOMP3F program (ScMo X-ray tube) with pressed powder pills

ppm	**Y**	**Rb**	**Ni**
AWQUARTZ	<1	<1	<1
TASBAS	20.0	16.5	151
TASBAS(expected)	19.5	16.4	150
LN54	**32**	**34**	**63**
LN55	**27**	**29**	**61**
LN94	**21**	**36**	**60**
LN107	**26**	**46**	**59**
LN67repeat	**29**	**81**	**59**
LN118	**20**	**111**	**27**
LNX-15	**17**	**142**	**13**
G-2	8.9	166.3	3.4
G-2 expected	9.4	166	*<5*
GSR-4	22.5	28.1	15.4
GSR-4 expected	21.5	29	16.6
AGV-1	18.3	67.7	14.5
AGV1 erxpected	20?,18.7, 17.8	67.3+/-0.9	16+/-3
GSR-1	63.2	468.4	4.6
GSR-1 expected	62	466?	2.3
TASGRAN1(8)	32.3	251.2	3
TASGRAN1(8) expec.	32.7	252	2.7
TASGRAN1(10)	32.0	249.7	3.6
TASGRAN1(10)expec.	32.5-33	251	3.5,2.9
detection **limit(ppm)**	1	1	1

Note:- Rb not requested but required to correct the Y analysis. (overlapping line)

Appendix 2B. Raw data used to create geochemical plots

Ident	Si02	Ti02	A1203	FeO	Fe2O3	Fe2O3*	MnO	MgO	CaO	Na20	K20	P205	Loss	Total	S	Nb	Zr	Sr	Cr	Ba	Sc	V	Y	Rb	Ni		Zr/Nb	Zr/Y	Rb/Ba	Ti/V	Ti/Sc	Sr/Ba	Cr/Sc
LN54 BASALT	55.20	0.74	14.36	nld	10.20	10.20	0.17	5.57	9.99	1.97	0.44	0.13	0.90	99.66	0.04	5.5	120	145	64	298	41	258	32	34	63		21.89	3.82	0.11	17.11	107.79	0.48	1.55
LN107 BASALT	55.11	0.74	14.34	n/d	10.42	10.42	0.17	5.42	9.89	1.93	0.77	0.13	0.70	99.61	0.04	6.4	122	137	58	255	41	257	29	81	59		18.98	4.21	0.32	17.17	107.24	0.54	1.41
LN55 DOL	55.52	0.73	14.30	n/d	10.36	10.36	0.19	5.66	10.14	1.89	0.48	0.12	0.77	100.16	0.03	6.4	120	162	60	276	40	249	27	29	61		18.70	4.40	0.11	17.55	109.41	0.59	1.49
LN94 DOL	54.95	0.76	14.42	nld	10.99	10.99	0.18	5.67	9.26	1.87	0.98	0.11	0.66	99.86	10.01	5.5	113	124	79	266	41	286	26	46	59		20.47	4.29	0.17	16.00	112.66	0.47	1.94
LN118	80.57	0.25	6.38	nld	4.47	4.47	0.02	1.10	0.27	0.16	3.81	0.04	2.58	99.65	10.01	4.8	93	27	13	687	9	37	20	111	27		19.31	4.72	0.16	40.18	168.40	0.04	1.51
LNX15	76.29	0.35	9.02	n/d	4.39	4.39	0.02	1.11	0.30	0.57	4.83	0.03	2.87	99.77	10.01	41	84	44	14	1205	9	61	17	142	13		20.41	5.02	0.12	34.50	247.56	0.04	1.60
LN67	51.46	0.96	19.40	n/d	7.29	7.29	0.06	3.61	0.67	1.36	31 6	0.04	11.81	99.82	<0.01	8.5	166	72	82	1457	54	343	21	36	60		19.48	7.94	0.02	16.84	106.43	0.05	1.51
Trss P57511	68.16	0.66	15.33	nld	n/d	nld	0.06	1.17	1.35	3.55	3.00	0.17	3.31	nld	n/d	8	159	373	41	737	11	90	24	92	30		19.88	6.63	0.12	43.96	359.70	0.51	3.73
P57578	71.57	0.67	14.39	nld	nld	n/d	0.15	0.86	0.42	1.55	1.98	0.11	4.88	nld	n/d	10	296	76	45	416	11	84	30	73	36		29.60	9.87	0.18	47.82	365.15	0.18	4.09
P57576	68.86	0.60	15.31	nld	nld	n/d	0.10	0.71	0.91	3.87	1.96	0.14	3.23	n/d	n/d	9	152	145	49	614	11	77	24	83	22		16.89	6.33	0.14	46.71	327.00	0.24	4.45
P57555	65.04	0.90	16.14	n/d	nld	n/d	0.05	1.47	1.08	2.09	2.30	0.18	6.74	n/d	n/d	11	189	296	63	501	17	153	27	80	28		17.18	7.00	0.16	35.26	317.38	0.59	3.71
P57556	66.73	0.79	16.24	n/d	nld	n/d	0.04	1.43	1.08	2.86	2.55	0.17	4.72	nld	n/d	11	187	108	51	617	12	106	25	92	25		17.00	7.48	0.15	44.68	394.67	0.18	4.25
P57574	73.85	0.40	11.94	nld	n/d	nld	0.08	0.63	0.40	0.03	1.35	0.04	4.52	nld	n/d	8	148	34	45	291	8	90	27	62	32		18.50	5.48	0.21	26.64	299.75	0.12	5.63
P57554	89.31	0.34	4.15	nld	n/d	n/d	0.05	0.11	1.60	0.04	0.49	0.01	2.86	nld	n/d	13	174	34	13	129	2	25	8	17	4		13.38	21.75	0.13	81.53	n/d	0.26	6.50
KB.81-2-1	54.15	0.59	16.23	7.33	1.44	8.63	0.17	6.42	11.36	1.85	0.41	0.08	nld	nld	nld	4	90	119	170	173	n/d	220	23	33	71		22.50	3.91	0.19	16.08	n/d	0.69	n/d
KB.81-2-2	53.73	0.59	15.96	7.42	1.45	8.72	0.19	6.62	11.43	2.28	0.25	0.08	nld	n/d	n/d	5	85	103	164	122	n/d	202	20	10	84		17.00	4.25	0.08	17.51	n/d	0.84	nld
KB.81-2-30	55.25	0.63	14.66	7.87	1.54	9.26	0.17	6.62	10.81	1.93	0.43	0.09	n/d	nld	n/d	5	105	123	100	164	n/d	237	25	35	67		21.00	4.20	0.21	15.94	n/d	0.75	n/d
KB.81-2-48	55.48	0.68	14.49	7.96	1.55	9.35	0.18	6.46	10.67	1.95	0.50	0.09	n/d	n/d	nld	5	99	137	92	231	n/d	234	24	25	75		19.80	4.13	0.11	17.42	n/d	0.59	n/d
KB.81-2-4	53.44	0.59	16.44	7.45	1.47	8.77	0.19	6.66	11.65	1.77	0.19	0.07	nld	n/d	nld	5	85	103	164	122	n/d	202	22	7	64		17.00	3.86	0.06	17.51	nld	0.84	n/d
KB.81-2-9	54.45	0.55	13.88	7.59	1.48	8.92	0.18	9.03	10.56	1.61	0.62	0.08	nld	nld	n/d	4	88	111	266	170	n/d	237	21	33	109		22.00	4.19	0.19	13.91	nld	0.65	n/d
KB.81-2-8	54.51	0.60	14.37	7.70	1.52	9.07	0.17	7.83	10.44	1.74	0.97	0.08	n/d	n/d	n/d	5	95	112	198	189	nld	257	23	26	94		19.00	4.13	0.14	14.00	nld	0.59	n/d
KB.81-2-11	55.95	0.82	14.27	8.90	1.74	10.47	0.18	5.20	10.08	1.95	0.82	0.12	nld	nld	n/d	6	130	129	31	235	n/d	239	31	55	65		21.67	4.19	0.23	20.57	n/d	0.55	n/d
KB.81-2-16	54.55	0.62	14.96	7.67	1.50	9.02	0.17	6.83	11.11	1.69	0.54	0.09	nld	n/d	n/d	5	102	118	126	171	n/d	232	25	29	80		20.40	4.08	0.17	16.02	n/d	0.69	n/d
KB.81-2-23	53.10	0.55	14.69	8.00	1.56	9.40	0.18	9.05	10.80	1.61	0.42	0.07	n/d	n/d	n/d	4	83	109	151	166	n/d	196	22	22	172		20.75	3.77	0.13	16.82	n/d	0.66	n/d
KB.81-2-26	53.96	0.56	16.43	7.20	1.40	8.46	0.16	6.44	11.88	1.46	0.44	0.08	n/d	nld	nld	4	81	167	164	175	nld	202	21	23	89		20.25	3.86	0.13	16.62	n/d	0.95	n/d
KB.81-2-42	54.34	0.63	15.22	7.70	1.50	9.05	0.15	8.40	9.60	1.60	0.84	0.09	nld	n/d	nld	5	87	103	225	168	n/d	199	21	32	98		17.40	4.14	0.19	18.98	n/d	0.61	n/d
TasDol NF87-783468	53.80	0.62	14.40	8.20	0.85	8.96	0.17	7.20	10.90	1.80	0.69	0.08	n/d	n/d	nld	6	108	101	171	209	35	252	nld	31	99		18.00	n/d	0.15	14.75	106.20	0.48	4.89
TasDol	53.18	0.65	15.37	8.33	0.76	9.01	0.15	6.71	11.04	1.65	1.03	0.08	n/d	nld	n/d	nld	nld	130	n/d	n/d	nld	nld	n/d	33	n/d		n/d	n/d	nld	nld	nld	n/d	n/d
Mt. Wellington dol 1	54.02	0.44	14.59	nld	nld	8.92	0.13	8.40	11.64	0.91	0.54	0.02	0.08	99.72	n/d	4	67	116	265	184	42	240	18	17	76		16.75	3.72	0.09	10.99	62.51	0.63	6.28
Red Hill dol 4	55.11	0.69	14.90	n/d	n/d	10.56	0.18	5.48	10.31	1.71	0.87	0.10	0.22	100.27	n/d	6	102	137	28	256	45	241	25	24	85		17.00	4.08	0.09	17.16	91.52	0.54	0.62
Red Hill dol 3	54.75	0.66	16.02	n/d	n/d	nld	0.13	4.49	10.55	1.33	0.91	0.06	n/d	n/d	n/d	6	102	145	18	279	42	250	25	26	18		16.72	4.08	0.09	15.83	95.11	0.52	0.43
Ben Lomond 6	53.29	0.44	13.66	n/d	n/d	n/d	0.19	9.05	11.89	1.21	0.55	0.06	n/d	nld	n/d	3	60	106	108	170	45	250	18	12	130		19.35	3.33	0.07	10.55	59.28	0.62	2.43
Ben Lomand 7	52.89	0.38	14.65	nld	n/d	nld	0.17	9.26	12.43	1.23	0.47	0.05	n/d	n/d	n/d	3	55	107	212	104	47	217	14	12	136		16.18	3.93	0.12	10.50	48.06	1.03	4.47
Red Hill 5	55.67	0.81	15.34	nld	n/d	n/d	0.17	3.84	9.27	1.85	1.12	0.11	0.48	99.45	nld	8	120	135	10	258	41	214	29	34	62		15.38	4.14	0.13	22.69	117.29	0.52	0.24
T-TasBas-1	44.46	2.00	13.25	9.41	3.63	12.68	0.18	9.63	8.57	3.85	1.53	0.70	nld	99.35	nld	44	201	794	325	135	nld	165	19	9	nld		4.57	10.58	0.07	72.67	n/d	5.88	n/d
T-TasBas-2	39.27	3.03	8.60	8.34	5.07	12.90	0.23	13.21	14.69	3.36	1.25	1.51	nld	99.49	nld	111	442	1297	521	514	n/d	254	35	23	246		3.98	12.63	0.04	71.52	nld	2.52	n/d
T-TasBas-3	51.73	1.57	13.14	9.51	1.73	11.07	0.16	8.79	8.86	2.60	0.31	0.21	nld	99.68	n/d	13	92	249	392	102	n/d	159	18	8	n/d		7.08	5.11	0.08	59.20	n/d	2.44	n/d
T-TasBas-4	44.55	2.21	14.61	7.26	4.70	11.49	0.17	8.68	11.03	2.55	0.79	0.42	n/d	99.36	n/d	42	152	580	299	218	n/d	235	25	6	n/d		3.62	6.08	0.03	56.38	n/d	2.66	nld
T-TasBas-5	36.69	2.71	9.32	8.44	5.44	13.34	0.21	14.91	13.23	3.82	1.44	1.32	n/d	99.29	n/d	116	268	1258	442	566	nld	233	28	32	n/d		2.31	9.57	0.06	69.73	n/d	2.22	n/d
T-TasBas-6	42.93	2.73	12.95	9.92	3.65	13.20	0.21	9.01	9.49	4.69	1.44	0.93	nld	99.58	nld	110	410	1150	260	510	n/d	190	39	31	260		3.73	10.51	0.06	86.14	nld	2.25	n/d
T-TasBas-7	44.96	2.22	13.27	9.34	4.41	13.31	0.18	6.65	7.87	4.45	2.36	1.27	n/d	99.01	n/d	116	507	1295	234	660	n/d	57	39	62	n/d		4.37	13.00	0.09	n/d	n/d	1.96	n/d
T-TasBas-8	46.81	2.72	14.15	8.85	3.33	11.85	0.17	7.03	7.65	3.22	1.81	0.95	n/d	99.39	n/d	69	425	1000	153	395	n/d	105	34	36	118		6.16	12.50	0.09	nld	n/d	2.53	n/d
T-Tas-Bas-9	48.31	1.23	15.18	5.21	5.67	10.31	0.21	5.26	5.95	6.89	2.58	0.62	n/d	99.39	n/d	130	730	1000	160	165	n/d	125	22	24	115		5.62	33.18	0.15	58.99	n/d	6.06	n/d
T-TasBas-10	39.41	2.79	11.60	9.64	3.57	12.85	0.20	11.14	13.58	3.09	1.63	1.03	n/d	99.89	n/d	115	250	830	240	720	n/d	340	25	46	170		2.17	10.00	0.06	49.19	n/d	1.15	n/d

Triassic sandstone P57511-P57554 from Grapes et al. (1996). Kirkpatrick Basalt KB 81-2-1 to KB 81-2-42 from Siders and Elliot (1985). TasDol NF87-783468 from Everard (1987). TasDol from Compston et al. (1968). Mt. Wellington dol 1-Red Hill 5 from Brauns et al. (2000). TasBas 1-10 from Sutherland (1989). **nld = no data**

Appendix 3. Microprobe data

	plg	plg	plg	amp	amp	amp	ilm
SiO2	58.23	59.29	58.65	38.98	42.63	46.97	0.16
TiO2	0.00	0.02	0.01	2.68	2.68	1.67	49.81
Al2O3	24.91	24.47	24.57	14.20	10.32	5.54	0.24
Cr2O3	0.01	0.00	0.00	0.02	0.00	-0.01	0.02
MgO	-0.02	0.01	0.03	13.12	12.86	12.34	3.84
CaO	8.43	7.66	7.83	12.09	11.44	11.06	0.09
MnO	0.01	0.01	0.02	0.14	0.54	0.55	1.22
FeO	0.19	0.20	0.36	10.97	14.28	17.26	46.28
NiO	0.00	0.02	0.02	-0.01	0.00	0.00	-0.01
Na2O	6.80	7.01	7.03	2.48	2.04	1.59	0.00
K2O	0.51	0.59	0.37	0.80	0.80	0.74	0.00
Total	99.09	99.27	98.90	95.49	97.58	97.72	101.65
O=	0.00	0.00	0.00	0.00	0.00	0.00	0.00
Total	99.09	99.27	98.90	95.49	97.58	97.72	101.65
Mg#				68.07	61.62	56.03	
An	56.64	53.36	54.33				

For microprobe raw data see data disk file "Appendix 3-Microprobe raw data"

Appendix 4. Vitrinite Analysis

1) Organic petrology and maturation of a suite of outcrop samples from the Jurassic of Tasmania. Prepared by Alan Cook, Kieraville Konsultants. See data disk file "Appendix 4- A.C. Cook.doc"

2) Outcrop samples: Maturity assessment and maceral analysis. Prepared by Wayne Knowles, Mirror Image, UK. See data disk file "report2.pdf and VRdata.xls"

PLAN VIEW
1 : 50

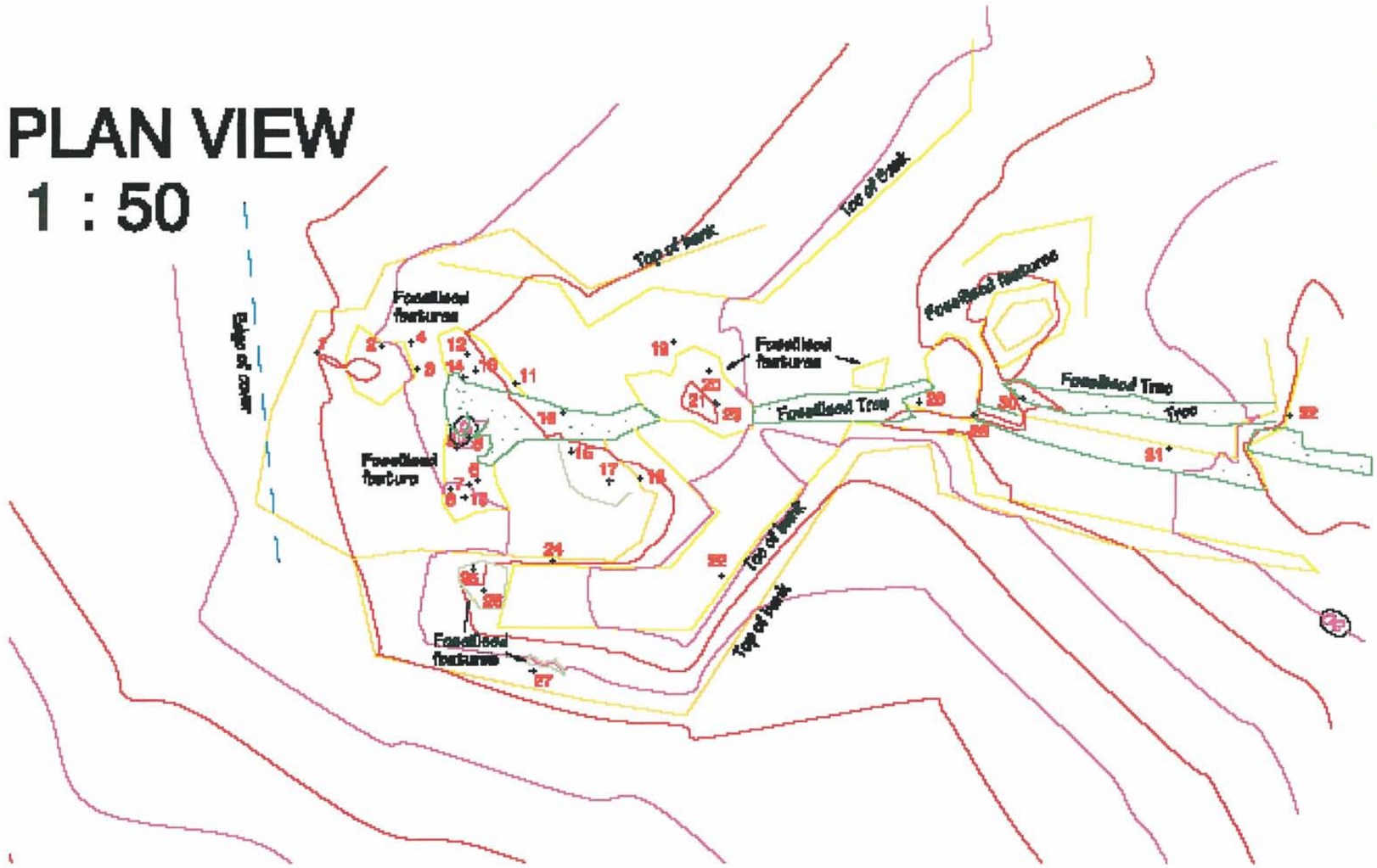

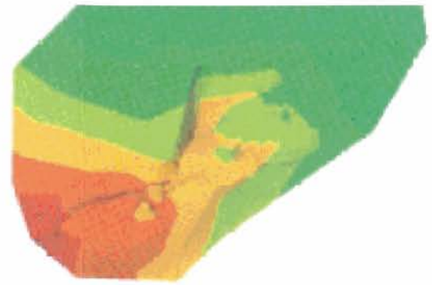

N

MGA

Approximate Centroid of Site

E 492045
N 5166677 (MGA - GDA94)
RL 61.0 (Above MSL)

Forestry Tasmania
GROWING OUR FUTURE

C	-	-	
B	-	-	
A	-	-	
Issue	Revision	Date	

Project: **Lune Fossilised Tree Project**

Project No.

Drafted	Hans	Scale	1:50 @ A3
Project Mgr	K Sykes	Date	25/03/2004
Drawn	MSG	Cont. Int	0.5 metres
Designed	-	CAD File	Lune Fossil.pro
Checked	-	Surveyor	MR

Client
Kate Greenfield
&
Forestry Tasmania

SHEET 1 of 1

Appendix 6 Literature Review: Australian Mid-Mesozoic floras and their application to Jurassic climatology. See data file "Literature review"

Appendix 7. Stratigraphic logs from the fossil site at Lune River

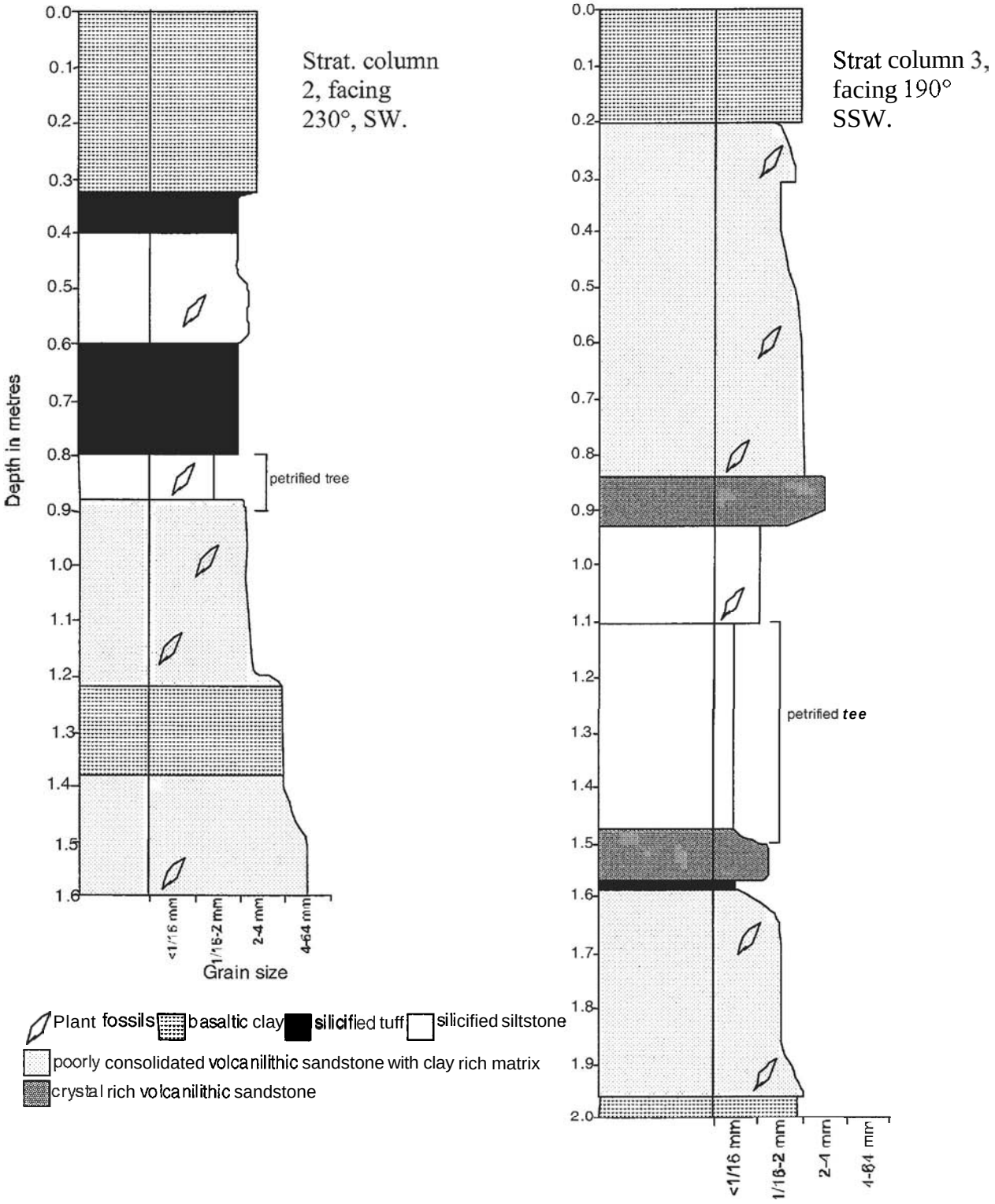

Appendix 8. Rock catalogue.

Utas#	Field Number	Rock Name	Rock Mineral 1	Rock mineral 2	Texture	Period1 System	Early/Middle/Late	Hand specimen	Powder	Thin Section	Polished block	Other Comments
154333	LNX15	Sandstone	Quartz	Feldspar group		Jurassic	Early	R	PD			
154334	LN97	Sandstone	Quartz	Feldspar group		Jurassic	Early	R				
154335	LN77	Sandstone	Quartz	Feldspar group		Jurassic	Early	R		1TS		
154336	LN28	Basalt	Clay			Jurassic	Early	R		1TS		
154337	LN107	Basalt	Pyroxene group	Plagioclase group	glassy	Jurassic	Early	R	PD	1TS		
154338	LNX21	Basalt	Pyroxene group	Plagioclase group	pillow basalt	Jurassic	Early			1TS		
154339	LN109	Basalt	Clay			Jurassic	Early	R				
154340	LNX22	Basalt			peperitic	Jurassic	Early	R		1TS		core from MRT rockstore
154341	LNX23	Basalt			glassy	Jurassic	Early	R		1TS		core from MRT rockstore
154342	LN118	Dacite	Clay			Jurassic	Early	R	PD			

154343	LN67	Basalt	Clay			Jurassic	Early	R	PD			
154344	LN55	Dolerite	Feldspar group	Pyroxene group		Jurassic	Middle	R	PD			
154345	LN54	Basalt	Pyroxene group	Feldspar group	porphyritic	Jurassic	Early	R	PD			
154346	LN94	Dolerite	Feldspar group	Pyroxene group		Jurassic	Early	R	PD	1TS		
154347	LN24		Clay			Jurassic	Early	R				
154348	LN30		Clay			Jurassic	Early	R				
154349	LN39		Clay			Jurassic	Early	R				
154350	LN59		Clay			Jurassic	Early	R				
154351	LN26		Clay			Jurassic	Early	R				
154352	LN76					Jurassic	Early	R		1TS		Palynomorph
154353	LN105	Mudstone				Jurassic	Early	R				
154354	LN102	Mudstone				Jurassic	Early	R				

154355	LN103	Mudstone				Jurassic	Early	R				
154356	LN10				wood	Jurassic	Early			3TS		slides of permineralised wood
154357	LN88				wood	Jurassic	Early	R				permineralised wood
154358	LN87				wood	Jurassic	Early	R		1TS		permineralised wood
154359	LN11				wood	Jurassic	Early	R				permineralised branch
154360	LN120	Mudstone				Jurassic	Early	R				leaf impression
154361	LN84	Mudstone				Jurassic	Early	R				leaf impression
154362	LNX9	Mudstone				Jurassic	Early				PB	gymnosperm branch
154363	LN113A					Jurassic	Early	R				leaf impression
154364	LNX27					Jurassic	Early	R				permineralised stem
154365	LN23					Jurassic	Early				PB	permineralised stem
154366	LNX10					Jurassic	Early				PB	permineralised stem

154367	LNX20					Jurassic	Early	R				permineralised stem
154368	LN98					Jurassic	Early				PB	permineralised stem
154369	LNX30					Jurassic	Early			1TS		
154370	LNX23	Mudstone				Jurassic	Early	R				leaf impression
154371	LNX25	Mudstone				Jurassic	Early	R				leaf impression
154372	LN80	Mudstone				Jurassic	Early	R				leaf impression
154373	LNX24	Mudstone				Jurassic	Early	R				impression
154374	LN52					Jurassic	Early	R				equisetum in canister
154375	LN83					Jurassic	Early	R				permineralised wood

Appendix 9. Reference spectra for PIMA.